



Skolkovo Institute of Science and Technology

PHYSICAL AND NUMERICAL MODELING OF THERMAL METHODS OF EOR
AND IMPROVEMENTS OF OIL RECOVERY

Doctoral Thesis

by

AYSYLU ASKAROVA

DOCTORAL PROGRAM IN PETROLEUM ENGINEERING

Supervisor
Associate Professor of Practice, Alexey Cheremisin

Moscow - 2020

© Aysylu Askarova 2020

I hereby declare that the work presented in this thesis was carried out by me at Skolkovo Institute of Science and Technology, Moscow, except where due acknowledgement is made, and has not been submitted for any other degree.

Candidate (Aysylu Askarova)

Supervisor (Associate Professor of
Practice, Alexey Cheremisin)

Abstract

Currently, the oil and gas industry faces a variety of challenges against the backdrop of ongoing events such as the depletion of existing reserves, drop in oil prices, sanctions, new regulations due to global warming, and the development of new technologies able to achieve ultimate recoveries. The interest of this research was in thermal enhanced oil recovery (EOR) methods due to their extensive technical and commercial development among other techniques and great potential for heavy-oil recovery. The main objective of this study was to conduct a comprehensive experimental and numerical modeling of thermal EOR to select a development methodology on the example of specific objects. The methodology was based on experimental and numerical modeling of hot water injection (HWI), supercritical water injection, high-pressure air injection (HPAI), and *in-situ* combustion (ISC) techniques on carbonate and unconventional reservoirs to predict the feasibility of the method. Subsequent experimental and numerical simulations were carried out to obtain insights into the kinetics, physics of the thermal processes, to determine optimal operational parameters, and to estimate the applicability of the method considered. These tests were conducted on high-pressure ramped temperature oxidation (HPRTO), medium-pressure combustion tube (MPCT), and high-pressure combustion tube (HPCT) equipment under reservoir conditions using oil and core samples from target fields to mimic the real processes. “Aquathermolysis” reactions were firstly introduced during simulation of HWI due to the presence of the products of the chemical reactions at the temperature ranges studied. The proposed kinetic model considers the chemical interactions of heavy oil with hot water. Also, field-scale simulation of supercritical water revealed some software limitations, featured aspects of upscaling the kinetics, and optimization options. The inability of the simulation software to separate the “bonded” components and mobile oil, and to set bitumen in different phases were addressed. The noticeable influence of the specification of the distribution of OM groups in the reservoir on the results of calculations and efficiency of thermal EOR was determined. Feasibility studies of the HPAI method were conducted through subsequent laboratory-scale HPRTO and MPCT experiments, their further 3D numerical simulation, and validation against experimental results. A numerical model of the MPCT employs a comprehensive formulation capable of representing the major phenomenological effects such as mass-heat transfer taking into account the properties of the medium, convection, combustion delay, heat losses, and the support of secondary reactions. Results of numerical simulations were used for the field upscaling and such problems such as low air injectivity, convergence difficulties, areal heterogeneity, and displacement effectivity were resolved. The development system was optimized to avoid uncertainties and risks. Important factors affecting the overall performance of the ISC were distinguished during a unique set of forward and reverse combustion tests on the HPCT installation, and the process of reverse combustion at reservoir condition was studied experimentally under reservoir conditions for the first time. A methodological approach that combines laboratory and numerical studies validated during HPAI simulation was successfully applied for numerical simulation of the forward ISC process. Numerical simulation of forward combustion displayed a satisfactory correlation with experimental results and can be further employed during the field-scale simulation.

Publications

1. A.Askarova, A.Turakhanov, S.Markovich, E.Popov, K.Maksakov, G.Usachev, V.Karpov, A.Cheremisin. Thermal Enhanced Oil Recovery in deep heavy oil carbonates: experimental and numerical study on a hot water injection performance, *Journal of Petroleum Science and Engineering*, 2020, Nov; 194, 107456, <https://doi.org/10.1016/j.petrol.2020.107456>
2. A.Askarova, A.Cheremisin, J.Belgrave, A.Soloviev, S.A. (Raj) Mehta, A.Cheremisin. Evaluation of the subject geological area suitability for oil recovery by High-Pressure Air Injection method. *Advances in Geoscience*, <https://doi.org/10.5194/adgeo-54-7-2020>
3. A.Askarova, E.Popov, M.G. Ursenbach, R.G.Moore, S.A. (Raj) Mehta, A.Cheremisin. Experimental investigations of forward and reverse combustion for increasing oil recovery of a real oil field, *Energies* **2020**, *13*, 4581; [doi:10.3390/en13174581](https://doi.org/10.3390/en13174581)
4. L.Khakimova, A.Askarova, E.Popov, R.G.Moore, A.Solovyev, Y.Simakov, I.Afanasiev, J.Belgrave, A.Cheremisin. High-Pressure Air Injection laboratory-scale numerical models of oxidation experiments for Kirsanovskoye oil field. *Journal of Petroleum Science and Engineering*, 2020 May; 188, 106796, <https://doi.org/10.1016/J.PETROL.2019.106796>

Conference proceedings:

1. A.Askarova, A.Turakhanov, E.Mukhina, A.Cheremisin, A.Cheremisin. Unconventional Reservoirs: Methodological Approaches for Thermal EOR Simulation, Unconventional Resources Technology Conference (URTeC), <https://doi.org/10.15530/urtec-2020-2112>
2. E.Mukhina, A.Askarova, A.Cheremisin et.al., Hydrocarbon Saturation for an Unconventional Reservoir in Details, SPE Russian Petroleum Technology Conference, [DOI: 10.2118/196743-MS](https://doi.org/10.2118/196743-MS)
3. A.Askarova, A.Turakhanov, E.Popov et al., Experimental and numerical simulation of hot water injection to deep carbonate reservoir, 19th SGEM International

Multidisciplinary Scientific GeoConference, [DOI: 10.5593/sgem2019/1.2/S06.108](https://doi.org/10.5593/sgem2019/1.2/S06.108)
[2017;15\(3\):169-182](#)

4. Cheremisin, A., Askarova, A., Bondarenko, T., Spasennykh, M., Moore, R.G., Mehta, S.A., and Ursenbach, M.G., Physical and Numerical Modeling of Air Injection EOR in a Heavy Oil Reservoir, presented at 2016 World Heavy Oil Congress, Calgary, Alberta, 6 – 9 September 2016.

5. A.Askarova, L.Khakimova, T.Bondarenko, A.Cheremisin, A.Myasnikov, R.G. Moore, S.A. Raj Mehta, M. Ursenbach, D. Mallory, Adaptation of laboratory experiments on modeling of thermal methods for increasing oil recovery at Usinsk oil field presented at the conference, Thermal EOR 2017, Kazan, Russia, 19-23 June 2017.

Acknowledgements

This work would not be possible without my supervisor Alexey Cheremisin who provided his excellent guidance, support, and showed extraordinary patience throughout my studies.

I also would like to extend my deepest gratitude to the following individuals and organizations for their priceless support during my Ph.D. studies at the Skolkovo Institute of Science:

- Members of the Integrated Center of Hydrocarbon Recovery: Prof. Mikhail Spasennykh, Prof. Dimitri Pisarenko, Prof. Yuri Popov, and Prof. Sergey Stanchits;
- My Individual Doctoral Committee members, Prof. Mikhail Spasennykh, Prof. Marwan Charara, and Prof. Dmitry Eskin;
- Prof. Raj Mehta, Prof. Gordon Moore, and Matthew Ursenbach from University of Calgary for productive collaboration, insightful conversations and enormous help;
- Special thanks to my teacher, idol, and inspiration – the late Dr. John Belgrave;
- Aman Turakhanov, Aliya Mukhametdinova, Evgeny Shilov, Strahinja Markovic, Dr. Elena Mukhina, Dr. Alexander Cheremisin and Dr. Evgeny Popov for creating a productive, friendly and happy environment;
- Amazing people from Education and Admission offices, Administration team of the Integrated Center of Hydrocarbon Recovery who made my journey comfortable and joyful;
- My wonderful family and all my friends for their unconditional love, encouragement, and for always standing by my side! It is not possible to list you all, but you all are parts of my heart!

Table of Contents

Abstract	3
Publications	4
Acknowledgements	6
Table of Contents	7
List of Symbols, Abbreviations	10
List of Figures	11
List of Tables	13
Chapter 1. Introduction	14
1.1 Recovery techniques	14
1.2 Purpose of the Thesis Study.....	16
1.3 Outline of the Thesis	17
Chapter 2. Literature review	19
2.1 Petroleum classification	19
2.2 Types of oil production.....	20
2.3 Thermal EOR methods.....	23
2.3.1 <i>Hot water injection</i>	24
2.3.2 <i>Steam injection</i>	25
2.3.3 <i>Steam-Assisted Gravity Drainage</i>	26
2.3.4 <i>HPAI</i>	27
2.3.5 <i>In-situ combustion</i>	28
2.3.5.1 <i>Forward combustion</i>	28
2.3.5.2 <i>Reverse combustion</i>	29
2.4 Thermal EOR projects	30
2.4.1 <i>Projects with hot water and steam flooding</i>	30
2.4.1.1 <i>HWI and steam flooding</i>	30
2.4.1.2 <i>Supercritical water injection</i>	33
2.4.2 <i>HPAI and ISC projects</i>	35
2.5 Conclusions	39
Chapter 3. Primary objectives	40
Chapter 4. Hot water flooding in a carbonate reservoir	41
4.1 Hot water flooding	44
4.1.1 <i>Rock samples</i>	44
4.1.2 <i>Oil samples</i>	45
4.1.3 <i>Cementation technology</i>	46

4.2	Experimental section.....	48
4.2.1	<i>Experimental modeling of cyclic HWI on the HPRT0 setup (Dome A) at different temperatures. Experiment 1</i>	49
4.2.2	<i>Experimental modeling of cyclic HWI on the MPCT setup (Dome B) with different injection rates. Experiment 2</i>	50
4.3	Numerical section	52
4.3.1	<i>The numerical model of Experiment 1 for Dome A</i>	52
4.3.2	<i>The numerical model of Experiment 2 for Dome B</i>	53
4.4	Hot water flooding experiments results	57
4.4.1	<i>Experimental and numerical results of Experiment 1</i>	57
4.4.2	<i>Experimental and numerical results of Experiment 2</i>	61
4.5	Conclusions	66
Chapter 5. Supercritical water flooding in an unconventional reservoir		68
5.1	Field-scale modeling of the supercritical water injection process	68
5.1.1	<i>Methods</i>	69
5.1.2	<i>Pyrolysis and SARA analysis</i>	69
5.1.3	<i>Parameters of HDS</i>	69
5.1.4	<i>The results of the modeling</i>	74
5.2	Methodological approach.....	77
5.2.1	<i>Methods</i>	79
5.2.2	<i>Autoclave experiment</i>	79
5.2.3	<i>Numerical simulation of autoclave experiment</i>	81
5.2.4	<i>Results</i>	85
5.3	Conclusions	86
Chapter 6. High-pressure Air Injection method.....		89
6.1	High-pressure air injection on a laboratory scale.....	89
6.1.1	<i>Experimental setup</i>	89
6.1.1.1	<i>High-pressure ramped temperature oxidation</i>	90
6.1.1.2	<i>Medium pressure combustion tube</i>	91
6.1.2	<i>Experimental results</i>	92
6.1.2.1	<i>High-pressure ramped temperature oxidation</i>	92
6.1.2.2	<i>Medium pressure combustion tube</i>	93
6.1.3	<i>Numerical modeling of the HPAI experiments</i>	95
6.1.3.1	<i>High-pressure ramped temperature oxidation numerical model</i>	95
6.1.3.2	<i>Medium pressure combustion tube numerical model</i>	95
6.1.4	<i>HPAI numerical simulation results</i>	99
6.1.4.1	<i>Fluid and kinetic model for Kirsanovsk oil field</i>	99
6.1.4.2	<i>MPCT: history matching</i>	100
6.2	Numerical simulation on a field-scale	102

6.3	Conclusions	107
Chapter 7. Forward and reverse <i>in-situ</i> combustion		110
7.1	Experimental study of forward and reverse combustion	110
7.1.1.	<i>Experimental part</i>	113
7.1.1.1	<i>Forward combustion</i>	113
7.1.1.2.	<i>Reverse combustion</i>	113
7.1.2.	<i>Experimental results</i>	114
7.1.2.1	<i>Forward combustion</i>	114
7.1.2.2	<i>Reverse combustion</i>	118
7.2	Numerical simulation of forward combustion	123
7.2.1	<i>A common approach to numerical modeling of combustion tube test</i>	124
7.2.2	<i>Numerical modeling of forward ISC</i>	125
7.3	Conclusions	129
Chapter 8. Summary, conclusions, and recommendations		132
8.1	Summary	132
8.2	Conclusions	132
8.2	Contribution to the knowledge	133
8.4	Recommendations	135
8.4.1	<i>HWI</i>	135
8.4.2	<i>Supercritical water injection</i>	135
8.4.3	<i>HPAI</i>	135
8.4.4	<i>ISC</i>	136

List of Symbols, Abbreviations

EOR – enhanced oil recovery;
HPAI - high-pressure air injection;
mb/d - million barrels per day;
OPEC – The Organization of the Petroleum Exporting countries;
USGS - United States of Geological Survey;
ISC – *In-situ* combustion;
CSS - Cyclic steam injection;
SAGD – Steam-assisted gravity drainage;
CMG – computer-modeling group;
HPRTO - high-pressure ramped temperature oxidation;
MPCT - medium-pressure combustion tube;
HPCT - high-pressure combustion tube;
BF – Bazhenov formation;
API – American Petroleum Institute;
HO – heavy oil;
LO – light oil;
bb1 - billion barrels;
HWI - Hot water injection;
HTO – high-temperature oxidation;
LTO – low-temperature oxidation;
PV - pore volumes;
PVT – Pressure, Volume, Temperature;
HMWG - High molecular weight gas;
HDS – hydrodynamic sector;
BHC – Bonded hydrocarbons;
OM – Organic matter;
SARA – saturates, aromatics, resins, asphaltenes;
HCG – Hydrocarbon gas;
EPT – effective permeability dependence in temperature;
 E_a – activation energy, [J/mole];
HPDSC - High-pressure differential scanning calorimetry
A – Frequency factor, [];
H – Enthalpy of the reactions [J/mole];
CT – combustion tube.

List of Figures

Figure 1. Evolution of EOR projects in the USA (Alvarado and Manrique, 2010)	15
Figure 2. Recovery methods. <i>Source: www.scmdaleel.com</i>	20
Figure 3. Number of EOR projects in operation globally (McGlade et al., 2018)	21
Figure 4. Screening criteria for EOR methods and methodology of its application. <i>Source: Enhanced oil recovery Shell</i>	23
Figure 5. Porosity (a) and permeability (b) distributions for the formations under study.....	44
Figure 6. Temperature dependence of the oil sample density at different pressures: Dome A (left) and Dome B (right).....	45
Figure 7. Temperature dependence of oil sample viscosity at different pressures: Dome A (left) and Dome B (right).....	46
Figure 8. Core model for Experiment 1 – HPRT0	47
Figure 9. Quality of cementing on a computed tomography scan.....	47
Figure 10. Schematic diagram of the HPRT0 setup.....	49
Figure 11. Scheme of the upgraded HPRT0 reactor with inlet water heater	49
Figure 12. Scheme of the large core holder for MPCT setup.....	51
Figure 13. The numerical model of the HPRT0 experiment in CMG: (a) model grid, (b) distribution of oil saturation, and (c) porosity in the reactor.....	52
Figure 14. Modified relative permeability: (left) water-oil; (right) gas-liquid.	53
Figure 15. The numerical model of the CT equipment in CMG: a) grid model; b) porosity; c) initial oil saturation	54
Figure 16. Relative permeability: (left) water-oil ; (right) gas-liquid.....	55
Figure 17. The temperature on the outer wall of the model in the middle part	57
Figure 18. The molar fraction of produced hydrocarbon gases	58
Figure 19. X-ray scans after Experiment 1	60
Figure 20. Temperature profile during the injection of heat agent into the HPRT0	60
Figure 21. Cumulative water (left) and oil (right) production for experiment and simulation	60
Figure 22. Temperatures on the outer wall of the model and cumulative gas volume	61
Figure 23. The molar fraction of produced hydrocarbon gases (left) and aquathermolysis produced cumulative gas mass (right).....	62
Figure 24. X-ray scans after Experiment 2.....	63
Figure 25. Temperature profiles (left) and cumulative water and oil (right) in CMG.....	64
Figure 26. Cumulative gases.....	65
Figure 27. The HDS-section, used for numerical simulations.	71
Figure 28. Relative phase permeability curves, oil-water (left) and oil-gas (right) for two regions: main reservoir (up) and fractures (bottom).....	73
Figure 29. Distribution of initial content of bitumen (left) and kerogen (right) in the HDS section.	74
Figure 30. Cumulative oil production, sensitivity analysis (EPT and E_a).....	75
Figure 31. Distribution of initial concentration of the combined solid component BITUM*/KER* (left) and distribution of total porosity (right) the HDS section.	76
Figure 32. Cumulative oil production for the base case and cases 2. BITUM* and 3. KER*.	77
Figure 33. (a) Experimental set-up scheme; (b) Injection pressure (green) and cumulative water volume (blue) profile	79
Figure 34. Autoclave in CMG format: a) grid mesh; b) oil and c) water initial saturations	81
Figure 35. Distribution of: a) Heavy Oil; b) Light Oil; c) Hydrocarbon Gas - mole fractions	82
Figure 36. (a) Cumulative oil; (b) cumulative HO and LO production	83
Figure 37. (a) Initial saturation of LB; (b) initial oil saturation	84
Figure 38. Comparison – (a) cumulative oil production; (b) cumulative HO and LO production	85
Figure 39. Liquid bitumen gas mole fraction changes overtime: (a) initial, (b) after 1.55 h, and (c) after 3.3 h.....	86

Figure 40. Scheme of the HPRT0 setup (Khakimova et al., 2020).	90
Figure 41. Scheme of the MPCT installation (Khakimova et al., 2020).	91
Figure 42. Centreline temperatures by zone gas mole concentrations.....	92
Figure 43. Temperature profiles on the centreline (top); Combustion gas mole concentrations (bottom).....	94
Figure 44. (a) MPCT equipment and its digital model in CMG STARS: (b) model grid, (c) initial porosity distribution, (d) initial permeability distribution	96
Figure 45. MPCT setup diagram and its cross-section.....	97
Figure 46. Temperature profiles: Zone 1 (left); Zone 6 (right).....	100
Figure 47. (a) Cumulative O ₂ , (b) CO ₂ , (c) water, and (d) oil production for experiment and simulation ..	101
Figure 48. Oil saturation distribution of different subsections	103
Figure 49. Cumulative oil production for 4 subsections (a,b,d,e) and temperature profiles for scenario 2 in subsection 2 (c); subsection 3 (f)	105
Figure 50. Optimization scenario (left) and cumulative oil production (right) for Subsection 3 before air breakthrough	106
Figure 51. High-pressure combustion tube experimental setup.....	111
Figure 52. Forward combustion test temperature profiles	115
Figure 53. Forward combustion front locations	116
Figure 54. Produced combustion gas compositions for forward combustion test.....	116
Figure 55. Forward combustion oil and water production cumulative masses	117
Figure 56. Reverse combustion test temperature profiles	118
Figure 57. Reverse combustion front locations	119
Figure 58. Reverse combustion produced combustion gas compositions.....	119
Figure 59. Reverse combustion oil and water production cumulative masses.....	121
Figure 60. A numerical model of the HPCT installation in CMG: (a) initial oil saturation; (b) permeability; (c) porosity	124
Figure 61. The difference in viscosity extrapolations for heavy oil using the Andrade and Walther equations	126
Figure 62. Simulation results: forward combustion temperature profiles	128
Figure 63. Simulation results: forward combustion produced combustion gas compositions (left); forward combustion oil and water cumulative production (right)	128

List of Tables

Table 1. Screening criteria for the EOR method (World Energy Outlook, International Energy Agency). ..	22
Table 2. Reservoirs and their parameters	44
Table 3. Characteristics of the two water injection experiments to determine k_{dis}	48
Table 4. Initial conditions	56
Table 5. Parameters of the experiment during water saturation and HWI (Experiment 1)	58
Table 6. Results of oil Rock-Eval pyrolysis	59
Table 7. Production of oil and water for Experiment 1	61
Table 8. Parameters of the experiment during water saturation and HWI (Experiment 2)	63
Table 9. Mass of oil and water produced for Experiment 2	64
Table 10. Mass of gases produced for Experiment 2	65
Table 11. The list of pseudo-components in calculation cases	72
Table 12. Molecular weights of pseudo-components	81
Table 13. Material balance	83
Table 14. The list of pseudo-components in the calculations - Cases 1 and 2	84
Table 15. MPCT specifications	91
Table 16. The porosity, permeability, and diameters of the tube layers	97
Table 17. Kinetic parameters obtained from the history match	100
Table 18. Mass of the products for the experiment and simulation	101
Table 19. Characteristics of the model.....	103
Table 20. Input parameters of forward and reverse combustion tube tests	112
Table 21. Summary of stabilized combustion parameters	122
Table 22. Comparison of the cumulative production for the experiment and simulation	129

Chapter 1. Introduction

1.1 Recovery techniques

There have been warnings of oil exhaustion from the early nineteenth century and according to predictions, the global oil was supposed to run out by the 2000s. The World's original endowment of recoverable oil was estimated to be roughly 2000 billion barrels. (R. W. Bentley, 2002) Geopolitical issues, production losses due to sanctions, over-supplied markets, the predicted fall in global oil demand, and efforts to improve energy sustainability, introduced major challenges into the oil industry. Nevertheless, the capacity of the world's oil production is expected to grow by 5.9 million barrels per day (mb/d), where OPEC and non-OPEC are expected to contribute 1.4 and 4.5 mb/d of crude and natural gas liquids capacity, respectively (IEA, 2020). According to the United States of Geological Survey (USGS), the total oil reserves in the world amount to three trillion barrels (400 billion tons) (Terry, R.E., 2001). Over 50% of the oil in place in the average reservoir counts as unrecoverable. Firstly, it is because the injected fluid can contact just a limited area of the reservoir. Secondly, only the limited fraction of the oil which is in contact with injected fluid can be displaced. Thirdly, heavy oils are more often too hard to move towards production wells by conventional means at economically sufficient rates. (Speight, 2013)

The past decade was characterized by the significant growth of technically recoverable light oil and shale gas resources, as more unconventional formations have gone into production. The development of unconventional hydrocarbon resources, including heavy oil fields, can lead to a significant boost in petroleum production worldwide. These "untapped" resources have attracted more attention in recent years and they will be able to satisfy the future growth of oil demand. The estimates of technically recoverable crude oil and natural gas resources change over time as new information is gained through drilling, production, and technological development. (U.S. Energy Information Administration, 2020) These uncertainties and assumptions must be studied more closely. The main challenge is to develop effective, fast, and cheap technologies for

the extraction of heavy and extra-heavy oil. Technological improvements and innovations may bring new resources into play. (McGlade et al., 2018)

Currently, EOR methods include thermal, chemical, gas, and hybrid methods. Application of EOR projects depends heavily on oil prices and economics, investment, and willingness of companies to invest, take risks, and the availability of other options. The general tendency of the EOR project evolution in the US is presented in Figure 1.

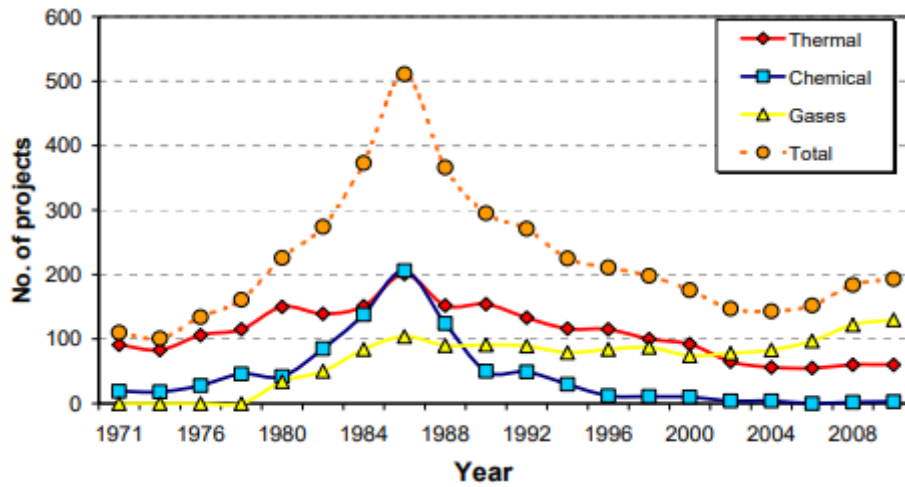


Figure 1. Evolution of EOR projects in the USA (Alvarado and Manrique, 2010)

The research in this thesis is devoted particularly to thermal methods of enhanced oil such as hot water injection (HWI), *in-situ* combustion (ISC), and HPAI. As was already mentioned, the choice of the particular technique is a challenging task and many features of reservoir and oil samples must be taken into account.

Thermal EOR projects have been spread geographically over such countries as Canada, Former Soviet Union countries, the USA, Venezuela, Brazil, and China. Cyclic steam injection (CSS) or Huff & Puff, steam flooding, and steam-assisted gravity drainage (SAGD) are the most commonly used recovery methods for heavy and extra-heavy oil production in sandstone reservoirs in the last few decades. Thermal EOR projects in their turn were not as popular in carbonate formations. However, recent studies show a steady increase in air injection projects in carbonate reservoirs, and they

have proved to have made an improvement on oil recovery in both mature and water flooded carbonate reservoirs. (Alvarado and Manrique, 2010)

This research includes several case studies with subsequent laboratory investigations, numerical simulation, and validation against experimental data, and further field-scale simulation. Simulation of the experimental tests is important for the design and optimization of the process, as well as for calculation of the decision variables like cumulative oil, recovery factor, and net present value. Numerical modeling serves as a tool to distinguish the process features, to interpret the laboratory combustion tests, and to assess the performance of the method. The model of kinetic reactions obtained and validated during “history matching” of the processes obtained in this research can be used to make reasonable and comprehensive decisions at the stage of early planning of reservoir development.

1.2 Purpose of the Thesis Study

Although a substantial amount of oil remains residual in unconventional reservoirs, the application of EOR methods can increase the average oil recovery factor. The degree to which the EOR methods can be effectively applied depends on many factors, such as an understanding of the fluid chemistry, phase behavior, physical properties, and accuracy of geology and reservoir engineering. Thus, the main goal of this study is to conduct a comprehensive experimental and numerical modeling of thermal EOR to select a development methodology based on the examples of specific reservoirs. The methodology is based on experimental studies and numerical modeling, using these experimental data to predict the feasibility of the method. The key objectives will be derived after careful study of existing approaches, methods, experimental procedures, and current progress described in the literature in Chapter 2.

The workflow of the research consists of the following steps:

- 1) To analyze the experimental tests of HWI, ISC, and HPAI under conditions close to the laboratory experiments, to analyze the experimental results, and to define the parameters of the oxidation kinetics;

2) To create digital models of these tests in the Computer Modeling Group (CMG) STARS and to conduct numerical experiments;

3) To validate and optimize the digital models in CMG, to tune, history match, and compare the simulation results against experimental data;

4) To specify the optimal operational parameters and to generate the kinetic models for aquathermolysis during HWI, supercritical water injection, HPAI, and ISC corresponding for each oil sample and field, including activation energies, stoichiometric constants, and reaction velocities.

5) To determine the dominant mechanisms affecting the recovery and upgrading of oil in the methods examined by analyzing experimental and numerical results.

6) To perform the up-scaling and to estimate the feasibility of the method applied to the reservoir, to identify the ways to optimize the method, based on the result of the simulations.

7) To demonstrate the efficiency of the chosen method and higher oil production of the target oil field taking into account the existing field development system.

1.3 Outline of the Thesis

This thesis has been organized into eight chapters and has 63 figures and 22 tables. Chapter 1 gives a brief introduction to the research topic. Chapter 2 presents a literature review on main enhanced recovery techniques with a focus on thermal methods, relevant definitions for this thesis, examples of field applications, and some previous work in the related area. Chapter 3 summarizes the main objectives of the thesis. Chapter 4 focuses on hot water flooding: experiments on modified HPRTO and MPCT setups, and their further numerical simulation. An “aquathermolysis” kinetic model was adapted from the steam injection process and implemented to the numerical model of HWI for the first time. The data obtained during this research, such as cementation technology, fluid model, history matched relative permeability curves, kinetic model, and optimized operational parameters are crucial during further field-scale modeling. Chapter 5 presents another case study of the hot water injection (HWI) process on a field scale in an unconventional reservoir, describes some drawbacks of the existing commercial software,

and offers a new methodological approach to solve some problems encountered during the simulation. The importance of the detailed OM distribution is described and the inability of the software to set a few different mobile liquid phases of hydrocarbons with different parameters was challenged. Chapter 6 is devoted to air injection-based methods, such as HPAI. Consequent experimental tests (HPRTO, MPCT) were conducted to estimate the method efficiency in the Kirsanovsk oil field. Further, these tests were recreated numerically and validated against experimental results. A comprehensive formulation of the numerical model that is capable of reproducing the major phenomenological effects observed during MPCT tests was introduced into the numerical model. This chapter also introduces the problem of upscaling kinetics for field-scale simulation and takes into account the areal heterogeneity, displacement effectivity due to low air injectivity, convergence difficulties caused by high-residual oil saturation, and high critical water saturation in the same grid block. The feasibility of HPAI projects was considered to predict the method's potential. Chapter 7 is devoted to unique forward and reverse combustion experiments conducted on HPCT equipment. The analysis of exclusive data for reverse combustion that was not available before under reservoir conditions. Conditions, where the application of reverse combustion becomes favorable, were described. The subsequent numerical simulation of forward combustion was studied in this chapter too. Chapter 8 draw conclusions of the research conducted and suggest some directions for further work.

Chapter 2. Literature review

2.1 Petroleum classification

Resources can be subdivided into three main classes such as reserves, contingent, and prospective resources. Generally, reserves are the quantities of petroleum that are expected to be recovered with some level of uncertainty. There is a strong need to keep track of such factors as economical/field project feasibilities, proven geology, and status of the commercial projects. The uncertainty depends on the reliability of the geological, engineering data, financial, political, and contractual situation in the petroleum industry. According to (Martinez and McMichael, 1998) reserves can be classified as proved and unproved. Proved reserves can be sub-divided into probable and possible reserves, where the possible reserves have the highest level of uncertainty. Proved reserves include developed and undeveloped, while developed reserves can be producing and nonproducing.

Crude oil can be classified according to its API (American Petroleum Institute) gravity. Crude oil can be identified as Heavy Oil (HO) and Light Oil (LO). LO is characterized by low density, low viscosity, high API gravity. HO, in its turn, has a higher density, higher viscosity, and lower API gravity. The heavy oil is defined as having a gravity of lower than 20° API and the oil with 10.0° API is considered as extra heavy. However, the API gravity does not fully reflect the flow properties, which can be better represented by the oil viscosity. There is also the term “bitumen” closely associated with heavy oil that has an API gravity less than 10°, but it represents the heavier part of the heavy oil spectrum. The term “tar sand” used in the literature describes a naturally occurring viscous mixture heavier than pentane with sulfur compounds and it cannot be recovered at an economically profitable rate. It should be noted, that similarly to tar sands, heavy oil consists of asphaltenes, sulfur, and metal content. Content of asphaltenes in heavy oil reservoirs such as Athabasca or Cold Lake (the heaviest part that can be separated by precipitation using paraffinic hydrocarbons) can be 10-100 times higher in comparison with conventional reservoirs. (Briggs et al., 2007)

2.2 Types of oil production

The production of conventional crude oil can generally be divided into the following stages: primary, secondary, and tertiary (see Figure 2). Primary recovery is a process where oil recovery takes place due to the natural pressure of the reservoir. In secondary recovery, the pressure is provided by injecting water or gas into the formation. (McGlade et al., 2018).

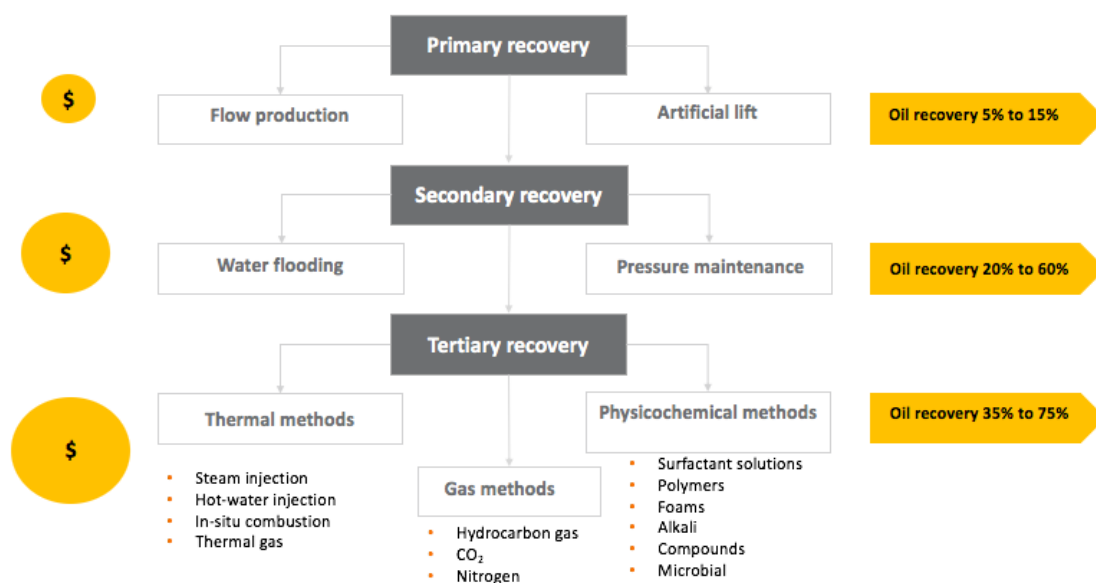


Figure 2. Recovery methods. *Source: www.scmdaleel.com*

The natural drive stage and secondary methods together recover up to 30% of the oil (R W Bentley, 2002; Pu, W. et al., 2019; Thomas, S., 2008), with 70% remaining in the ground. As a consequence, when it comes to unconventional reservoirs, neither primary nor secondary recovery method can be applicable (Speight G.J., 2016; Speight, 2013; Terry, R.E., 2001). The way to reverse the decline of recovery and increase of recovery indicators can be found in the implementation of EOR methods. Their development requires a suitable EOR method based on comprehensive studies, including physical and numerical modeling on reliable experimental data and modern software, as well as pilot tests on representative sites of the reservoir (Fadaei, H. et al., 2010; Shojaepour, M. et al., 2014; Taber, J. J. and Martin, F. D., 1983). Figure 2 presents the

main classes of EOR technologies with a tendency to increase the recovery factor, as well as a number of capital investments from primary to tertiary recovery methods. Tertiary methods of recovery can be classified as thermal, gas injection, chemical, and hybrid methods. (Alvarado and Manrique, 2010; Terry, R.E., 2001). Nevertheless, thermal methods account for almost 50% of the world's EOR- based output, while gas and chemical methods have 45% and 5% of the share, respectively.

There is a steady growth of interest and a number of investments in EOR methods. The main aim is to develop and implement innovative solutions to improve the efficiency of the unconventional reserves (Kamari and Mohammadi, 2014; Terry, R.E., 2001) According to one estimate (McGlade et al., 2018), there are approximately 375 EOR projects currently operating globally, accounting for over 2 mb/d of oil (see Figure 3). The share of global crude production using EOR methods has remained stable over time accounting for 2% of global oil production. However, the geography of EOR production has changed in recent years since several countries (Malaysia, United Arab Emirates, Kuwait, etc.) have started some pilot projects with the application of EOR methods. It also should be noted, that about 15 offshore projects have been started, mainly by natural gas injection. (McGlade et al., 2018)

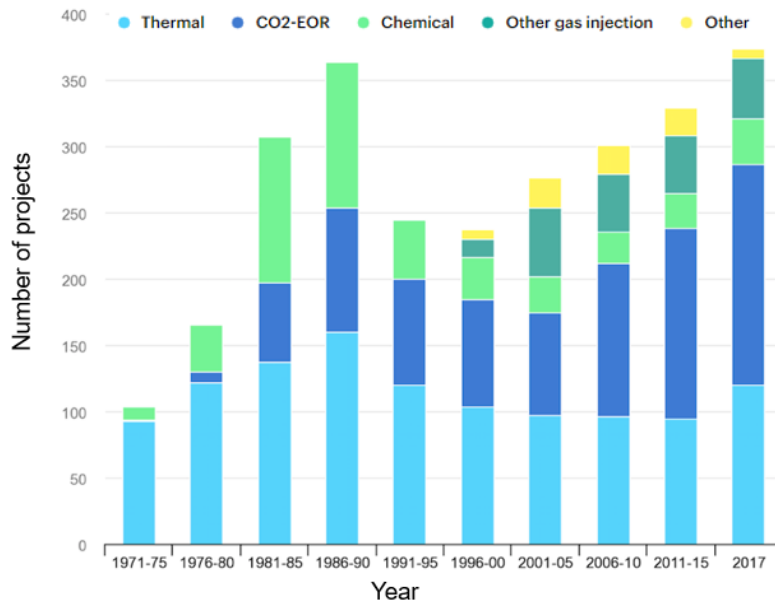


Figure 3. Number of EOR projects in operation globally (McGlade et al., 2018)

While the lifecycle cost of EOR can be competitive with other production techniques, it is often associated with high capital investment and long pay-back periods. Thus, before choosing the method there is a list of checkpoints that should be considered. The EOR technique selected must be carefully examined taking into account all the reservoir's properties (Jha, B. and Verkoczy K. N., 1985) and the feasibility of the project (Dickson, J. L. et al., 2011) must be ensured.

The driving factors affecting the choice of EOR technologies or screening criteria are listed in the table (see Table 1), and include the physicochemical properties of oil such as gravity and viscosity, and injectant availability (Surguchev, L.M. et al., 2010; Taber, J. J. and Martin, F. D., 1983).

Table 1. Screening criteria for the EOR method (World Energy Outlook, International Energy Agency).

Type of EOR	Reservoir type	Oil Gravity API	Depth (ft)	Permeability (mD)	Temperature (°C)
CO ₂ –EOR	Sandstone or carbonate	>25	>2000	NC	NC
Hydrocarbon	Sandstone or carbonate	>35	>4000	NC	NC
Nitrogen injection	Sandstone or carbonate	>35	>4000	NC	NC
ASP flooding	Sandstone	>20 up to 35	>9000	>10 up to 450	<93 up to 26
Surfactant EOR	Sandstone	>20 up to 35	>9000	>10 up to 450	<93 up to 26
Polymer Flooding	Sandstone	20-35	5000-6000	500-5000	>93 to 60
Steam injection	High porosity Sandstone	>8 to 13.5	1500 to <4500	>200 to 2540	NC
In-situ	High porosity Sandstone	>10 to 16	3500 to <11500	>50	>37 to 57
SAGD		7 to 11		NC	NC

The choice of the EOR method for a particular project depends on these parameters (Dickson, J. L. et al., 2011). The efficiency of certain methods can overlap (see Figure 4) for the range of similar input parameters. Thus, the screening of the

projects and the choice of best fit is a challenging task. As was already mentioned, the implementation of EOR methods requires high capital investment, and is time and labor-intensive (Taber, J. J. and Martin, F. D., 1983). The prior appropriate planning, which includes technical, and economic screening, modeling, and engineering design are essential steps (see Figure 4), that can help in the success of the project.

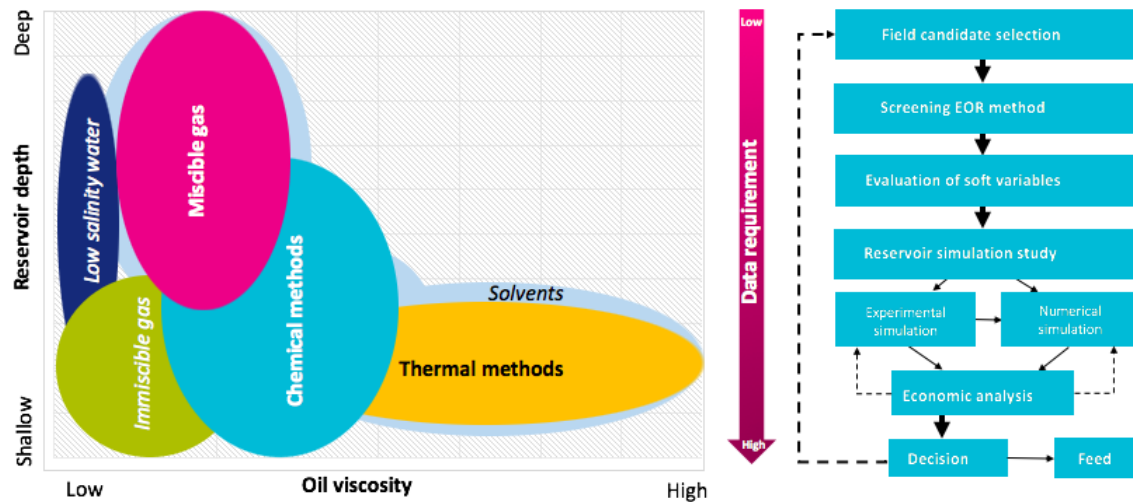


Figure 4. Screening criteria for EOR methods and methodology of its application. *Source: Enhanced oil recovery Shell*

Improvement of existing methods of EOR, their systematic adaptation, and utilization across the world can potentially unlock up to 300 billion barrels (bbl) of oil. In reality, only a fraction of this potential is being exploited and the growth in EOR production is rather modest. Several measures and initiatives are required to increase the contribution of EOR techniques.

2.3 Thermal EOR methods

Thermal EOR methods are the most widely applied and well-studied techniques (Belgrave et al., 1993; Gutiérrez, D. et al., 2012; Kim, T.W. and Kovscek, 2017). These methods provide almost half of the enhanced oil production globally and they are believed to be very promising. All of them are based on the heating mechanism as the heat supplied reduces the oil viscosity. (Bousaid, I.S. and Ramey, H.J., 1968; Kapadia, P.R. et al., 2010, 2009) The classification depends on the mechanism of heat generation

in the reservoir. Thermal processes generally can be divided into the categories of hot water injection (HWI), steam injection, and ISC (Pwaga et al., 2010; Terry, R.E., 2001).

2.3.1 Hot water injection

In HWI a significant amount of hot water is injected into the wells to reduce the heavy oil viscosity and subsequently displace the oil more easily towards oil production wells (Alajmi, A. F. et al., 2009; Pwaga et al., 2010). HWI has some drawbacks in comparison with steam EOR such as lower transport capacity, heat losses in transport, and displacement efficiency. HWI might be a preferable option in deep reservoirs where high injection pressure is needed and delivery of high-quality steam is not possible (Terry, R.E., 2001). Among several thermal methods, the HWI method is a less expensive process, it requires a lower investment and lower levels of heat in comparison with steam injection (Alajmi, A. F. et al., 2009; Pwaga et al., 2010; Rego, F. B. et al., 2017; Sola, B.S. and Rashidi, F., 2008; Terry, R.E., 2001). However, the design of steam and HWI projects requires estimation of casing temperatures and wellbore heat losses, by using methods of determining the overall heat transfer coefficient from the process variables (Stone, T. W. et al., 2013).

Several factors must be considered during the water flooding process. Generally, during water flooding, higher pressure is maintained such that oil is swept towards the production end. This pressure in the reservoir causes stress redistribution and higher stress near the wellbore (material damage and permeability change). The pore structure of reservoir rocks can change after long-term water flooding due to the physical and chemical action of fluid and rocks, which will affect the displacement. Also, relative permeability can be changed due to the varying formation temperature. (Hao et al., 2016)

The wettability of the porous media affects the placement of the fluids in the porous media and relative permeability. It can be affected by various factors such as aging time between the fluids and the rock surface, surface heterogeneity, roughness, and mineralogy of the rock surfaces, the composition of the brine and crude oils. It determines the oil recovery factor and relative permeability curves. It can be explained by

fluid-fluid and fluid-rock interactions that, in their turn, control rock wettability, capillary pressure, and relative permeability curves (Ehlim, E.O. and Orisa, E.F., 2018).

It is shown that as wettability changes from oil-wet to water-wet, oil recovery and relative permeability to oil increases because the wetting phase adheres to the reservoir rock while the non-wetting phase moves freely. Because the impact of wettability extends from pore scale to reservoir scale, wettability can affect the project economics. Through the parameters S_{wi} and S_{or} , wettability influences oil recovery. In addition, the relative permeabilities of oil and water vary with formation wettability. (Abdallah et al., 2007).

One of the most important aspects of thermal EOR methods is to take into account the extent of chemical transformations from reactants to products, e.g., how fast do the chemical reactions occur and how much of the reactant is used. These chemical transformations cannot be neglected, particularly at temperatures higher than 235°C (Kapadia, P.R. et al., 2012). There are several reaction schemes for aquathermolysis published in the literature (Belgrave et al., 1993; Clark, P. D. et al., 1987; S. Guangshou et al., 2009; Hyne et al., 1982; Lamoureux-Var, V. and Lorant, F., 2005; Moore, R. G. et al., 1996; Tamanyan, B.P., 2015) describing different features such as an “aquathermolysis window” in the ranges of 170-300°C; bitumen decomposition where reservoir minerals act as catalysts, etc. (Kapadia, P.R. et al., 2012). The special term, aquathermolysis, describes chemical reactions occurring during steam or HWI in the presence of certain reservoir minerals such as calcite, dolomite, etc. (Fan, 2003; Hyne et al., 1982).

2.3.2 Steam injection

Steam injection (Alvarado and Manrique, 2010) has a long history and nowadays, it is the most widely used and advanced thermal EOR method. Steam is generated on the surface and is pushed down along the injection wells, into the reservoir under high pressure. When steam enters the reservoir, the temperature of the formation significantly increases and the oil viscosity is reduced accordingly. Such mechanisms as thermal expansion of the oil and reduction in capillary forces, also result in additional oil

recovery. However, along the reservoir, as the steam cools down and condenses, the lighter hydrocarbons are vaporized or turned into gases by hot water. With time, the gases cool down, as they move ahead of the steam and condense back to the oil. These phenomena give additional gas drive and are called steam stripping (Pwaga et al., 2010; Speight G.J., 2016; Terry, R.E., 2001). However, in deep and thin reservoirs steam injection faces difficulties due to overburden heat losses (Rego, F. B. et al., 2017).

There is a modification of the steam injection technique called “Huff-and-Puff” or CCS. In this case, steam is injected into a well with alternate “soak” periods. The oil is produced from the same well where the steam was injected (Pwaga et al., 2010). Steam flooding has advantages such as controllability of the process due to low operating temperatures and the absence of environmentally unwanted gases. However, there is a need for a considerable amount of high-quality hot water and steam generators. (Pwaga et al., 2010).

2.3.3 Steam-Assisted Gravity Drainage

The concept of using continuous heating and production as well as advanced horizontal drilling technology served as the basis for the development of SAGD (Speight, 2013). It was initially proposed by (Butler, R.M., 2004) and was developed in Canada for deposits with immobile bitumen. This method requires horizontal injector/producer well pairs that are drilled about 400 meters beneath the surface. Low-pressure steam is injected continuously to the upper well of two horizontal and it creates a steam chamber. This chamber heats the highly-viscous bitumen and mobilizes the oil towards the lower well which then pumps it to the surface.

The key benefits of the SAGD process are an improved steam-to-oil ratio and high ultimate oil recovery (up to 60-70%). Additionally, SAGD has advantages such as reduced environmental footprint, scalability, and a possibility to improve the recovery rates and energy efficiency at a lower cost. This process is stable since the process zone grows only due to gravity segregation. Also, it allows such pressure-driven instabilities as channeling, conning, and fracturing to be avoided. However, the cost of the heat, the heat losses, and the deceleration of lateral growth are the major constraints. In terms of

thermal effect, SAGD is highly likely to be twice as efficient as CSS for reasonably thick deposits. There are several variations of the SAGD process described in (Speight, 2019)

2.3.4 HPAI

HPAI is one of the thermal production methods with a possibility of reducing the production cost since the process is without steam and water cycling (Yoshioka et al., 2017; Ursenbach et al., 2010) particularly in the case of light oils in deep, thin, high-pressure, low permeability fields, where other EOR methods are not profitable. (Gutiérrez et al., 2008; Montes et al., 2018; Moore, R. G. et al., 1996; Sutherland, R. B. et al., 2007). Compressed air is injected into a high gravity, high-pressure reservoir in the HPAI process to mobilize the oil and increase the sweep efficiency. The process is governed by the combustion kinetics initiated by the spontaneous ignition of injected air. (Yoshioka et al., 2017) The compressed air reacts with some fraction of oil in place acting as fuel at high-temperatures and high-pressures. In cases when the oil is not reactive enough for spontaneous ignition, it might be supported by the injection of a special chemical mixture or by the use of a downhole heater. (Moore, R. G. et al., 1996; Sutherland, R. B. et al., 2007) It has such advantages as a high recovery coefficient, less energy, and less water consumption for oil production. Some of the oil is consumed to provide heat. (Yoshioka et al., 2017).

The growing interest in HPAI is dictated by the increase in oil demand, as well as the economic success of HPAI projects within the last few decades. There is a list of successful projects at various types of reservoirs, and companies started to investigate the applicability of this process both on their onshore and offshore fields. (Gutiérrez et al., 2008; Ismail et al., 2016; Moore, R.G. et al., 2007a; Sutherland, R. B. et al., 2007)

A few key factors affect the overall performance of HPAI project design such as air compressors, screening of the prospects, laboratory screening of candidate reservoirs, numerical modeling, etc. The increase in the recovery coefficient can be achieved only by employing good quality experimental data, numerical studies, and history matching on the samples of the target field to avoid any uncertainties. Despite the wide availability of the published literature, the behavior of oxidation kinetics, the nature of the fuel for

combustion kinetics, and the importance of thermal effects are still subject of numerous studies (Barzin et al., 2010; Gutiérrez et al., 2008; Khakimova et al., 2020; Montes et al., 2018).

2.3.5 In-situ combustion

In the ISC method, the injected air initiates combustion, the combustion front generates the energy and moves towards the production well mobilizing the heavy oil. Sometimes a special heater in the well is required to ignite the oil in the reservoir, in case it is not reactive enough. (Bousaid, I.S. and Ramey, H.J., 1968; Gutiérrez, D. et al., 2012; Gutiérrez et al., 2012; Kisler, J. P. and Shallcross, D. C., 1997; Mallory et al., 2018; Moore, R. G. et al., 1996; Moore, R.G. et al., 2007a; Rodriguez et al., 2012; Xu, H. H. et al., 2001; Yang, M. et al., 2017; Yang, X. and Gates, I. D., 2009; Yang and Chen, Z., 2016). Several factors influence the performance of ISC such as the quantity of initial oil in the rock, the quantity of air required to burn the portion of the oil, the distance where combustion can be sustained without great heat losses, and the mobility of the air.

Although this method was extensively studied and is believed to be promising, there are still unresolved problems with the kinetics of the reactions, controllability of the process, and prediction of the correct operational parameters. Planning and management of thermal EOR processes are conducted extensively using commercial reservoir simulators. Numerical simulations are highly valuable since they can help to assess the applicability of the method in different scenarios and conduct the optimization measures in the numerical simulator. There are some studies (Bousaid, I.S. and Ramey, H.J., 1968; Burger, 1978; Hayashitani et al., 1978) reporting that three major reactions occur during ISC: Thermal Cracking, High-Temperature Oxidation (HTO), and Low-Temperature Oxidation (LTO) (Belgrave et al., 1993; Gates C.F. and Ramey H.J., 1980; Moore, R. G. et al., 1996; Moore, R.G. et al., 2007b; Yang and Chen, Z., 2016).

2.3.5.1 Forward combustion

During forward combustion, the combustion zone moves towards the production well in the same direction as the airflow (Kristensen et al., 2006). In the first step, the crude oil near the wellbore needs to be ignited using gas burners, electrical heaters, using

chemical agents, or steam injections. After that, continuous air injection leads to the movement of the combustion front towards the production wells. Ideally, it results in the almost complete removal of all reservoir liquids from the swept zone (leaving behind a hot, clean rock) (Reed and Tracht, 1960). Sometimes, ignition can occur spontaneously if the temperature in the reservoir is high enough and the oil is reasonably reactive (Bhattacharya et al., 2016; Fassihi et al., 1984).

Forward combustion can be divided into “dry” and “wet” categories. It is called “Dry” (or O₂-enriched combustion) when only air (or enriched air) is injected. The concept “wet” describes the situation when air and water are co-injected.

Wet combustion can be classified as incomplete, normal, and quenched. During incomplete combustion, water is converted into superheated steam with only partial heat recovery from the burning zone. Normal combustion is a process during which all the heat is recovered. In turn, during quenched/super wet combustion the front temperature falls due to the temperature of the injected materials.

2.3.5.2 Reverse combustion

Reverse combustion is a method, which also can be used for the production of oil that has high viscosity. Air is introduced into the injection well while the ignition takes place in the production well. The combustion zone that is created moves away toward the injection well, in the opposite direction from the airflow (Perry et al., 1960; Speight G.J., 2016; Speight, 2013, 2019; Stosur, 1977). Two dependent parameters that are important in terms of defining the progress of the combustion process are the maximum temperature achieved within the combustion zone and the front velocity (Berry and Parrish, n.d.; Warren.J.E. et al., 1960). They can provide insights into recovery efficiency, oil, and gas production rates, and average air requirements.

A few drawbacks of reverse combustion limit its application. The first is the probability of spontaneous ignition (Dietz and Weijdema, 1968). In the case of spontaneous ignition near the injector, the oxygen would be consumed and the process would revert to forward combustion. To avoid the spontaneous ignition near the injector the reservoir should be preheated before the air injection (Burger, 1978; Elkins et al.,

1974; Tadema and Wiejdema, 1970). Secondly, reverse combustion can be often unstable with narrow combustion channels and resulting in a poor burn (Gunn and Krantz, 1987, 1980; Johnson L A et al., 1978). However, the main issue is the lack of new experimental studies on reverse combustion within the last few decades despite the improvements in the technologies. Nevertheless, the successful application of reverse combustion is possible with desired air permeability, oil saturation, and a sufficient rate of reaction (Perry et al., 1960; Reed and Tracht, 1960). It might be applicable for very heavy oils of gravity 5-20° API at very low reservoir temperatures due to the slow spontaneous ignition of up to several years (Stosur, 1977). Another favorable condition for reverse combustion can be low effective permeability that helps to minimize the plugging of the reservoir by the mobilized fluids (Speight, 2013). Reverse combustion plays an important role in coal and tar sands since it can develop highly-permeable paths between production and injection wells where, at the second stage, forward combustion can be used (Gunn and Krantz, 1980).

2.4 Thermal EOR projects

As was already mentioned, every reservoir can be worked either from its natural energy or, with the application of secondary and tertiary methods of oil recovery. The choice of method is a complex task where production should be optimized from the point of view of cost effectiveness. A suitable reservoir should be selected based on the reservoir characteristics. (Wu and Liu, 2019)

2.4.1 Projects with hot water and steam flooding

2.4.1.1 HWI and steam flooding

HWI can lead to an ultimate oil recovery greatly exceeding the cold-water flood values. However, it can have a drawback such as lower maximum energy injection rates compared to steam injection, due to the higher energy content in saturated steam vapor. The laboratory experiments demonstrated, that a steam flood following a hot water flood recovered more oil than a steam injection alone. (Alajmi, A. F. et al., 2009; Hong, 1987; Shen, 1989).

The paper (Dornan, 1990) discusses the application of hot water flood after steam flooding in the Kern field, California. The switch to HWI was considered since there was a problem with a steam override. The steam and reservoir fluids had different densities that led to gravity segregation. The reservoir rock and fluid properties prevented the formation of an effective displacement bank. The oil resaturation took place in the areas where water filled the steam swept zones. Also, HWI was insufficient at transferring heat to the lower portions of the reservoirs. The reduction of steam injection volumes was required from an economic perspective. However, HWI was ineffective at transferring heat to certain areas of the reservoir. Authors (Messner and Stalling, 1990) demonstrated a dual injection of hot water and steam in the same field. Both methods showed a favorable production behavior. The project was considered as a low to mid-quality (10-40%) steam flooding where the introduction of HWI after steam flood led to several benefits. The main impact was due to the heat transfer between the tubing and the annulus. (Bousaid, 1991) carried out lab experiments to understand the effect of variation of injection rate both for HWI and steam flooding on the oil samples of the previously mentioned reservoir. The results showed, that HWI produces effective oil mobilization above a specific temperature and at higher injection rates; the heat moved further and oil mobility was improved. The oil response and recovery at steam breakthrough increased when the steam rate also was increased. A paper (Goodyear et al., 1996) discusses the possibility of HWI application compared to cold water injection on a North Sea reservoir with viscous oils and high permeability sands. The numerical simulations discovered that HWI into a reservoir with 400 cp oil with underlying water can lead to 18% of OIIP in comparison to cold water injection.

A paper by (Pederson and Sitorus, 2001) proposed using the geothermal reservoir water into an oil reservoir to reduce the cost associated with HWI projects in the fields with shallow, high viscosity waxy oil formations and deeper water-bearing formations with relatively low salt concentrations. The field simulation study showed that incremental recovery can be increased by up to 7.5% compared to cold water injection. The paper (Bhat and Kovscek, 1998) described a problem of an increase in permeability

and clogging due to silica dissolution and redistribution. The authors performed a permeability alteration in the modeling and found a relationship describing the changes in permeability as a function of the porosity changes. Permeability change affects the networks with low connectivity or small pore throats that are connected to relatively large bodies dramatically. (Kovscek et al., 2000) suggested considering the role of rock compression during HWI into diatomite reservoirs. HWI also can be used to improve the wettability of oil-wet reservoirs as described in (Al-Hadhrami, H. S. and Blunt, M.J., 2001) in the example of oil-wet fractured carbonate reservoir in Oman with 30% oil recovery over 700 days against the current 2% of oil recovery after 20 years of production. These results are due to a favorable mobility ratio and wettability alteration (Tang and Kovscek, 2008).

There is a project of HWI proposed by (Cassinat et al., 2002) in the Senex field in Alberta, Canada, to overcome the effect of viscosity and permeability reduction due to paraffin deposition. The results demonstrated a 25% increase in oil recovery. The HWI also can be enhanced by the simultaneous injection of chemicals.

The paper (Adams, R.H. and Khan, 1969) describes the drilling in the Tar pool started in 1924, in the Huntington Beach oil fields in California where oil had a 12° API gravity. Initially, the primary development was implemented and then a cyclic steam stimulation pilot project was introduced in 1964. The steam drive was more effective taking into account the crude oil characteristics. The best results depend on the optimum soak and injection periods. Another example of the cyclic steam injection application in the Santa Barbara field, Eastern Venezuela is shown in the paper (Bowman, C.H. and Gilbert S., 1969). This field is accepted as a “California-type” and demonstrated a superior response to steam stimulation than the typical domestic projects showed. (Adams, R.H. and Khan, 1969)

An example of steam injection project in diatomite with heavy oil (~12° API) collected in the South Belridge Field, Kern Country, California was presented in (Murer, A.S. et al., 2000). As a result, the oil was mobilized and steam injection showed itself to

be a promising method for heavy oil diatomite or other shallow heavy oil reservoirs with high porosity and low permeability.

Some objectives that should be addressed in the implementation of steam injection processes such as steam optimization, are the steam breakthrough at the producers, and the development and maintenance of effective monitoring programs. (Castrup, 2019) Also, the presence of chemical conversions of hydrocarbons and their transformations should be taken into account. For example, the paper by (Kapadia *et al.*, 2012) describes how significant are the chemical reactions on the growth of the SAGD steam chamber and introduces the aquathermolysis reactions. This is due to the product gases such as hydrogen sulfide, methane, and hydrogen gas identified by gas chromatography. (Hyne *et al.*, 1982; Kapadia *et al.*, 2012).

2.4.1.2 Supercritical water injection

The conventional method for oil shale processing is mining with further surface retorting. However, since the middle of the 20th century, significant theoretical and experimental modeling has been performed by world-leading scientific groups to develop *in-situ* retorting methods successfully on a commercial scale. The research resulted in Shell ICP (Ryan *et al.*, 2010), Exxon Mobil Electrofrac (Symington *et al.*, 2010), Total CCR (Burnham *et al.*, 2010), Chevron CRUSH (Crawford and Killen, 2010), and development of many other technologies. The most promising results of subsurface organic matter transformation today show the *in-situ* conversion process (Meijssen *et al.*, 2014) and high-pressure air injection (Gutierrez *et al.*, 2007; Kokorev *et al.*, 2014), but even these technologies do not satisfy existing economic and safety requirements.

Subcritical and supercritical ($T > 374^{\circ}\text{C}$, $P > 22 \text{ MPa}$) water injection in oil shale deposits is a promising technology to deliver sufficient enthalpy to generate liquid hydrocarbons *in-situ* and develop deep (2-3 km) unconventional reservoirs (Popov *et al.*, 2017; Sun *et al.*, 2019). At high temperatures, water's ability to solvate organic compounds of various polarities is comparable to organic solvents – acetone, toluene, and benzene (Luong *et al.*, 2015). Low values of the self-ionization constant in such conditions make water a powerful acid-base catalyst (Siskin and Katritzky, 2001).

Ultimately, a pilot project of in situ oil shale extraction by subcritical water is under development in Jilin Province, China (Sun et al., 2019).

Hydrous pyrolysis or pyrolysis in the presence of water was first used by (Lewan et al., 1979) to describe oil-generation kinetics of source rocks. It was showed that in the case of type II kerogen, hydrous pyrolysis water promotes thermal cracking reactions and inhibits carbon-carbon bond cross-linking in comparison with anhydrous conditions. It was shown that pyrolysates collected from the water surface at the end of the experiment have a SARA composition close to natural petroleum (Lewan, 1997). Comparative analysis of type III kerogen pyrolysis in open-system, closed-system anhydrous, and hydrous conditions showed that maximum hydrocarbon gas yield was observed in open-system conditions, and a minimum one in closed-system hydrous pyrolysis. Liquid hydrocarbons' yield was maximum in open-system and closed-system hydrous pyrolysis, whereas it was three times lower in closed-system anhydrous conditions. The observed result was attributed to the extra high yield of aromatic and polar compounds in comparison with closed-system anhydrous pyrolysis (F. Behar et al., 2003).

Many numerical modeling studies are devoted to development of *in-situ* retorting simulation procedure: acceleration of simulations using fast upscaled dynamic models (Alpak and Vink, 2018), parameter space reduction and sensitivity analysis (Bauman and Deo, 2011), estimation of reaction parameters using inverse modeling (Lee et al., 2018a), simulation with fully coupled thermal-hydraulic-mechanical properties (Wang, 2017), application of various operator splitting techniques (Maes et al., 2016), and different kinetic models and heat delivery methods application (Lee et al., 2018b, 2017; Youtsos et al., 2013).

However, to specify the optimal *in-situ* oil shale retorting conditions and predict quantity and quality of produced hydrocarbons, it is important to obtain a reliable kinetic model of specific oil shale organic matter transformation; account for porosity, permeability, and evolution of geo-mechanical properties during *in-situ* retorting.

2.4.2 HPAI and ISC projects

HPAI and ISC are similar in many ways, but ISC is targeted toward heavy oil reservoirs. It means that the knowledge about the ISC process is valuable and adaptable to the application of HPAI, and the kinetic models and fluid phase behavior require further attention. (Barzin et al., 2013)

The paper by (Erickson, A. et al., 1993) presents a performance of a few quite large HPAI projects compared with other conventional alternatives. HPAI proved itself as a more viable alternative on deeper, low permeability reservoirs that are too tight for HWI. There are several successful HPAI field pilots in deep light-oil reservoirs with low permeability, high reservoir temperature, high reservoir pressure, low oil density and viscosity. One of the successful examples of the application of HPAI is a pilot project in the Buffalo field, Southern slope of the Williston basin, South Dakota, USA. (Gutiérrez et al., 2008; Moore, R.G. et al., 2007a). According to the results (Glandt et al., 1999) of South Buffalo, Red River Unit, production rates double the initial values obtained by primary recovery. HPAI was also successfully implemented in 1980 in the Coral Creek field (CCF) (Glandt et al., 1999). It was accepted as an ideal candidate for application of HPAI due to its size and relatively low water-cut of 70%. The field is a low-permeability, non-fractured, porous carbonate that has a 30-40% residual oil after waterflood. Field AOR values for Medicine Pole Hills and South Buffalo are 7 and 14 Mscf/stb, respectively. The work presented in (Watts and Hall, 1997) presents laboratory experiments conducted to obtain the kinetic model and a few numerical simulations on the samples from Horse Creek field, Bowman County, North Dakota. ARC and combustion tube results provided the kinetic parameters and indicated the applicability potential of the HPAI process. The economic feasibility of HPAI in Medicine Pole Hills Unit, North Dakota and West Hackberry, LA is discussed in a paper (Fassihi et al., 1996). They proved themselves to be economically and technically viable even at low oil prices. Capital spending has the greatest effect on the results. (Moore, R.G. et al., 2007a) demonstrates the strategies for successful design and application of air-injection based methods, with a focus on differences between air injection in light and heavy reservoirs.

Although the ISC process has a long history and it has been on the stage for more than a century, it is also one of the most complex and high-risk. (Ismail et al., 2016) However, there are four major and long-term ISC projects including Bellevue (USA), Suplacu de Barcau (Romania), Balol, and Santhal (India) that have proved successful. The number of current running ISC projects in the United States has reached seven, while six of them produce from the carbonate reservoirs. The following projects are examples of combustion projects.

The first example is a double displacement process on West Hackberry at a 2280-2740 m depth. This field has a porosity in the range of 24-28%, permeability 300-1000 mD, and 9 m net pay. The oil sample has a 33° API gravity and its viscosity is 0.9 cp. The ultimate recovery factor, in this case, was increased from 50-60% to 90%. Wet combustion was implemented after waterflooding at AMOCO's Sloss Field project at a 1890 m depth. The porosity of this field was 19.3%, permeability 191 mD, and net pay 4.4 m. Oil saturation after waterflooding was in the range of 20-40%. The oil had a 38.8° API gravity and a viscosity of 0.8 cp. Results of an initial five-spot (40 ac) pilot were sufficiently encouraging to warrant expansion. A full-scale tertiary wet combustion project was undertaken from 1967 to 1971. The main challenges and issues that were faced: 1) low oil saturation after waterflood; 2) emulsions brought on by corrosion products; 3) lateral and vertical permeability anisotropy resulting in poor volumetric sweep efficiency (14%); 4) low crude prices. In the pilot and expansion areas, 32% and 11% of the remaining oil after waterflood was recovered by air injection. Thus, the process is unaffected by high water saturation, as would be the case with steam injection. It has a high displacement efficiency and significant incremental oil recovery can be achieved after water-drive. (Belgrave, 2019).

BP Canada's Wolf Lake Air Injection Project is an example of CSS followed by ISC. The field belongs to Alberta Oil Sands Deposits. The depth is 450 m, net, and gross pay thickness are 23 m and 34 m, respectively. Porosity is 30%, permeability is 1-3 Darcy, initial oil saturation is 64% with 10° API gravity. The recovery factor was doubled from 15% to 30%. The key observation is that the combustion would propagate only if

the flue gases could flow. There is an initial mobility requirement for oil displacement by combustion. For this particular case, combustion demonstrated a superior displacement efficiency over the steam injection process. Recovery factor increased from 15% to 30% (Belgrave, 2019).

The cyclic *in-situ* combustion is efficient in increasing oil recovery from the oil fields. Also, it has advantages such as a reduction of the sand influx in the unconsolidated formation and upgrading the oil (Belgrave, 2019). An Exxon project on Pleito Creek, California is an example of Cyclic Combustion in San Joaquin Basin, USA. This is a sandstone reservoir, the formation lies at depth 3600-4500 feet, with a thickness of 130 feet. The porosity varies from 25 to 31%. The oil has a 14-18° API gravity. The application of this process resulted in a production increase from 5 b/d to 95 b/d in one well and increased 7.5 times from the pre-stimulation rate in the second well. In both cases, the API gravity was increased (up to 44° API). The degree to which the oil was upgraded shows that thermal cracking plays a significant role. Liners, pulled after cyclic combustion, were found to be plugged with coke. The mechanism of coke generation has to be realistically incorporated in combustion modeling (McGee, R. et al., 2011). Another example is presented in a paper on the oil field Patos-Maranza in Albania, where cyclic ISC also proved to be successful to consolidate the formation sand and significantly increase oil production (Gjini et al., 1999).

In 1994 the Amoco Canada and the Alberta Department of Energy tested “Horizontal Well Cyclic Combustion” in thin heavy oil sands in the Wabasca Area, Alberta. The primary production with horizontal wells was economic for the reservoirs with 14° API gravity. However, the recovery factor was estimated to be only 5-10 % of the original oil in place. The injector was initially preheated with steam and then the air was injected for more than 4 months while the producers were shut-in to pressurize the reservoir. Once the air injection was terminated, production was initiated in the producers. The production response was favorable and oil analysis did not show any problems with upgrade or emulsion. Also, no oxygen breakthrough was observed at the

producers. Thus, the gas drive effects of combustion is an important oil displacement mechanism. (Belgrave, 2019).

The application of ISC to the carbonate reservoir is associated with high complexity due to the reactivity of these reservoirs. The presence of calcite and dolomite also can be associated with such issues as high-temperature decomposition of carbonates, development of fractures, scale deposition, combustion sustainability, etc. (Hascakir and Kovsky, 2014) report an unpredictable and complex behavior of oil-carbonate rock interactions. Also, clay presence might affect the combustion front behavior.

In contrast to forward combustion, a very limited amount of open published literature is available for reverse combustion, with limited insights into the process. The paper by Reed and Tracht (Reed and Tracht, 1960) discusses uncertainties related to the temperature redistribution near the wall due to the short length of their reactor in late 1960. The deficiency in experimental data is another issue that authors have faced. Different conditions under which reverse combustion becomes attractive must be studied as well as its application to the conventional as well as heavy oil fields rather than just in oil sands (Reed and Tracht, 1960). Laboratory experiments on reverse combustion also conducted in 1960 demonstrated much lower oil recovery value (50% of OOIP) compared to that for forward combustion (85-95%). The higher amount of oil consumed as fuel during reverse combustion and the front velocity was relatively slower (Perry et al., 1960).

Another one-dimensional laboratory study was described in the paper (Romanowski L J and Thomas, 1985) in 1985 that was conducted to evaluate reverse combustion application: 1) as a recovery process; 2) as a reservoir preheating technique before steam displacement. Reverse combustion served as an effective preheating method for the tar sand and the development of plugging was avoided. It was possible to increase the combustion temperatures with air flux alterations. Due to the coking of the remaining bitumen very small amount of oil was available for steam-flooding recovery. Low-temperature oxidation (LTO) reactions were dominant which resulted in a low level of carbon oxides, increased H/C ratio, increased water production, and increased oxygen in

the product. The oil produced had increased API gravity values and significantly decreased viscosity (Romanowksi L J and Thomas, 1985). Preheating treatment can be beneficial in the cases when the oil saturation is sufficiently high and the effective permeability is low to avoid reservoir plugging. For example, reverse combustion was applied to the tar sands of the Orinoco deposit and the Athabasca (Speight, 2019).

The paper (Lasaki et al., 1985) performs a field case numerical study of *in-situ* reverse combustion and steam flooding. Experiments were also conducted on oil sands. In this case, reverse combustion shifted to forward mode and served as a preheating procedure before steam injection. The reported oil recovery by reverse combustion was in the range of 2-5% original oil-in-place (OOIP), but recovery was accelerated further. Stable reverse combustion can be achieved by a high-communication path or, for example, in fractures. (Lasaki et al., 1985)

The number of experimental and numerical studies of application of ISC is remarkable both for heavy and light reservoirs for sandstone reservoirs extensively and for carbonate reservoirs. Combustion tube tests are used generally to assess the applicability of the ISC process (Belgrave, J.D.M. et al., 1997; Fadaei et al., 2011; Gutiérrez et al., 2012; Hascakir and Kovscek, 2014; Sibbald, L. et al., 1988). Nevertheless, the creation of an appropriate kinetic model, well patterns, and prediction of field performance remain challenging.

2.5 Conclusions

Any project should be initially evaluated against the performance of similar reservoirs at similar conditions, carefully analyzed, and deeply studied. The preliminary screening process of technology selection for the candidate reservoir includes mainly the reservoir properties. Other parameters that should be considered during decision making are air injectivity, stability, initial oil saturation, etc. The main goal of this study is to conduct a comprehensive experimental and numerical modeling of thermal EOR to select a development methodology on the example of specific reservoirs and to choose the appropriate technique for a particular field.

Chapter 3. Primary objectives

The primary objectives of the thesis are listed below:

1. To construct a numerical model of experimental equipment that is capable of representing the major phenomenological effects.
2. To determine the recovery coefficient in unique HWI experiments in a deep heavy carbonate oil field and evaluate the effect of the temperature on the oil properties, and oil displacement, to implement aquathermolysis reaction and to obtain relative permeability curves, kinetic model, and optimal operational parameters.
3. To conduct sensitivity studies and assess the application of supercritical water injection at an unconventional reservoir, to estimate the extent of chemical transformations, to implement the changes in fluid and matrix properties, viscosity, density, thermal properties, porosity. To determine the effect of the specification of initial matrix saturation with OM and the number of pseudo-components and reactions, taking into account the available computing capacity. To overcome the limitations of existing commercial software such as an inability to set a few different mobile liquid phases of hydrocarbons with different parameters (viscosity-temperature dependence, flowing).
4. To evaluate the feasibility of the HPAI method for carbonate reservoir development, to build and validate the kinetic model. To create a 3D digital model of the combustion tube multilayer design; work of the heaters; reproduction of the processes preceding the air injection to take into account the unique phenomena such as mass-heat transfer taking into account the properties of the medium, convection, heat losses, and secondary reactions. To carry out field-scale modeling using experimental and numerical results, to avoid the risks and uncertainties and optimize the development system.
5. To analyze the results of unique forward and reverse combustion under reservoir conditions and assess their applicability, to distinguish the possible favorable conditions of reverse combustion, and to consider vapor phase combustion.

Chapter 4. Hot water flooding in a carbonate reservoir

Currently, thermal methods of enhanced oil recovery are the most efficient methods in the development of heavy oil reservoirs. This chapter is devoted to the assessment of HWI efficiency to engage in the active development of high-viscosity oil reserves in a deep carbonate reservoir. Oil-bearing formations at depths of 1100–1500 m require technology that can achieve sufficiently high fluid temperature (250-300°C) in the bottom-hole zone to be successful.

The development design of most carbonate reservoirs, described in the literature, is based on the continuum theory. They are highly heterogeneous both laterally and vertically. It is due to the wide variety of environments in which the rocks were deposited and by the susceptibility of the rocks to diagenetic alteration (Jardine and Wilshart, 1982). It is crucial to provide simulation models in the form of the vertical and lateral distribution of the reservoir rock types, reservoir rock characteristics, reservoir continuity, and barriers to flow. Several technologies were developed to improve the production and EOR of carbonate reservoirs such as ultra-deep geophysical description, discrete geology modeling, ultra-deep complex wells, deep large-scale reservoir simulation, water flooding, and gas flooding (Li et al., 2018).

When there is a question of choosing the appropriate thermal method (Belgrave et al., 1993; Gutiérrez, D. et al., 2012; Kim, T.W. and Kovscek, 2017) for a particular field, it is necessary to carefully weigh all the advantages and disadvantages of the options under consideration and conduct the required preliminary screening. The selected EOR technique must fit the reservoir, its rock, and fluid environment (Jha, B. and Verkoczy K. N., 1985) and ensure the feasibility of the project (Dickson, J. L. et al., 2011). The driving factors affecting the choice of EOR technologies or screening criteria are the depth of the reservoir, porosity, permeability, initial oil saturation, properties of the core, physicochemical properties of oil such as gravity and viscosity, and injectant availability (Surguchev, L.M. et al., 2010; Taber, J. J. and Martin, F. D., 1983). Depending on these parameters the injection type and EOR method can be chosen for the particular project (Dickson, J. L. et al., 2011).

For this research, *in-situ* combustion was removed from consideration due to the unfavorable number of existing wells and their relative positions in the field along with, high initial oil saturation and low native oil mobility (Oskouei et al., 2010). On the other hand, the steam injection method was already examined as one of the most promising techniques. However, analytical calculations, trial numerical simulation, and a wide range of publications (Huygen, H.H.A. and Huitt, J. L., 1996; Satter, 1965; Stone, T. W. et al., 2013) indicated that high heat losses might be expected at the targeted depth (1200-1300 m), which corresponds to high pay zone. This method becomes unfeasible at this depth due to the high reservoir pressure (water-steam phase state boundary). Also, steam injection requires expensive casing designs to provide high-quality steam at the bottom hole, as well as ground equipment. Other methods, such as gas and polymer injection were also examined. A detailed description of huff-and-puff CO₂ injection on the same field is presented in the paper by (Shilov et al., 2019) where the recovery factor was 43%. Polymer flooding was rejected due to reported problems with polymer injectivity and economical concerns (Needham, R.B. and Doe, P.H., 1987; Rego, F. B. et al., 2017). Due to these factors, it was decided to further proceed with the HWI method.

The HWI method can be applied for carbonate reservoirs at depths of 1200-1300 m as an alternative to steam injection. Due to the limitations of maximum injected temperatures the hot water flooding also can become inefficient due to heat losses (Rego et al., 2017). Successful implementation of HWI requires the selection of optimal conditions for the injection process, especially the temperature and dynamics of injection and production. The heat exchange process leads to changes in the properties of oil after heat exposure and the composition of the gases produced. The nature and rate of these changes strongly influence the feasibility of the selected method. Thus, for the successful realization of the thermal EOR project, the quantification of these processes is of crucial importance. The most reliable way to achieve this is by performing simulations using both physical and numerical models and these models must be obtained before the design of the pilot works. It is necessary to identify all the uncertainties, determine the optimal parameters, and make a prediction of its applicability to the field under consideration. In

this study, experimental results from the HWI treatment of the naturally consolidated carbonate reservoir rock under *in-situ* conditions were presented. Following the in-depth analysis of the experimental results, the numerical simulation was conducted to history-match the HWI process and associated chemical reactions. The results of this analysis laid down a foundation for further development of the upscaled model for the given heavy oil carbonate reservoir. Consequently, the study was performed in two stages – experimental modeling and numerical modeling.

The following difficulties were revealed during the experimental and numerical modeling:

- The temperatures and pressures for operating this experiment surpass the P-T ratings for most of the common core flooding equipment. In other words, it is difficult to safely replicate the high pressure and temperature (P-T) conditions in a deep carbonate reservoir. The natural permeability and porosity of the system are hard to preserve in the unconsolidated (crushed) core samples packed in the reactor tube.

- Thus, an improved technique for injecting a heat-resistant cement is required that enables the void space between the steel core holder and unconsolidated core samples inside it to be filled, preventing the fluids from bypassing the sample pore space.

- There is no information about relative permeabilities, thus history matching is required to obtain these values.

- The extent of chemical transformations from reactants to products during HWI is not taken into consideration.

The screening was conducted, analytical calculations were performed to evaluate the heat losses along the tube, and preliminary numerical tests were carried out. Experiments of water flooding were designed to determine the recovery coefficient in different injection modes, and to evaluate the effect of the temperature on the oil properties and oil displacement.

4.1 Hot water flooding

4.1.1 Rock samples

The samples for the study were selected from a carbonate reservoir under study: Dome A, Formation F₁; and Dome B, Formations F₂, and F₄ (see Table 2). The distribution of porosity and permeability for a given reservoir is presented in Figure 5. Formation F₁ is 300 meters deeper than formation F₂-F₄. The parameters of the formations are shown in Table 2.

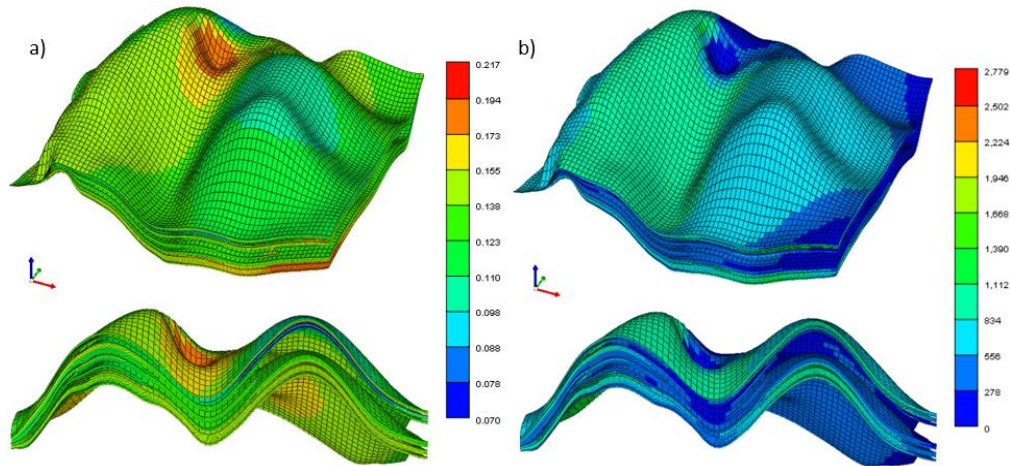


Figure 5. Porosity (a) and permeability (b) distributions for the formations under study

Table 2. Reservoirs and their parameters

Formation	Average porosity, %	Average permeability, mD	Depth, m	Lithology	Core samples diameter	Experiment
F1	13	1410	1400-1450	Carbonate calcite	15-19	Experiment 1
F2	13	1924	1100-1150	Carbonate organogenic-clastic	49-51	Experiment 2
F4	17	993		Carbonate		

- 1) Formation F₁ is composed of 100% carbonate, calcite material.
- 2) Formation F₂ is qualified as a carbonate; limestones consist mainly of calcite (95% -100%) with an admixture of dolomite (7.3% - 42.6%).

3) Formation F₄ is predominantly carbonate and to a much lesser extent clay-carbonate deposit. The F₄ formation consist mainly of calcite (67% -100%) with an admixture of dolomite (0% -32.6%).

A total of 121 full-sized core samples were taken for drilling cylindrical core plugs of 30 and 50 mm in diameter for laboratory tests. Samples were taken based on well log data from sections determined as pay zone and non-pay zone for the application of laboratory analysis data in hydrodynamic modeling.

4.1.2 Oil samples

Each oil sample is a wellhead sample; thus, an oil recombination procedure was required to restore the initial gas content. The obtained oil samples were thoroughly homogenized using an overhead stirrer. The density measurements of the oil samples were carried out on a DMA 4200M laboratory densitometer. Temperature dependencies of oil sample density and viscosity at different pressures are given in Figure 6 and Figure 7, respectively.

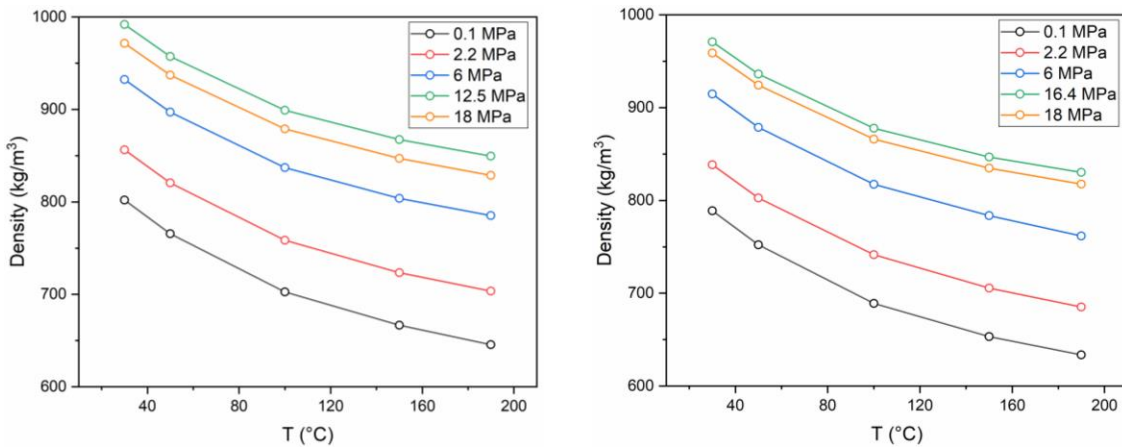


Figure 6. Temperature dependence of the oil sample density at different pressures: Dome A (left) and Dome B (right)

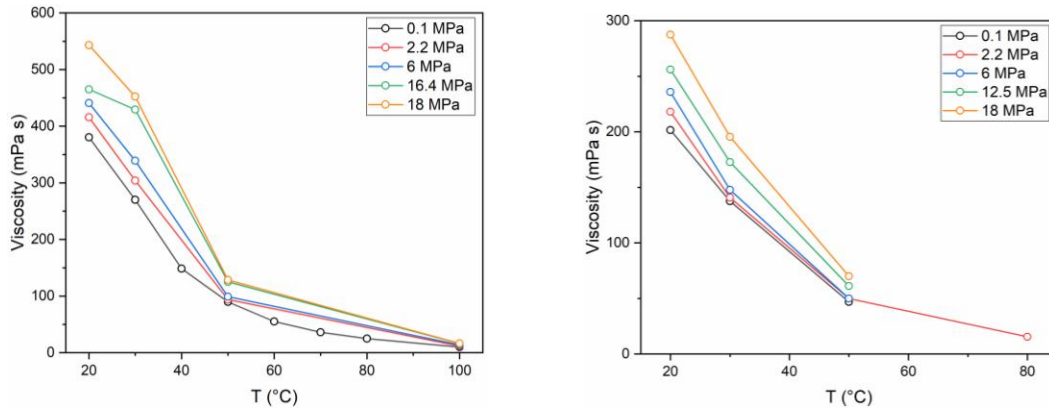


Figure 7. Temperature dependence of oil sample viscosity at different pressures: Dome A (left) and Dome B (right)

Thus, the density and viscosity of oil samples from Dome A and B were measured under wide range thermobaric conditions for their subsequent use in the CMG WinProp simulator and the development of the 3D models of laboratory setups in CMG STARS, for further studies of the possible application of cyclic steam or HWI technology for given reservoirs. As expected, a temperature increase has a greater effect on the viscosity of oils than pressure.

4.1.3 Cementation technology

The temperatures and pressures for operating this experiment surpass the P-T ratings for most of the common core flooding equipment, (e.g. sealing gels and heat shrinkable tubes (Kim and Kovscek, 2017)). Therefore, two hot water flood experiments were performed on two different setups: MPCT and HPRTO. Typically, in these setups, unconsolidated (crushed) core samples are packed in the reactor tube, together with homogenized sand packs (Fadaei et al., 2011), (Pu et al., 2019), due to which natural permeability and porosity of the system are not preserved. This issue is addressed by improved cementation technology for filling out the annular space and sealing the naturally consolidated core samples, thus preventing the fluids from bypassing the sample pore space.

For Experiment 1 in the HPRTO setup, a core model was placed into a 316 steel reactor tube. A high-temperature, chemically resistant cement was used to fill up the space between the core model and the reactor wall. The cement permeability and porosity were determined using Automated Permeameter-Porosimeter, and they were found to be 0.138 and 0.56 mD, respectively. Compared to the average porosity (11%) and permeability (14 mD) of core samples, it was expected that most of the injected liquid, would flow through the sample pore matrix. The alignment of the samples before the cementation is shown in [Figure 8](#).



Figure 8. Core model for Experiment 1 – HPRTO

Parameters of the core model and a detailed description of the process are given in the paper ([Askarova et al., 2020c](#)). Following the core sample insertion into a vertically mounted core holder, the cement mixture was injected from bottom to top using a custom-made pressure-feed pump.

The quality of cementation was evaluated using aCT scanner ([Figure 9](#)).

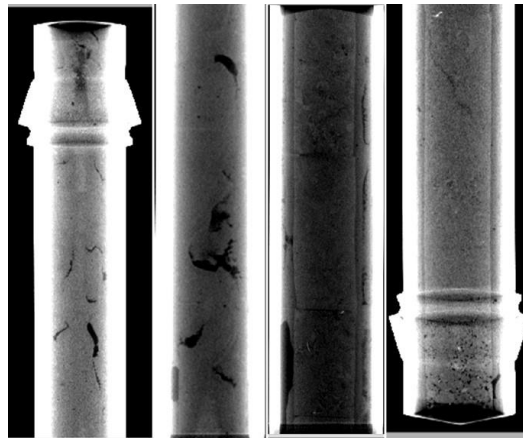


Figure 9. Quality of cementing on a computed tomography scan

Although the scanner can be used to reconstruct and quantify the cement pore space, this was impossible given the core holder steel density. However, the scanner's depth of investigation and resolution of the scans were suitable for visual examination of large connected voids, through which a fluid can bypass the rock matrix. After an inspection in both vertical and horizontal planes, no significant interconnected void space was found within the cement mass. [Section 3.2](#) provides a detailed description of Experiment 1. The cementation procedure for Experiment 2 in the MPCT setup was carried out identically. The detailed description of Experiment 2 is presented in [Section 3.2](#).

4.2 Experimental section

Modified HPRTO and MPCT test design strategy and objectives are presented in [Table 3](#) where two laboratory units are compared. Although the transition to larger reservoir models will entail significant manufacturing costs in the preparation of the experiment, this solution is a step forward when conducting experiments on a whole core.

Table 3. Characteristics of the two water injection experiments to determine k_{dis}

Characteristics	Experiment 1	Experiment 2
Core holder inner diameter, mm	21.5	53
Length, mm	530-540	640-1000
Loading material	Whole core with a diameter of 15-19 mm	Whole core with a diameter of 49-51 mm
Packing method	Core cementing	Core cementing
Pore volume of the core model, cm ³	22.83	203.8
Porosity, %	Core porosity (11%)	Core porosity (14.7%)
Representativeness and reliability of results (K_{rec})	due to the small volume of fluid, the k_{rec} will probably be determined with a significant error	representative results
Experiment Modes	- various injection temperatures -different injection velocities	- various injection temperatures -different injection speeds -combination mode with a maximum model length

4.2.1 Experimental modeling of cyclic HWI on the HPRTO setup (Dome A) at different temperatures. Experiment 1

An experiment was carried out on the HPRTO setup that was adapted for HWI, the collection of a small amount of produced fluids and gases was obtained. Cementation technology is discussed in Section 3.1.3. A schematic diagram of the HPRTO setup, which is usually used for oil oxidation experiments with a linear temperature increase is given in Figure 10. Figure 11 represents the core holder cross-section of a tube with a cemented core column, injection and production lines, and installed heating elements.

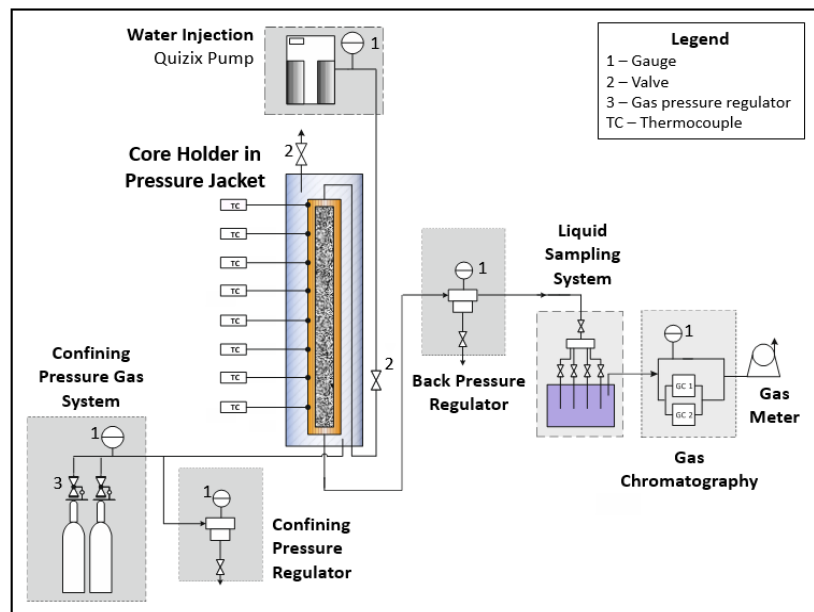


Figure 10. Schematic diagram of the HPRTO setup

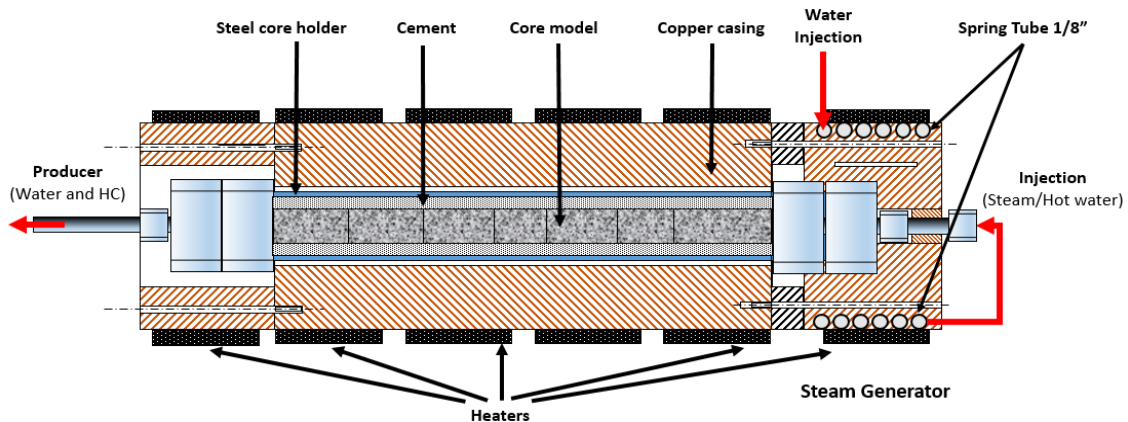


Figure 11. Scheme of the upgraded HPRTO reactor with inlet water heater

After preparing the consolidated core model using a described cementation procedure, the system was placed in the oven at 90 °C for 72 hours for cement drying. Following the drying, the model was then vacuumed using a proprietary pump at a pressure of -1 bar, for two hours. The model was then saturated with reservoir water by injecting two pore volumes (PV). The model was then stored at ambient conditions for an additional 24 hours to allow the rock-water system to reach ion equilibrium. Further oil saturation with heated (80 °C), non-recombined reservoir oil was established until the water content of produced fluid was negligible. Subsequently, 100% oil saturation was reached.

The experiment was carried out at gradually increased temperatures of 100, 200, and 300°C. The water injection rate was 0.1-0.12 ml per minute. Confining pressure was maintained at 21.5 MPa throughout the experiment, injection pressure was kept up to 14.5 MPa until the end of each stage when the pressure was relieved to ambient conditions to collect the displaced oil and clean up the outline with toluene. The water temperature reached the desired value in the first zone of the reactor. During the experiment, fluids displaced from the model were collected in a measuring vessel. The volume of outgoing gases was monitored by a gas meter. Gas samples were taken at regular intervals into the samplers for gas chromatography.

4.2.2 Experimental modeling of cyclic HWI on the MPCT setup (Dome B) with different injection rates. Experiment 2

Experiment 2 was conducted on the adapted MPCT laboratory setup (Kudryavtsev, 2014), equipped with a modified stainless steel core holder with an inner diameter of 53 mm and a length of 640 mm. The MPCT schematic diagram is shown in Figure 12.

The core holder was made of stainless steel alloy similar to the steel grade 304. The wall thickness was 2 mm. Before injection into the model, water was preheated in a custom-made heater with a 1/8-inch tube wound around 70 mm diameter copper cylinder with an annular electric heater installed on top of the tube. This tube was a conduit for heated water (270-280°C) into the core model.

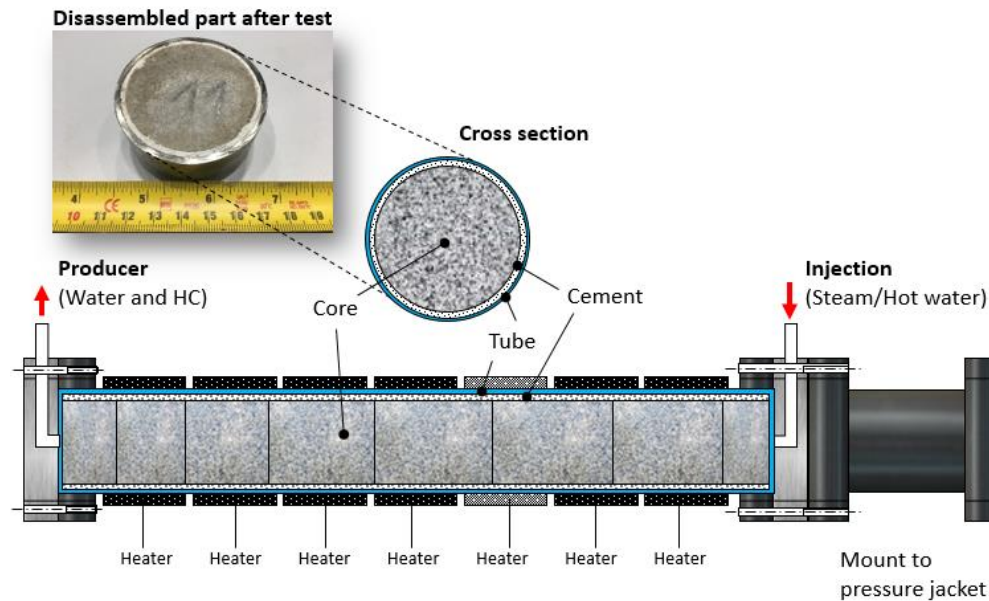


Figure 12. Scheme of the large core holder for MPCT setup

The core model was prepared from 17 stacked cleaned cylindrical core samples with a diameter of 49 mm selected from the same reservoir. The samples were cemented into the core holder with chemical- and heat-resistant cement. The average porosity of the core model was 14.7%. The cement mass was then inspected using an X-ray CT scanner, and no significant fractures were found. After drying and sealing, the consolidated core model was vacuumed, saturated with reservoir water, and left for 24 hours to allow the rock-water system to reach the ion exchange equilibrium. Then water was displaced from the core with recombined live oil at reservoir temperature and pressure maintained by the backpressure regulator until the water fraction in the produced fluid was negligible. After water displacement oil saturation reached 74%. The confining pressure was set by helium 5 MPa higher than reservoir pressure.

Eight annular heaters and thermocouples for temperature control were installed on the core holder. During the experiment, fluids displaced from the model were collected in a measuring vessel. The volume of the gases produced was monitored by a gas meter. Gas samples were taken at regular intervals into the samplers for subsequent analysis using gas chromatography.

4.3 Numerical section

4.3.1 The numerical model of Experiment 1 for Dome A

To conduct a series of numerical experiments, a 3D radial model of the HPRTO experiment setup was constructed, consisting of six grid blocks in the radial direction, one block in the azimuthal direction, and 27 blocks in the vertical direction (Figure 13). Six blocks are core, cement, steel wall, air gap, body, and heating blocks. The inner layer corresponds to the solid core with an effective porosity of 11% and a permeability of 1.4 mD. The initial oil saturation is 0.8; while the initial water saturation is 20%. The porosity and permeability characteristics of the layers and geometry are set taking into account the design of the experimental setup. The thermophysical parameters were calibrated so that the actual temperature on the wall of the HPRTO reactor coincides with the temperature of the corresponding layer in the numerical model. The obtained relative permeability curves used in the model are given in Figure 14 below.

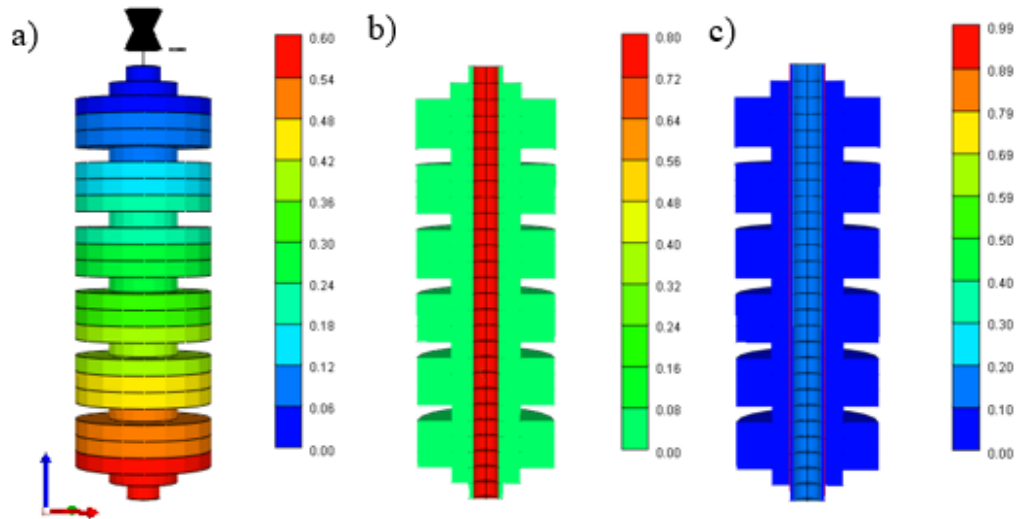


Figure 13. The numerical model of the HPRTO experiment in CMG: (a) model grid, (b) distribution of oil saturation, and (c) porosity in the reactor

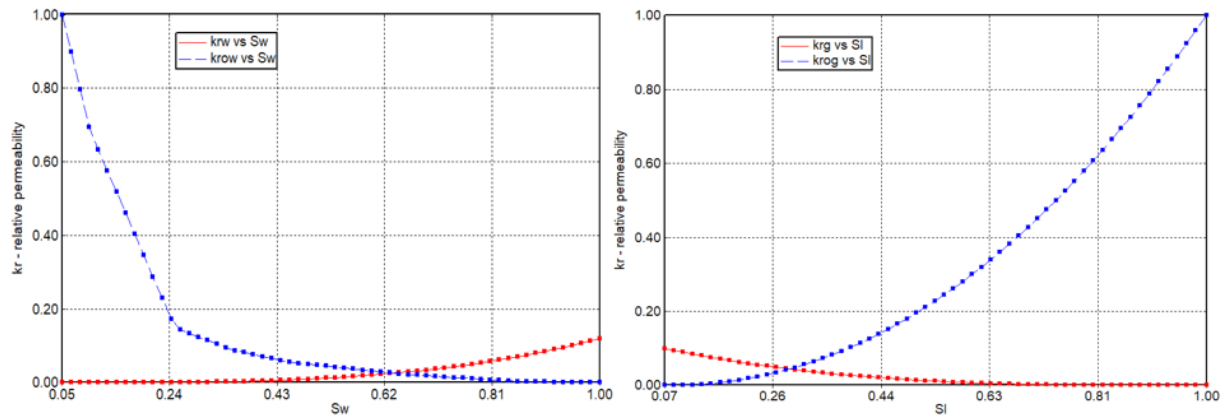


Figure 14. Modified relative permeability: (left) water-oil; (right) gas-liquid.

During the experiment, water is injected into the core model with a constant flow rate at three different temperatures in isothermal mode: $T_1 = 100^\circ\text{C}$, $T_2 = 200^\circ\text{C}$, and $T_3 = 300^\circ\text{C}$. The model is initially heated to 18°C , the fractional composition of the pseudo-component is also set at this stage. The initial temperature of the injected water is 50°C ; the injection pressure is 14 MPa. The subsequent stages of injection mean three different temperatures of the injected heat agent $T_1 = 100$, $T_2 = 200$, $T_3 = 300^\circ\text{C}$.

One of the main steps during the construction of the hydrodynamic model of the proposed oil displacement process is the creation of a representative fluid model. The development of the models is carried out in the format of the CMG WinProp 2017 commercial software. The reliability of the model significantly depends on the quality and integrity of the provided experimental data.

The initial pseudo-component composition of the fluid and initial parameters must be specified to determine the state of each pseudo-component (Water, Maltenes, Asphaltenes, N_2 , CO_2 , O_2) (T_c , P_c , w , ...) based on the physicochemical analysis of oil and data from the standard CMG WinProp library. To create a fluid model in WinGrop CMG format a PVT study of samples from Dome A was used.

4.3.2 The numerical model of Experiment 2 for Dome B

All parts of the combustion tube laboratory setup; including heaters, thermal insulation, and other elements were reproduced in the numerical model of the experiment.

Results such as temperature profiles, pressure drops, fluid production dynamics, and operational parameters, are further used in the numerical model of the experiment. The numerical simulation of the experiment was carried out with CMG STARS commercial software using the properties of the recombined oil sample of the studied carbonate oil field. The fluid model was built using WinProp. The core holder is modeled in a 3D radial coordinate system consisting of five grid blocks in the radial direction, one block in the azimuthal direction, and 26 blocks in the vertical direction (Figure 15).

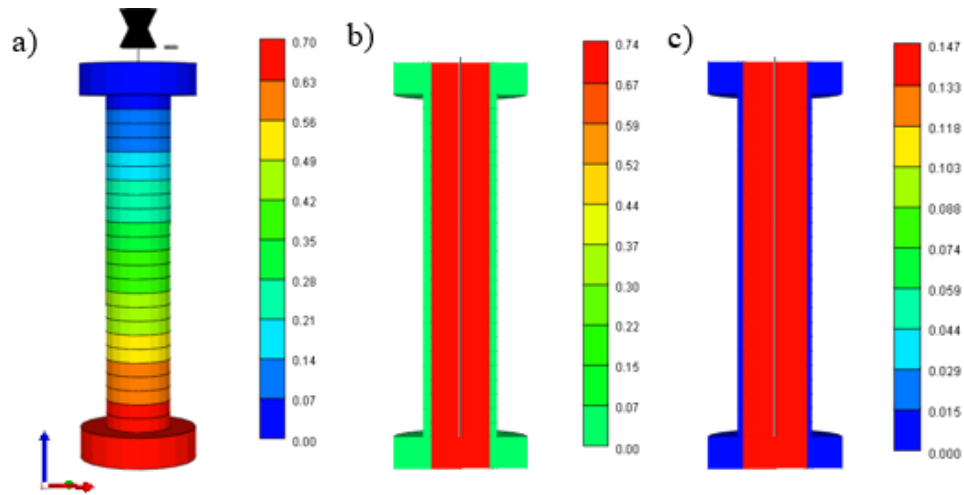


Figure 15. The numerical model of the CT equipment in CMG: a) grid model; b) porosity; c) initial oil saturation

The full geometry and heater regimes were recreated in the numerical model to take into account all the physical phenomena occurring during the experiment. (Khakimova et al., 2020) The relative permeability curves were modified (see Figure 16) to match the cumulative water and oil production. It was determined that the model is highly sensitive to changes in relative permeability.

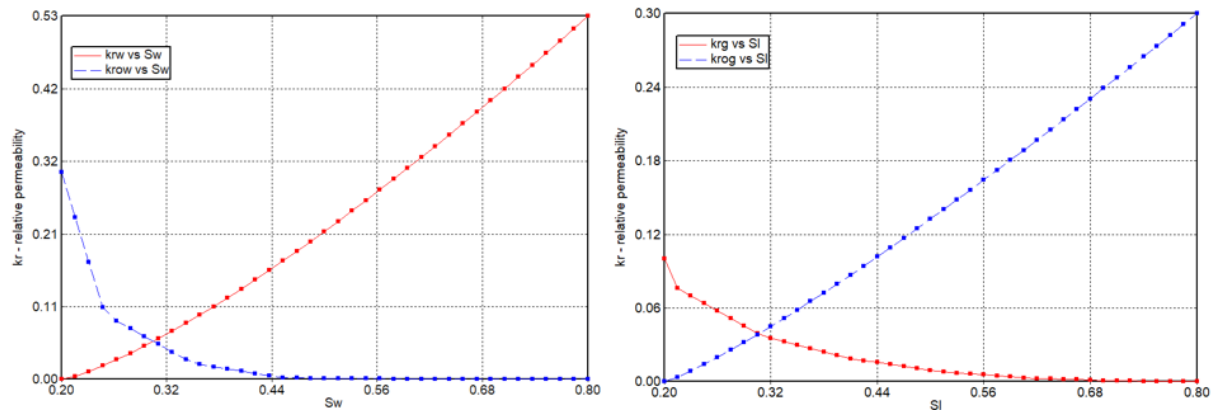


Fig. 13. - Modified relative permeability: 1) water-oil; 2) gas-liquid.

Figure 16. Relative permeability: (left) water-oil ; (right) gas-liquid

The first numerical model described in Section 3.1.1 did not include a chemical reaction model, due to low temperatures (100-200°C is not sufficient, while 300°C level was the last stage held for a short period with a low amount of hydrocarbons produced). Thus, it was decided to introduce the kinetic model during Experiment 2 modeling. The main reason to take aquathermolysis reactions into account is hydrogen sulfide, methane, and hydrogen gas presence in the products detected by gas chromatography. Chemical conversion of heavy fractions of oil in the presence of water demonstrated that aquathermolysis reactions could occur through the production of reactive species from organosulfur compounds with their consequent polymerization or reactions with water to produce smaller fragments such as CH₄, H₂, H₂S, and CO₂ (Hyne *et al.*, 1982; Kapadia *et al.*, 2012).

There are several reaction schemes for aquathermolysis published in the literature (B. Hyne *et al.*, 1982; Belgrave *et al.*, 1993; Clark *et al.*, 1987; Song Guangshou *et al.*, 2009; Lamoureux-Var, V. and Lorant, F., 2005; Tamanyan, 2015) describing different features such as “aquathermolysis window” in the ranges of 170-300°C; bitumen decomposition where reservoir minerals act as catalysts, etc. (Kapadia *et al.*, 2012). Kinetic models developed for ISC with pseudo-components can be taken as a basis (Belgrave, J.D.M. *et al.*, 1997; Belgrave *et al.*, 1993; Fadaei *et al.*, 2011; Gutiérrez, D. *et al.*, 2012; Kapadia *et al.*, 2012; Lin *et al.*, 1984; Ungerer *et al.*, 1988; Yang and Gates,

2009; Yasar et al., 2001) In the paper (Kapadia et al., 2012) a detailed description of the aquathermolysis reaction model with associated rate constants was proposed. It was used as an initial model and was history matched against the results of Experiment 2. The heavy fraction of the original oil (C_{8+}) is defined as a pseudo-component HO; HMWG (High Molecular Weight Gas) is also a pseudo-component that represent combustible hydrocarbon gases (C_{2-7}). HO is in the oleic phase, WATER in aqueous, and other components are in the gas phase. HO as a pseudo-component can be converted into different products and parallel reactions take place as described in (Kapadia et al., 2012). Carbon monoxide and WATER further react forming carbon dioxide and hydrogen through water gas shift reactions. However, carbon monoxide was not detected by gas chromatography. Thus, the mentioned reaction was omitted. The adapted (history matched) reaction scheme is presented below. Kinetic parameters of the reactions are taken from the experimental data and history matched according to the results of Experiment 2. It should be noted, that the activation energy (E_a) values were directly transferred from the (Kapadia et al., 2012), however, frequency factors (A) were adjusted. The inner layer corresponds to the solid core with an effective porosity of 11% and a permeability of 1.4 mD. The initial oil saturation is 0.8; while the initial water saturation is 20%. Details on properties of pseudo-components and kinetic parameters of the used reaction can be found in the article (Askarova et al., 2020c)

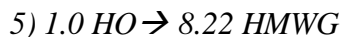
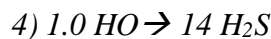
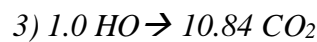
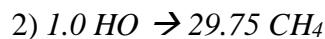
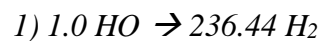


Table 4 lists the initial physical model conditions at the time when HWI started. The parameters are calculated based on the mass balance data and molecular weight of oil and its fractions.

Table 4. Initial conditions

Property	Value
----------	-------

Oil saturation	0.74
Water saturation	0.26
Gas saturation	0.0
Mole fraction of HMWG (in live oil)	0.0526
Mole fraction of HO	0.9427

4.4 Hot water flooding experiments results

4.4.1 Experimental and numerical results of Experiment 1

The temperature profiles of the injected water and temperature on the outer wall (Figure 17) show that the model was heated uniformly over the entire length.

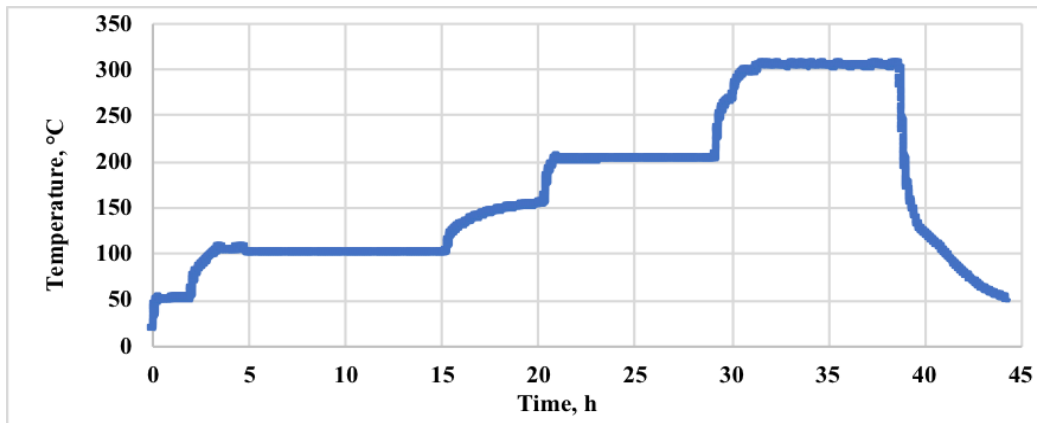


Figure 17. The temperature on the outer wall of the model in the middle part

During the first stage, 3 PV of 100°C hot water was injected into the model, which resulted in 58.2% oil displacement. Further temperature increases up to 200°C and an extra 4.5 PV injection did not result in extra oil recovery. The third stage consisted of 3.5 PV injection of 300°C hot water and allowed the total oil recovery to be increased only by 7%. Low extra oil recovery with temperature increase could be related to the degradation of permeability properties (Sola et al, 2008), which were evaluated during HWI when the stationary regime was reached. Finally, the experimental setup was disassembled and all the lines were rinsed with toluene. The tube with a core model was extracted with the alcohol-benzene mixture. Since the dead oil was used to saturate the consolidated core model, a small amount of hydrocarbon gases was produced.

Table 5. Parameters of the experiment during water saturation and HWI (Experiment 1)

Stage	Cross-section $\times 10^{-4}$, m ²	Viscosity, mPa s	Length, m	Injection rate $\times 10^{-9}$, m ³ /s	Pressure drop, MPa	Permeability, mD
Water saturation	3.6	1.8	0.54	1.33	2.35	1.48
T=100°C	3.6	0.28	0.54	1.33	0.7	0.78
T=200°C	3.6	0.14	0.54	1.33	0.4	0.66
T=300°C	3.6	0.09	0.54	1.33	0.27	0.64

Gas product analysis shows three intervals of active gas release during the experiment that correspond to three different temperature regimes – 100, 200, and 300°C (Figure 18).

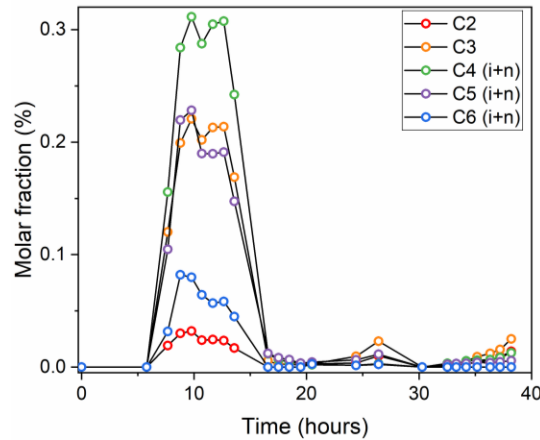


Figure 18. The molar fraction of produced hydrocarbon gases

Hydrocarbon gases are produced due to temperature increase and further distillation after 5 hours of the experiment. However, no peak corresponding to methane, hydrogen sulfide, or hydrogen gas was observed according to the results of gas chromatography. It means that not enough enthalpy was provided to the system to observe the effect of aquathermolysis reactions. Only the final stage of the experiment (300°C) could satisfy such conditions. However, even at this stage characteristic aquathermolysis products were not detected.

Colmatation (or clogging) of the pore space leads to significant permeability degradation. High-temperature cement and decomposition of calcium carbonate-containing minerals, mineral dissolution, and wettability alteration could explain the

observed effect. However, the same effects of damage to formation properties and plugging were observed by other researchers in HWI experiments without cementation (Sola et al, 2008). It also should be noted that the pH values of reservoir water used to saturate the model and produced water differ significantly (6.3 and 9.5, respectively). Thus, we can conclude that calcium carbonate decomposition resulted in the ultimate alkalization of the water produced and could cause the observed colmatation.

Oil density and viscosity measurements using standard methodology were complicated due to the low volume of oil produced. That is why oil density was estimated using the Rock-Eval pyrolysis technique, where S_0 and S_1 relate to gaseous and light hydrocarbons, S_{2a} , and S_{2b} show heteroatomic non-polar and polar hydrocarbon contribution (Table 6). The results show that oil produced at the first stage has close ° API value to the reservoir oil sample (13.8 and 16° API, respectively).

Table 6. Results of oil Rock-Eval pyrolysis

Stage	S_0 , mg HC/g	S_1 , mg HC/g	S_{2a} , mg HC/g	S_{2b} , mg HC/g	Density, g/cm ³	°API
Reservoir oil	41.90	204.35	764.2	730.41	0.959	16
T=100°C	14.78	115.83	325.67	362.97	0.974	13.80
T=300°C	2.43	33.83	274.04	598.11	1.027	6.24

Results of X-ray tomography after the experiment showed the formation of significant void space (Figure 19). However, created channels were not interconnected, which was indirectly proved by the observed permeability degradation.

Figure 20 shows the temperature reading of the central thermocouple of a numerical model of the reactor. The temperature profiles in this graph correspond to the chemical transformations occurring during the experiment.

The dynamics of water and oil production of the experiment and numerical simulation are given in Figure 21. The material balance of water and oil for the experiment and numerical simulation is given in Table 7. It should be noted, that for oil and water, it is possible to compare only the integrated total values, since the collection of products is discrete.

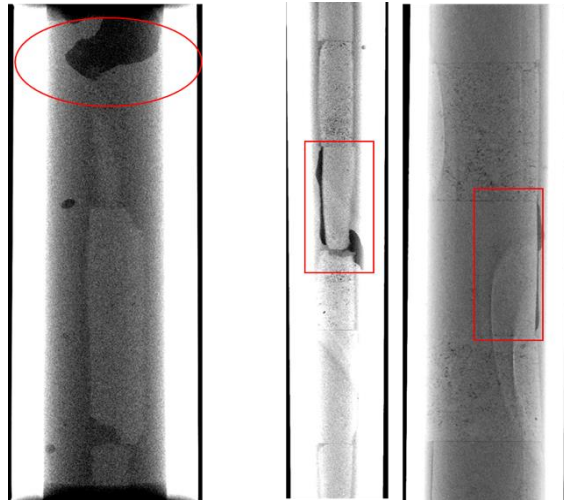


Figure 19. X-ray scans after Experiment 1

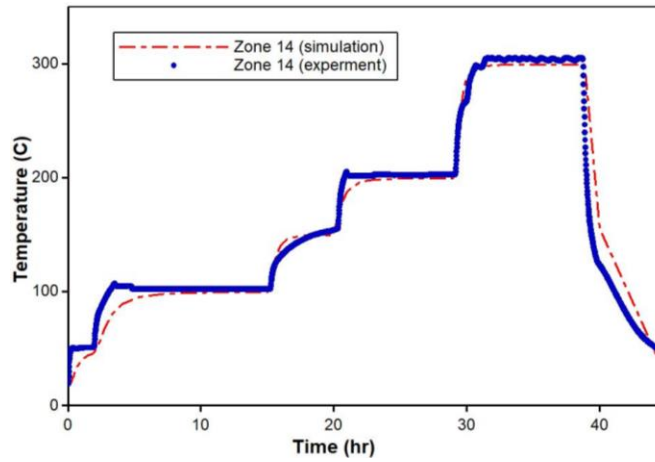


Figure 20. Temperature profile during the injection of heat agent into the HPRTO

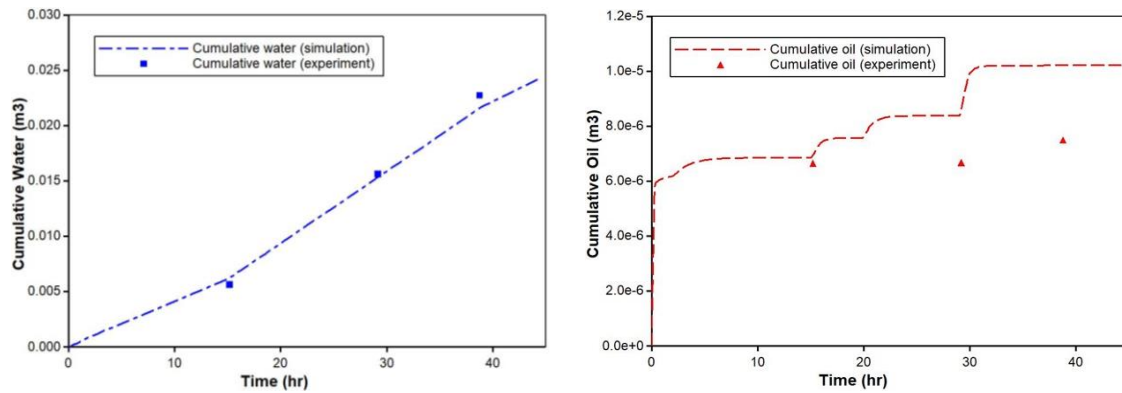


Figure 21. Cumulative water (left) and oil (right) production for experiment and simulation

Table 7. Production of oil and water for Experiment 1

Parameter	Experiment	Simulation	Error (fraction)
Mass of water produced, g	2270.0	2170.0	0.044
Mass of oil produced, g	7.12	9.69	0.361

4.4.2 Experimental and numerical results of Experiment 2

During the experiment, water preheated to 265-270°C was injected into the model along three stages at different injection rates (Figure 22).

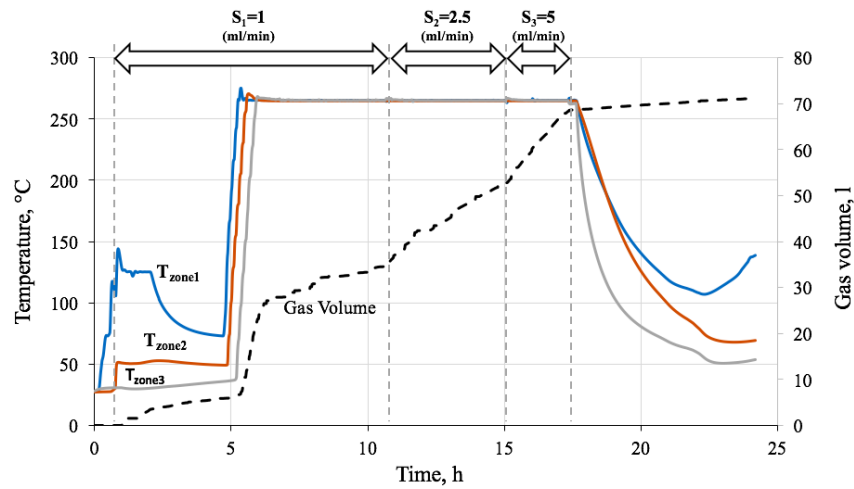


Figure 22. Temperatures on the outer wall of the model and cumulative gas volume

At the first stage, 2.7 PV was pumped through the model, then at the second and third stages, 3.3 and 3.4 PV were injected, respectively. During the first 5 hours of the experiment hot water did not heat the whole model due to significant heat losses on massive metal elements of the core holder, that is why the experiment was continued with sequential heating of the entire model to a temperature of 270-280°C using annular heaters.

Chromatography results of the gases produced showed that a large amount of hydrocarbon gases was obtained during the first 5 hours of the experiment due to the degassing of recombined oil (Figure 23). Further temperature increase resulted in the overlapping effect of hydrocarbon distillation and aquathermolysis reactions. When the

temperature of the system reached 250-260°C hydrogen sulfide, methane, and hydrogen gas were detected among gas products, which is the main criterion showing aquathermolysis reactions taking place. It resulted in a cumulative 1.5 g hydrogen sulfide, 0.011 g hydrogen gas, and 0.067 g methane production.

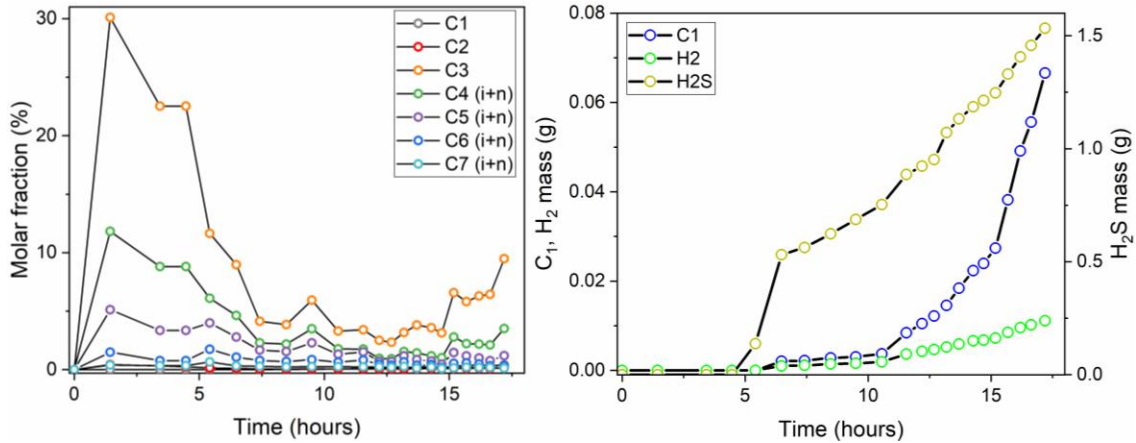


Figure 23. The molar fraction of produced hydrocarbon gases (left) and aquathermolysis produced cumulative gas mass (right)

The first stage of the experiment consisted of 1.1 PV and 1.6 PV of HWI into the consolidated core model before and after the sequential heating of the core holder. It resulted in a 35% and 17.3% oil recovery increase only at the first stage. Further rise of the injection rate up to 2.5 ml/min led only to an extra 6% of total oil recovery. The ultimate HWI rate of 5 ml/min resulted in only a 5% increase in oil recovery. Extra 3.7% of the oil was obtained after the pressure drop and rinsing the outgoing line with toluene. Finally, the experimental setup was disassembled.

Maltenes and asphaltenes concentration of the produced oil at the first stage of the experiment was 96.5% and 3.5%, however, for initial oil, it was 90.7% and 9.3%, respectively. Further analysis of the oil density and viscosity also showed that oil produced at the first stage was upgraded: 131 mPa s and 21.5°API in comparison with 406 mPa s and 19°API, respectively. It also should be noted that the pH values of reservoir water used to saturate the model and produced water differ significantly (6.3 and 8.8, respectively). Thus, we could consider that calcium carbonate decomposition

resulted in the ultimate alkalization of the produced water. However, during the experiment absolute permeability of the consolidated core model increased (Table 8), despite it was about a hundred times less than one estimated during water saturation at ambient conditions.

Table 8. Parameters of the experiment during water saturation and HWI (Experiment 2)

Stage	Cross-section $\times 10^{-4}$, m ²	Viscosity, mPa s	Length, m	Injection rate $\times 10^{-9}$, m ³ /s	Pressure drop, MPa	Permeability, mD
Water saturation	22.1	1.8	0.644	33.3	0.08	204.1
S ₁ =1 ml/min	22.1	0.11	0.644	16.7	0.17	3.06
S ₂ =2.5ml/min	22.1	0.11	0.644	41.7	0.23	5.44
S ₃ =5 ml/min	22.1	0.11	0.644	83.3	0.33	7.71

The X-ray tomography of the core holder after the experiment did not detect any filtration channels in cement or cracks (Figure 24). The volume of the oil samples collected during the last two stages was insignificant. It was difficult to separate the emulsion obtained at the last two stages, therefore, determination of the density and viscosity of the oil was not performed.

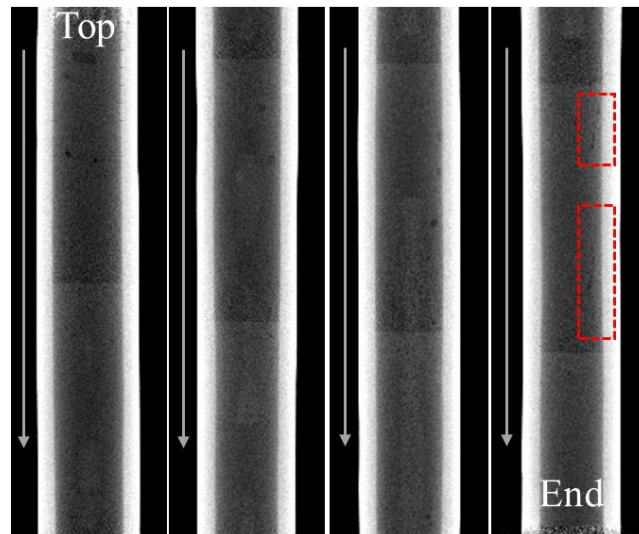


Figure 24. X-ray scans after Experiment 2

A comparison of experimental graphs of temperature changes with the corresponding zones of the model is presented in Figure 25 (left). During the initial period of the first injection stage at the rate of 1 ml/min, there was no significant increase

in temperature on the outer wall due to heat losses. However, even in the initial stage, water was pumped through the model and displaced oil (see Figure 25 (right)).

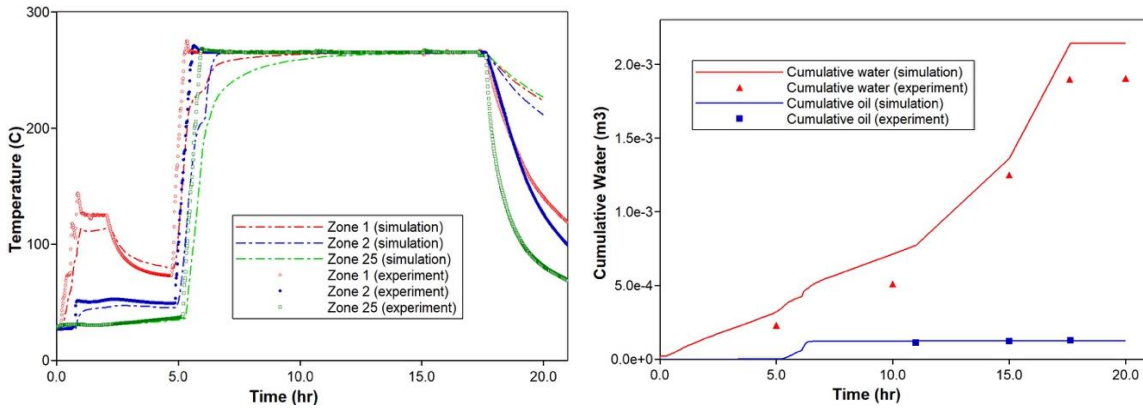


Figure 25. Temperature profiles (left) and cumulative water and oil (right) in CMG

Table 9 below provides a comparison of the cumulative production of water and oil for the experiment and numerical simulation.

Table 9. Mass of oil and water produced for Experiment 2

Parameter	Experiment	Simulation	Error (fraction)
Mass of water produced, g	1905.0	2126.0	0.116
Mass of oil produced, g	120.0	117.2	0.023

Figure 26 presents a comparison of the cumulative gas masses for experiment and simulation.

Table 10 gives absolute values of the produced HMWG, CO₂, H₂S, H₂, and CH₄. Results obtained during simulation demonstrate a comparatively good match within 3%, except for HMWG, which exceeds 6%. HMWG was initially in the oil phase (recombined oil sample), that could explain the results. There are two mechanisms taking place: degassing of original recombined oil (HMWG release) and reaction (5) from Section 3.2. K-values obtained in WinProp led to numerical problems and significant disagreement in cumulative oil production. Thus, during simulation, it was assumed that gas liberation occurred immediately, and HMWG was initially introduced as a pseudo-component in a gas phase.

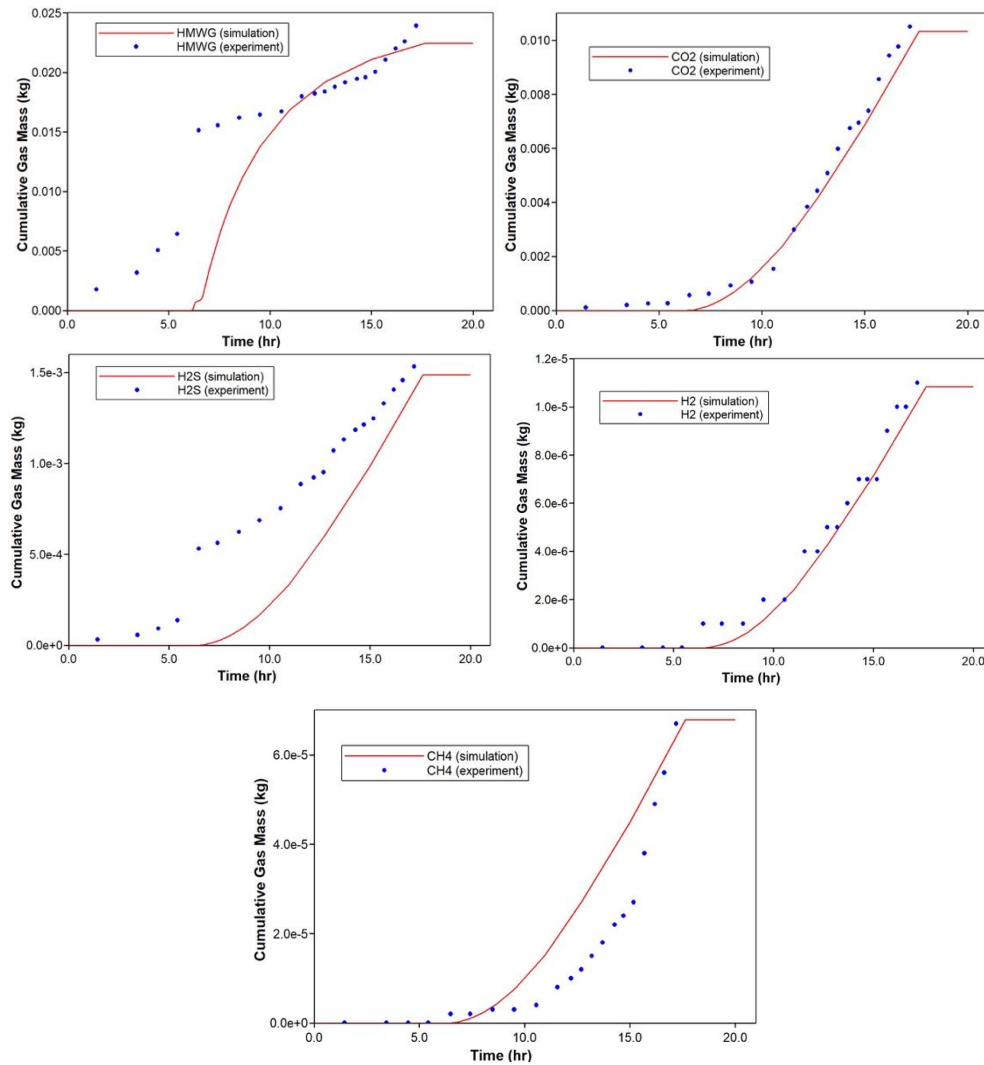


Figure 26. Cumulative gases

Table 10. Mass of gases produced for Experiment 2

Parameter	Experiment	Simulation	Error (fraction)
Mass of HMWG produced, g	23.918	22.451	0.061
Mass of CO ₂ produced, g	10.507	10.332	0.017
Mass of H ₂ S produced, g	1.533	1.488	0.029
Mass of H ₂ produced, g	0.110	0.108	0.018
Mass of CH ₄ produced, g	0.067	0.068	0.015

It is worth mentioning, that the CO₂ and H₂ curves demonstrate the best match in comparison with H₂S, CH₄, and HMWG. It could be explained by the variable heating of

the model at the first stage of the experiment before switching on the annular heaters. In addition, the sampling of the gases produced was discrete and it might differ from the continuous regime of gases produced. The relative permeability curves introduce additional uncertainty.

The products of the chemical reactions serve as a sign of the presence of aquathermolysis at the studied temperature ranges (200-270°C) or, so-called “aquathermolysis window”. Further increase of the temperature (above 300°C) could lead to the thermal cracking reaction and conversion of the heavy molecules into light hydrocarbons and coke (Hyne *et al.*, 1982; Kapadia *et al.*, 2012). The proposed kinetic model takes into account chemical interactions of heavy oil with hot water with consequent formation of acid gases such as carbon dioxide and hydrogen sulfide. H₂S due to its toxicity and environmental concerns has limitations on the percent of its recovery and is an important parameter that should be taken into account. Production of active species from organosulfur compounds and subsequent reaction of the smaller fragments generating CH₄, H₂, H₂S, and CO₂ was also demonstrated.

The results obtained during numerical simulation demonstrate an acceptable agreement of the temperature profiles, cumulative water, oil, and gas values. The model reflects the oil displacement in the first section when water is pumped at the rate of $S_1 = 1$ ml/min, followed by an increase at the transition to the speed of S_2 and S_3 . The main part of the oil displacement occurs at the first stage; however, with a further change in the pressure drop, there is a slight yield of oil. Thermal treatment reduces viscosity with a subsequent increase in oil yield.

4.5 Conclusions

The robust workflow of experimental and numerical modeling of HWI into the heavy oil deep carbonate reservoir was presented. The proposed technology of cementation of consolidated core samples into the core holder for the experiment at temperatures above 250°C works successfully. According to results obtained, the thermal effect of water injection at a temperature of 270-280°C reduces the viscosity of oil due to heating, increasing its mobility, which leads to high values of the recovery factor.

The model developed for Experiment 1 gives a good match of the temperature profile for a zone under investigation; a close agreement is obtained between the values of the produced water both numerically and in the experiment. The volume of accumulated oil in the experiment is small; the values obtained in the simulation are of the same order. The main effect of oil displacement is achieved by displacement with hot water at 100°C, which can be observed in the numerical model. A significant difference in the volume of oil in the second and third sections may be due to inaccurate relative permeability values and a very small amount of oil.

The simulation results of Experiment 2 demonstrate a close agreement of temperature profiles, as well as a good match of experimental and simulation values of cumulative fluid output. Gaseous products of aquathermolysis reactions were obtained: hydrogen sulfide, methane, hydrogen gas, carbon dioxide. A common kinetic model of aquathermolysis reactions was adjusted according to the results of the experiment. Cumulative gas masses obtained during numerical simulation demonstrated a desirable match with the experimental data. The model correctly reflects the dynamics of oil displacement at different rates of water injection. These experimental and numerical results can be further used for subsequent scaling to a hydrodynamic sector (HDS) model based on which the optimal rate, optimal injection temperature, and volume of the injectant in the reservoir are selected. The efficiency of oil displacement by HWI for studied oil field is confirmed by numerical simulation.

An “aquathermolysis” kinetic model was adapted from the steam injection process and introduced into the numerical model simulating the HWI process for the first time. The vigorous workflow that consists of a subsequent experimental and numerical study of HWI was also presented in this research. The data, such as cementation technology, fluid model, relative permeability curves, kinetic model, and operational parameters obtained during this research can be directly transferred to the upscaled model for further feasibility studies.

Chapter 5. Supercritical water flooding in an unconventional reservoir

5.1 Field-scale modeling of the supercritical water injection process

As was already mentioned, the boost of oil production from unconventional reservoirs led to the development of new technologies and an increased number of experimental and numerical studies. This chapter focuses on the development of an ultra-low permeability unconventional formation. It has great potential to generate synthetic oil due to its high content of organic matter. The target object belongs to a deposit of the Western Siberian part of the Bazhenov formation. (Mukhina et al., 2020) Its geology comprises interlayered kerogen-enriched mudstones with interbedded layers of sandstone. They also have distinctive characteristics as low open porosity, low absolute permeability, and practically unknown water saturation. (Kazak and Kazak, 2019)

As a result, the application of thermal EOR methods in unconventional reservoirs is featured with the transformation of kerogen (immature organic matter) due to its pyrolysis or oxidation during the injection of the heating agents (Erofeev et al., 2016; Fan et al., 2010). Kerogen (Chong et al., 2021; Lewan and Roy, 2011; Liang et al., 2020; Mukhina et al., 2020; Wang and Zhao, 2020) go through a series of chemical decomposition reactions and that results in the release of recoverable liquid and gaseous hydrocarbons (Lee et al., 2016). The injection of superheated steam or subcritical water considered in this chapter leads to the above-mentioned transformations, alteration of fluid and matrix properties, viscosity, density, thermal properties, porosity, etc. (Kang et al., 2020a). Thus, the hydrodynamic models created to predict the performance of such methods should take into account all the thermal and chemical processes with high complexity, precision keeping in mind the available computing capacity. (F Behar et al., 2003; Erofeev et al., 2016; Lewan and Roy, 2011). More information on the injection of superheated steam and supercritical water on oil shale can be found in (Dong et al., 2018; Kang et al., 2020b; Kazak and Kazak, 2019).

The simulations are associated with high risks due to uncertainties of reservoir properties, thermal parameters, technology parameters (injection rate, injection time,

production rate, frequency of cycles), etc. It was established that the performance of the selected thermal EOR is greatly affected by the distribution of kerogen, as well as the distribution of the “bonded” hydrocarbons (BHC) (Mukhina et al., 2020). The focus of the numerical simulation conducted within this research was made on the kerogen and bitumen transformations represented by the kinetic reaction model based on reaction rate laws expressed as concentrations of each pseudo-component in different phases (Fan et al., 2010).

5.1.1 Methods

The research was divided into two parts: an experimental investigation and numerical simulation. Specification of organic matter (OM) group distribution was carried out during laboratory experiments. Further numerical simulation was conducted to address the influence of the reservoir saturation matrix on the results of forecast calculations of injection of hot water in a Huff & Puff mode.

5.1.2 Pyrolysis and SARA analysis

The OM distribution was identified during the laboratory studies and the relative content of BHC was estimated using core samples obtained from the field under study. Pyrolysis was conducted of the prepared rock samples before and after extraction was conducted. Five packs were distinguished within formation based on the lithological and geochemical characteristics. Characteristics of the research samples used and the method for determination of OM distribution are described in (Mukhina et al., 2020). The results of pyrolysis and SARA (saturates, aromatics, resins, asphaltenes) analysis defined the following organic pseudo-components Hydrocarbon Gas (HCG); light oil (LO), kerogen (KER), bitumen (BITUM), heavy oil (HO) (Askarova et al., 2020d). The data obtained resulted in the detailed OM saturation matrix of the studied core sample and the relative distribution of pseudo-components in the oil phase.

5.1.3 Parameters of HDS

Numerical simulations were conducted on a thermos-HDS with a pseudo-compositional fluid model taking into account the geological structure of the target

reservoir. Additional laboratory studies on kinetic parameters were used in these forecast calculations.

The fundamental physical processes, which are necessary to take into account during the simulation of thermal recovery methods (Erofeev et al., 2016), are:

- 1) Three-phase multi-component fluid flow in the reservoir;
- 2) Phase-to-phase fluid transformations;
- 3) Heat transfer from heating agent to matrix and fluid;
- 4) Temperature and fluid, matrix properties change during thermal agency injection;
- 5) Kerogen pyrolysis by high temperatures and generating fluids from kerogen;
- 6) Porosity and permeability changing due to kerogen pyrolysis, compressibility, and thermal deformations;
- 7) Heat losses in surrounding formations.

All these phenomena were taken into account during the creation of the HDS model. Implementation of such technology requires the use of special equipment and thermally insulated tubing to provide minimal transport heat loss in well to avoid additional technical and economic constraints. The heat losses from the heating agent to an ambient formation strongly affect the oil recovery efficiency and require accurate calculation. (Yusupov et al., 2020) The effect of different system parameters plays a crucial effect on flow behavior. For example, a hydrostatic pressure increase with well depth greatly contributes to a pressure change along the injection tubing. The study by (Yusupov et al., 2020) demonstrates that the fluid (steam) quality increases with the well depth due to the specific behavior of both the liquid and vapor enthalpies near the critical point. The flow rate also an important parameter affecting the fluid quality distribution along the tube. Nevertheless, the study of heat losses within reservoir cross-section must be studied further.

The distribution of porosity, permeability, solid concentration, and fluid saturation were carefully determined in the experiment, and history matched in the target model. An active section for HDS was a part of the field near one of the fractures (Figure 27). The

calculations were carried out using a three-phase multicomponent commercial reservoir simulation software. The incorporation of the kerogen and bitumen transformation requires an introduction of a great number of reactions. Also, the oil sample consists of a large number of different hydrocarbon and non-hydrocarbon components. Thus, it was decided to use a simplified pseudo-component fluid model. (Chen, 2012).

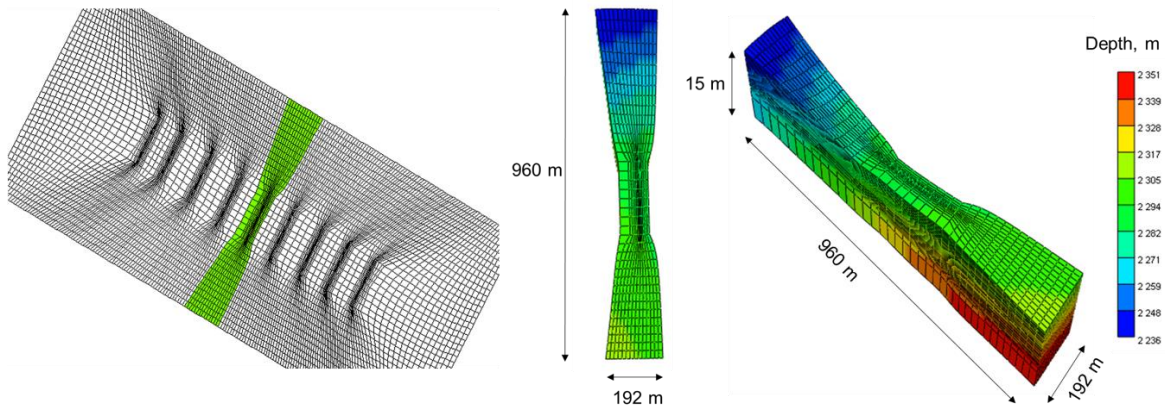


Figure 27. The HDS-section, used for numerical simulations.

Currently, there are some constraints in the commercial reservoir simulation software limiting the separation of the components of “bonded” and mobile oil. Thereby, the study was performed with an assumption about the identity of the properties of BHC and mobile oil. The influence of the saturation was estimated by a set of numerical calculations. Based on these forecast numerical runs the optimal parameters of thermal EOR technology were defined: injection temperature of 350°C, the injection pressure of 25 MPa, injection stage period – 5 months, imbibition stage – 1 month, production – 6 months in each injection cycle. The fluid model consisted of 9 pseudo-components, water (WATER) was specified as a liquid phase, the oil phase (oleic) was specified by the components CO₂, CH₄, HCG, LO, HO (the BHC content were added, although not separated); and KER (kerogen), BITUM (bitumen) and COKE components were presented as solid components (solid). The initial distribution of OM groups in the initial saturation matrix was varied while the total amount of OM was maintained.

Three forecast calculations were performed for supercritical water injection:

1. Base case (described above)
2. Use of one unified solid component that replaces KER and BITUM with the properties of BITUM;
3. Use of one unified solid component that replaces KER and BITUM with the properties of KER.

The identical initial parameters were used apart from the initial OM saturation matrix. The cases are presented in [Table 11](#).

Table 11. The list of pseudo-components in calculation cases.

Phase	Base case	Solid BITUM	Solid KER
Liquid	WATER		
Oil (liquid and gaseous), including BHC	LO, HO, HCG, CO ₂ , CH ₄		
Solid	BITUM, KER, COKE	BITUM*, COKE	KER*, COKE

Properties of the pseudo-component BITUM* were identical to the solid component BITUM used in the base case, and the concentration of the solid was specified as the sum of the initial concentrations of the solid kerogen and bitumen. The KER* pseudo-component with the properties of the KER component was defined similarly, using the same matrix of both solid component concentrations. The COKE component is the reaction product; it did not participate in the initial OM distribution specification. Additionally, the distribution matrices of kerogen and bitumen concentrations and thermal properties were used in the HDS with adjustment of the fluid PVT properties. Three sets of relative phase permeability curves in oil-water and oil-gas systems were input for two regions (see [Figure 28](#)). The first region was the main reservoir, the second region – fractures.

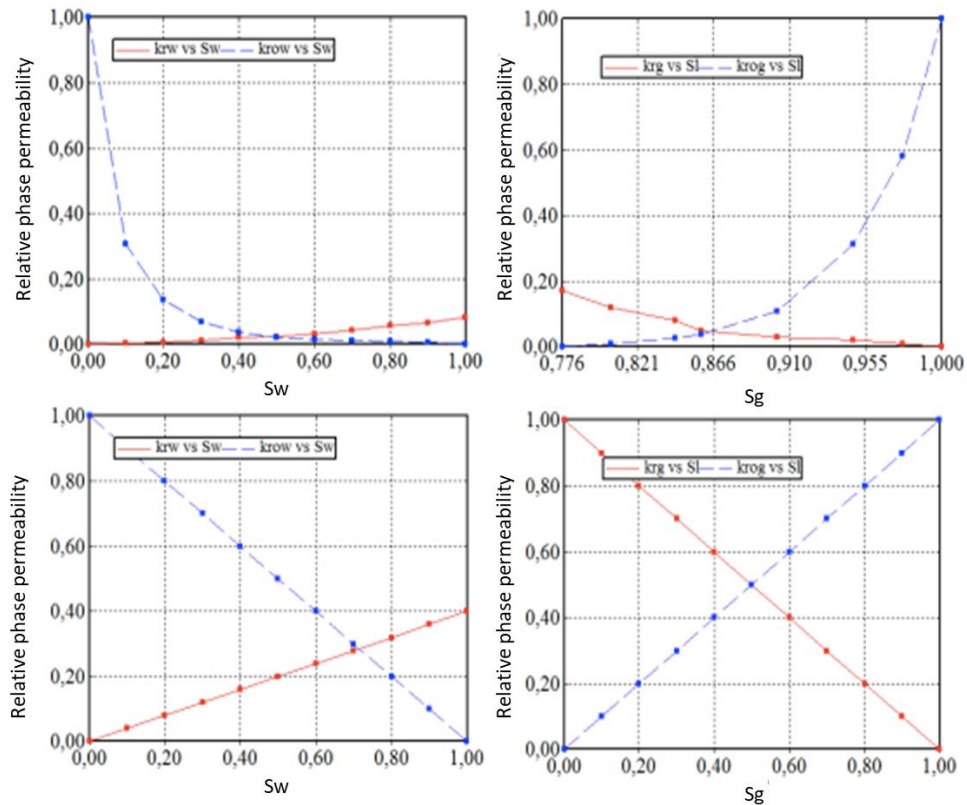


Figure 28. Relative phase permeability curves, oil-water (left) and oil-gas (right) for two regions: main reservoir (up) and fractures (bottom).

The kinetic model of organic matter transformation was characterized by 4 reactions, more details on the reactions can be found in (Mukhina et al., 2020).

1) *Reaction #1 – thermal cracking of bitumen*



$$E_a = 194.2 \text{ kJ/mol}, A = 3.6e^{18}$$

2) *Reaction #2 – thermal cracking of kerogen*



$$E_a = 224.1 \text{ kJ/mol}, A = 3.6e^{18}$$

3) *Reaction #3 – thermal cracking of heavy oil*



$$E_a = 230.0 \text{ kJ/mol}, A = 3.6e^{18}$$

4) *Reaction #4 – thermal cracking of light oil*



$$E_a = 260.0 \text{ kJ/mol}, A = 3.6e^{18}$$

Where:

E_a – activation energy;

A – pre-exponential factor.

The additional calculation 2. BITUM* excludes *reaction #2* and case 3. KER* excludes *reaction #1*. The composition of the light BHC in the reservoir according to the experimental study: 17.61% HCG, 31.35% LO, and 51.04% HO, while the average composition of the reservoir mobile oil is as follows: 20% HCG, 47% LO, 33% HO.

The data obtained of the OM distribution is representative only for selected core samples. Nevertheless, they are sufficient to clarify the OM matrix distribution groups in the rock.

5.1.4 The results of the modeling

1) Base case (all groups of OM are considered)

The base case calculations were performed with both solid components BITUM (Mukhina et al., 2020). The distribution of initial concentrations of bitumen and kerogen are illustrated in Figure 29.

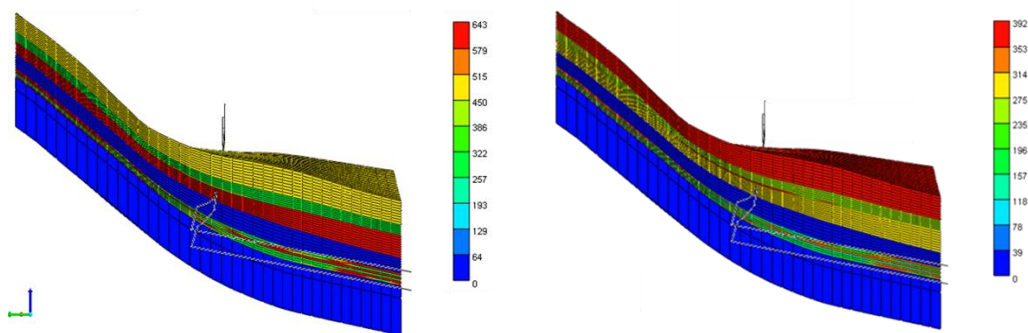


Figure 29. Distribution of initial content of bitumen (left) and kerogen (right) in the HDS section.

The optimization calculations were derived: temperature of 350°C, the pressure of 25 MPa, injection for 5 months, imbibition for 30 days, production for 6 months. The forecast of the calculations at the end of the calculation period (~ 3100 days) was 1237

m^3 of the cumulative oil production, its dynamics are presented in Figure 30. The HDS sensitivity was carried out with a variation of the effective permeability dependence on temperature (EPT) and activation energy (E_a). The results obtained allow us to evaluate the influence of these parameters on the forecast of oil production (Figure 30).

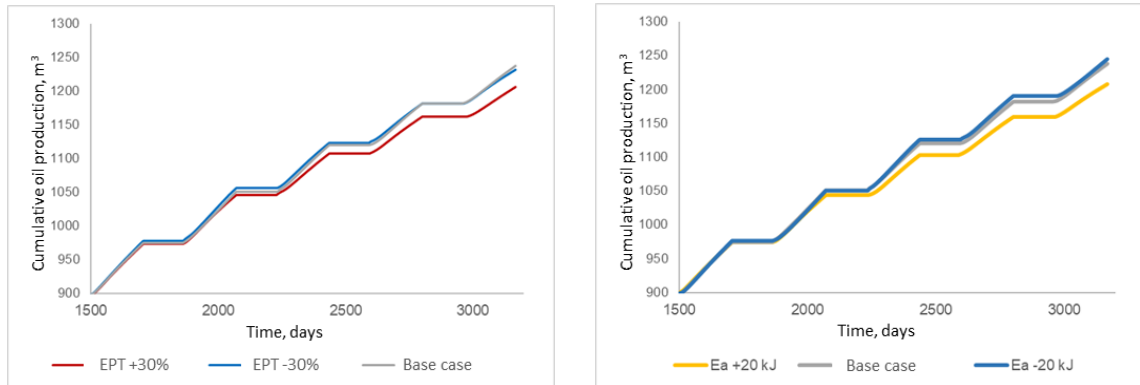


Figure 30. Cumulative oil production, sensitivity analysis (EPT and E_a).

The variation in EPT by $\pm 30\%$ from the original value (Mukhina et al., 2020) demonstrated the influence in cumulative oil production. The difference between the results of cumulative oil production in the case of EPT variation is 31 m^3 of oil. A decrease in the activation energy leads to a slight increase in the cumulative oil production. Increase of the activation energy results in lower cumulative oil production (difference $\sim 37 \text{ m}^3$). However, the influence of these parameters could not be quantitatively determined, since the four reactions are characterized by 12 degrees of freedom, which complicates the calculations. Hence, the base case and its optimized parameters were selected.

- 2) The calculation with the combination of solid components KER and BITUM with the properties of BITUM

The pseudo-components were chosen with the purpose of accurate representation of the reservoir oil properties, as well as the physical and chemical properties of the field. One of the requirements of numerical simulations is a choice of a reasonable number of the required pseudo-components to save the calculations time. The calculation time depends exponentially on the number of pseudo-components involved in the reactions.

Calculations in the second case were performed with the technological parameters of the base case, while the combined solid component BITUM* was characterized by $MW = 0.7 \text{ kg/mol}$ and $\rho_{\text{BITUM}} = 1020 \text{ kg/m}^3$. The distribution of the initial concentration of this solid component is calculated through the following formula:

$$\text{CONC_SLD 'BITUM*'} = \text{CONC_SLD 'BITUM'} + \text{CONC_SLD 'KER'}$$

Where CONC_SLD 'BITUM*' - the new solid component concentration;

In this case, the kinetics excludes *reaction #2 – thermal cracking of kerogen*.

- 3) The calculation with the combination of solid components KER and BITUM with the properties of KER

In these calculations, the combined solid component KER* was specified with the following properties $MW = 2 \text{ kg/mol}$, $\rho_{\text{KER}} = 1090 \text{ kg/m}^3$. The initial concentration of this pseudo-component is equal to CONC_SLD 'BITUM*' . The kinetic excludes *reaction #1 – thermal cracking of bitumen*. Figure 31 illustrates the distribution of total porosity. The calculation results for each case are presented in Figure 32.

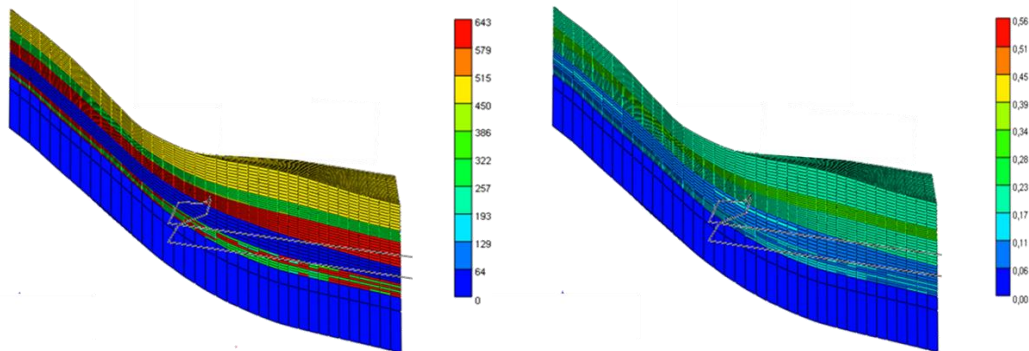


Figure 31. Distribution of initial concentration of the combined solid component BITUM*/KER* (left) and distribution of total porosity (right) the HDS section.

The calculations revealed that the determination of the single solid component by BITUM* properties leads to the increase in cumulative oil production by 247 m^3 . On the other hand, the calculation with KER* component leads to a reduction in oil production by 346 m^3 . The difference is primarily attributed to the simplification of the solid component properties – kerogen ($MW = 2 \text{ kg/mol}$, $\rho_{\text{KER}} = 1090 \text{ kg/m}^3$) transforms more slowly than the BITUM* component ($MW = 0.7 \text{ kg/mol}$, $\rho_{\text{BITUM}} = 1020 \text{ kg/m}^3$).

It was defined, that the detailed elaboration of initial matrix saturation with OM influences the results of forecast calculations of cumulative oil production. The selection, separation, and properties specification are crucial for accurate numerical simulations.

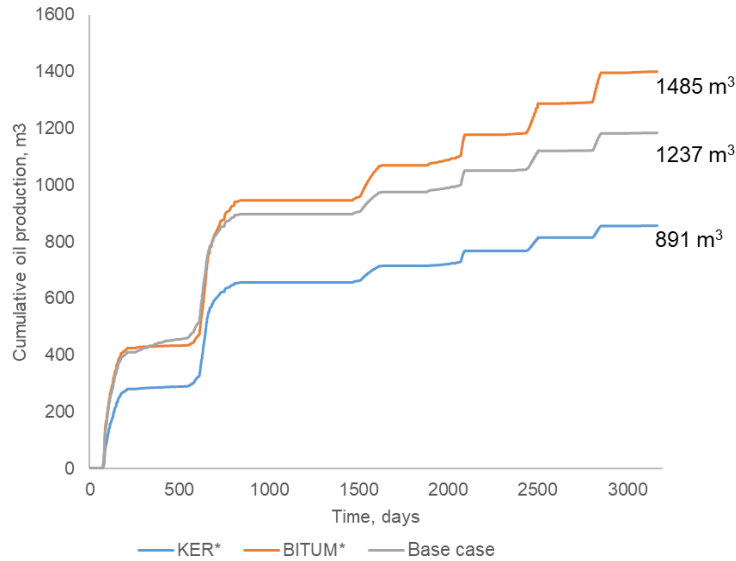


Figure 32. Cumulative oil production for the base case and cases 2. BITUM* and 3. KER*.

However, there are some limitations of modern commercial software such as the inability to set a few different potentially mobile HC liquid phases with different parameters. Thus, there should be a possibility to set the bitumen to have a separate liquid phase with its own flow properties (the flow is activated with a temperature increase) along with mobile oil. Chemical and phase transformations should be specified simultaneously for liquid components and mobility of the bitumen should change its phase at high temperatures.

5.2 Methodological approach

There is a variety of kinetic models available in the literature. However, all of them have their advantages and limitations. (Bauman and Deo, 2011; Braun and Burnham, 1992, 1990; Fan et al., 2010; Hazra et al., 2013; Jupp and Woods, 2003; Lee et al., 2014; White et al., 2010; Youtsos et al., 2013)

The kinetic reactions model is built based on the patent (Wellington, S.L. et al., 2005) and consists of five reactions and six lumped pseudo-components (HO, LO, HCG, kerogen, CO₂, N₂). The results of the modeling demonstrate good agreement with experimental data. However, it also has few limitations such as the absence of water components and aqueous phase, no involvement of solid components, no evolution of porosity, and permeability due to kerogen pyrolysis, and the coking reaction was not taken into account.

A paper by (Lee et al., 2016) includes kerogen pyrolysis and further cracking of its hydrocarbon products. The kinetic model used in this simulator is built based on the previous paper (Fan et al., 2010) and includes six reactions generally grouped to kerogen decomposition, cracking of heavy oil, cracking of light oil, and coking of hydrocarbon gas. Most of the components are represented in different fluid phases (aqueous, liquid organic, gaseous). However, the change of solid components phases was not taken into account in this research.

The phase change of the bitumen was considered in the paper (Gao and Chen, 2020), where this evolution believed to have a significant impact on the geomechanics and temperature distribution. According to these articles (Gao and Chen, 2020; Pang et al., 2019), bitumen phase change contributes to the effects of heat transfer, and mechanical deformation and must be taken into account.

The purpose of this chapter is to develop an approach including experimental studies and numerical simulation for the investigation of pyrolysis and cracking processes with a focus on the fluidity of the bitumen. Description of various methods for creating thermo-compositional fluids is provided – including all solid, liquid, and gaseous components, as well as mobile bitumen, transformations of light oil, heavy oil, and the adsorbed hydrocarbons. It should be mentioned that, currently, CMG software (CMG, 2016) is unable to introduce the solid component that changes its phase over time without additional components and reactions. The proposed method's focus on the introduction of the highly viscous liquid bitumen with decreasing viscosity at a higher temperature,

previously introduced into the model as a solid immobile component. The results of this study were published in (Askarova et al., 2020d)

5.2.1 Methods

The investigation conducted in Section 4.1 was continued. The same specification of distribution of OM groups was used further during an experiment in an autoclave, where subcritical water was injected at reservoir pressure. Numerical simulation subsequently recreated the autoclave experiment including the kinetic model.

5.2.2 Autoclave experiment

The autoclave experiment was performed in a one-liter Hastelloy C-276 autoclave (Parr, USA). A detailed description of the experimental procedure can be found in the article (Askarova et al., 2020d). Autoclave pressure during the temperature rise was maintained at 25 MPa using a back-pressure regulator to simulate reservoir conditions (see Figure 33).

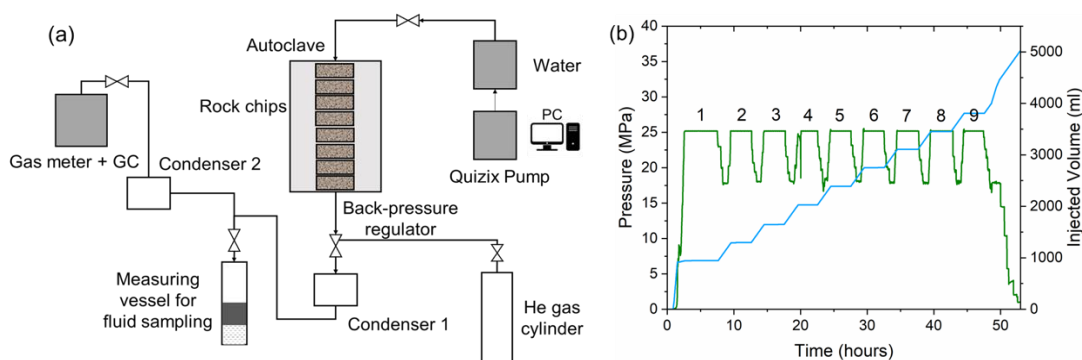


Figure 33. (a) Experimental set-up scheme; (b) Injection pressure (green) and cumulative water volume (blue) profile

Exposure temperature was chosen in accordance with the results of previous studies, which showed significant liquid hydrocarbon yield in laboratory conditions only starting from 350°C (Popov et al., 2017).

Results of the open-system Rock-Eval pyrolysis showed how organic matter distribution changed after the test. X-ray computed microtomography of original and spent oil shales revealed the creation of extra pore space. Microstructural properties of oil

shale samples were characterized based on the comparison of the same sections of samples before and after the treatment. Samples X₁ and X₂ were scanned and the porosity of the X₁ sample increased 3.3 times from 0.37% to 1.23%, specific pore surface increased significantly. The porosity of X₂ increased 155.6 times from 0.0056% to 0.8716%, and specific pore surface area raised from 10.9 m²/m³ to 897.8 m²/m³. 3D reconstruction of pore space shows interbedding behavior, which could be explained by the observation that pores and microfractures are generated primarily along with the organic-rich layers (Tiwari et al., 2013). It should be noted that visible fractures appeared in almost all the samples. Porosity and specific surface area rise significantly due to artificial maturation of organic matter, pores, and microfractures generation primarily along the organic-rich layers.

Based on the experimental results obtained an initial kinetic model containing 4 chemical reactions was constructed. The model is a derivative of a common kinetic model (Lee et al., 2016, 2018b) with the extra equation accounting for bitumen thermal desorption, and without high energy hydrocarbon gas and prechar cracking due to relatively low temperature (350°C) experimental conditions. This kinetic model was further used in the thermodynamic model created during numerical simulations. The molecular weight of the used pseudo-components is presented in Table 12.

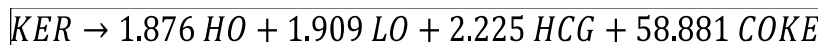
Reaction 1: Bitumen thermal desorption:



With the following kinetic parameters:

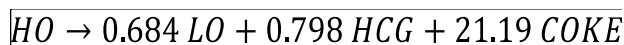
- Ea – 227.2 kJ/gmole; A – 6.94 e+10.

Reaction 2: Kerogen thermal cracking:



- Ea – 225.7 kJ/gmole; A – 6.94 e+10.

Reaction 3: Heavy Oil thermal cracking:



- Ea – 249.1 kJ/gmole; A – 6.94 e+10.

Reaction 4: Light Oil thermal cracking:

$$\overline{LO} \rightarrow 0.390 \overline{HCG} + 10.332 \overline{COKE}$$

- E_a – 259.2 kJ/gmole; A – 6.94 e+10.

Where:

- COKE – coke solid component;
- E_a – activation energy;
- A – pre-exponential frequency factor.

Table 12. Molecular weights of pseudo-components

Pseudo-components	KER	BITUM	HO	LO	HCG	Coke
MW, kg/gmole	2	0.7	0.4286	0.1572	0.0586	0.013

5.2.3 Numerical simulation of autoclave experiment

The autoclave experiment setup was constructed in the CMG STARS commercial simulator to validate the chemical reactions and their parameters. The digital model recreated the process of hydrous pyrolysis of core samples of the target reservoir deposit by a cyclic heating agent injection at a temperature of 350°C and a pressure of 25 MPa. The general view of the autoclave model, initial oil and water saturations are presented in Figure 34.

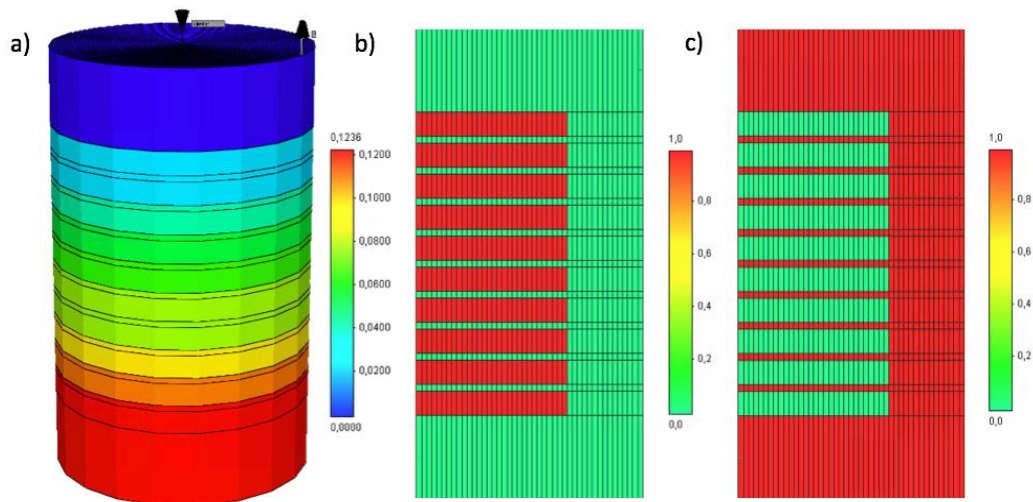


Figure 34. Autoclave in CMG format: a) grid mesh; b) oil and c) water initial saturations

The core samples had no initial water saturation, however, water was injected from the top and occupied the available space around the samples with porosity 100%.

The initial distributions of HO, LO, and HCG were taken from experimental studies and are shown in [Figure 35](#). Relative permeability curves, PVT properties of components, thermal properties of rocks, and saturating fluids were taken from the well located in the subject area.

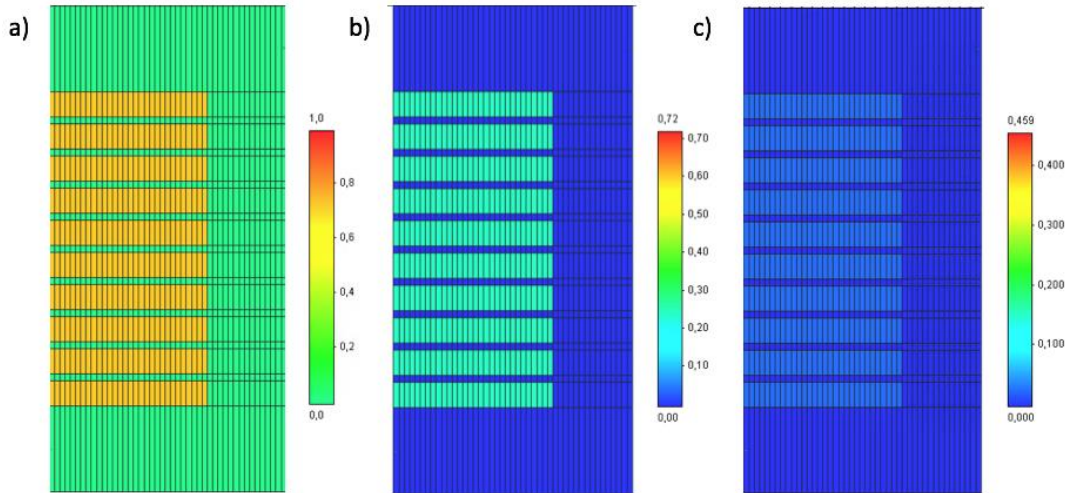


Figure 35. Distribution of: a) Heavy Oil; b) Light Oil; c) Hydrocarbon Gas - mole fractions

The chemical reaction scheme obtained from the autoclave experiment was used as an initial guess for further numerical modeling. Its results were analyzed and validated against the experimental data. The fluid model consisted of 9 pseudo-components: water (WATER) was specified as a liquid phase; the oil phase (oleic) was specified by the components CO₂, CH₄, HCG, LO, HO; and KER, BITUM, and COKE components were presented as solid components (solid). It should be noted, that initially the BHC content was added to HO.

The properties of the pseudo-components are presented in [Table 13](#). This case is accepted as a Case 1 - Base case. The dynamics of cumulative oil production is given in [Figure 36](#), as well as a comparison of the experimental and simulation results for the HO and LO. The material balance of oil and other oleic pseudo-components (HO, LO) are presented in [Table 13](#). As can be seen, the kinetic model obtained during the experiment gives a good approximation for cumulative oil production with a 1.1% error. However,

the given reaction scheme does not provide the desired precision, particularly for HO and LO production.

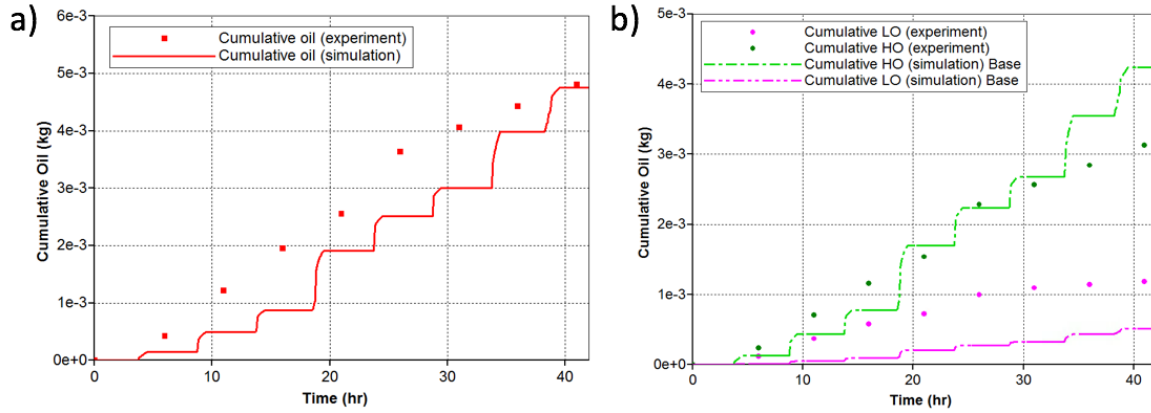


Figure 36. (a) Cumulative oil; (b) cumulative HO and LO production

Table 13. Material balance

Parameters	Experiment	Simulation	Error (%)
Mass of oil produced, g	5.10	5.152	1.10
Mass of HO produced, g	3.32	4.6	35.18
Mass of LO produced, g	1.24	0.56	52.7

Previously obtained results (Mukhina et al., 2020) demonstrated the influence of initial matrix saturation on the forecast calculations as well as pseudo-component selection and specification of their properties. Currently, commercial reservoir simulation software has some limitations when creating a multi-component OM model of the reservoir. Simulation software does not allow proper separation of the “bonded” components and mobile oil. The mobile oil cannot be set apart from light BHC of the same qualitative composition. Bitumen as a separate component can only be specified in the solid phase.

The purpose of this chapter is to develop a methodological approach by the introduction of a new chemical model, adjusted initial distribution of components, viscosities, and relative permeability, to obtain an authentic description and understanding of the nature of the process. The key issue of this research is to overcome

the difficulties of existing commercial software with its inability to set a few different mobile liquid phases of hydrocarbons with different parameters (viscosity-temperature dependence, flow). Thus, in Case 2 bitumen was introduced into the model as a liquid pseudo-component “BIT_liq” in the aqueous phase. It has very high viscosity at reservoir temperatures and lower viscosities at higher temperatures. Several numerical runs were conducted to demonstrate the influence of the parameters mentioned above. The cases are described in Table 14.

Table 14. The list of pseudo-components in the calculations - Cases 1 and 2

	Case 1	Case 2
Phase	Components	
Liquid	WATER	WATER, Bit_liq
Oil (liquid and gaseous)	LO, HO, HCG, CO ₂ , CH ₄	
Solid	BITUM, KER, COKE	KER, COKE

The model in Case 2 was adjusted accordingly: the solid concentration of bitumen was removed. The corresponding amount of Bit_liq was added through initial water saturation (see Figure 37, (a)) together with the amount of BHC previously considered as part of HO. The mole fraction of HO subsequently was decreased, while the fraction of LO was redistributed within total initial oil saturation. This assumption was possible since the initial model has no initial water saturation. The amount of BHC was subtracted from HO initial distribution and changed the total initial oil saturation Figure 37, (b).

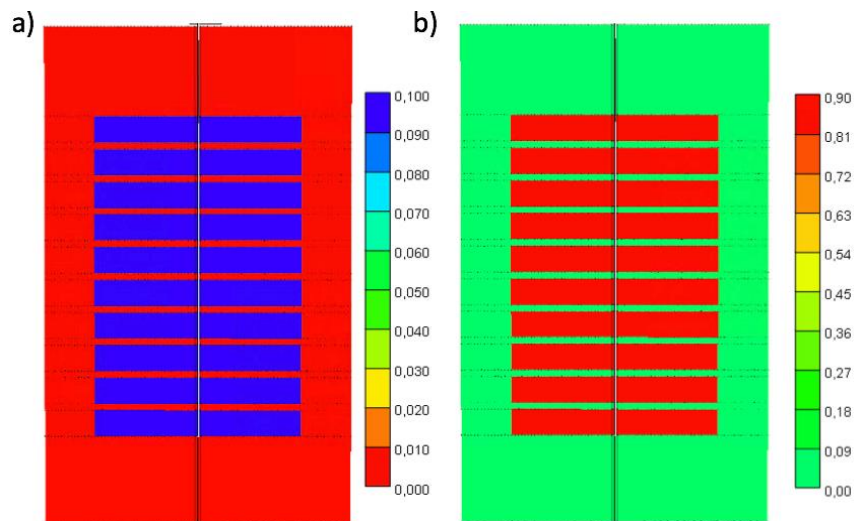


Figure 37. (a) Initial saturation of LB; (b) initial oil saturation

Further few adjustments were made to improve the results and validate the kinetic model. The viscosity of the Bit_liq at elevated temperatures was adjusted to match the viscosity of the liquid bitumen against permeability at its initial saturation.

5.2.4 Results

The kinetic model obtained during the autoclave experiment where subcritical water was injected at reservoir pressure was used as an initial guess (Case 1) in the numerical model and it presented a good physical description of the process. However, this initial Case 1 model did not involve the phase change of solid bitumen. Thus, Bit_liq pseudo-component was added in the aqueous phase that has very high viscosity at low temperatures and can mobilize when temperature decreases. Bitumen concentration was added as initial water distribution, while fractions of HO and LO were redistributed. Some adjustments in viscosity of Bit_liq and relative permeability curves were further made to history match the experimental data. The adjusted kinetic model (Case 2) was validated in the numerical simulation of the autoclave experiment (see Figure 38). The total cumulative oil production see Figure 38, (a) consisted of cumulative production of HO in the oleic phase, LO both in gaseous and oleic phases, and liquid bitumen in gas and aqueous phases. The difference between simulation and experimental results of cumulative oil production was 6.4%.

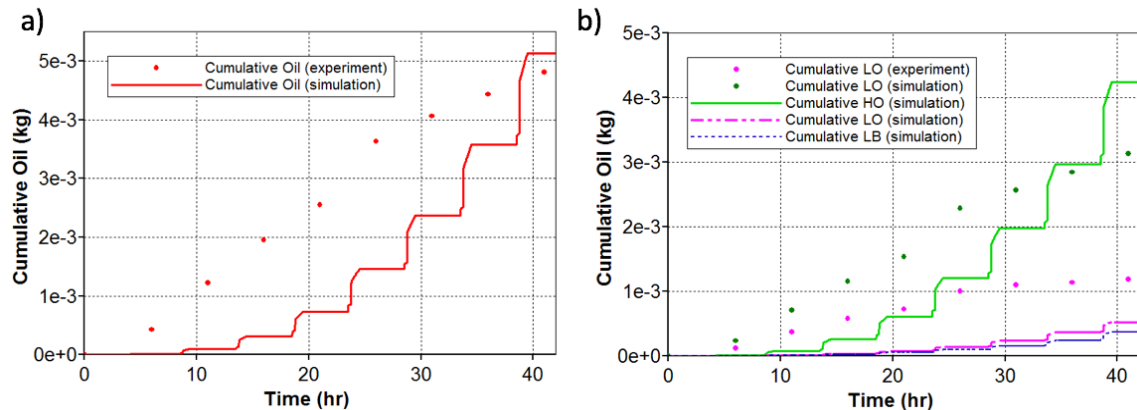


Figure 38. Comparison – (a) cumulative oil production; (b) cumulative HO and LO production

The discrepancies in HO and LO production (35% and 44%, respectively) as can be seen from Figure 38 (b), are due to the changes in their fractions in initial oil saturation. Changes of relative permeability curves during supercritical water injection also remain a challenge. Figure 39 demonstrates the changes in mole fractions for Bit_{liq} over time.

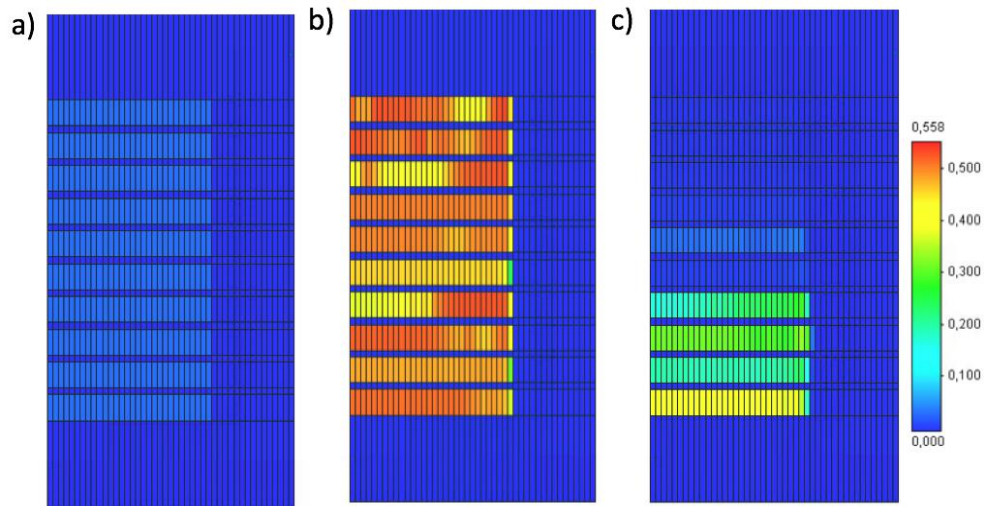


Figure 39. Liquid bitumen gas mole fraction changes over time: (a) initial, (b) after 1.55 h, and (c) after 3.3 h

The history match performed in this research shows reasonable agreement with experimental data. However, we understand that different sets of parameters can result in comparable agreement and multiple solutions are possible. This kinetic model can be enhanced with a greater number of adjustable parameters before its application to a full-field scale. Moreover, kinetic transformations of HO and LO separately in gas and oil phases could lead to a refinement of the model. Nevertheless, the results obtained provide a satisfactory degree of validation, improved methodological approach and they could help to avoid some limitations of the commercial simulator.

5.3 Conclusions

There are various aspects influencing the successful prediction of oil recovery in the EOR technique. One of the significant aspects of thermal EOR is a specification of a

group-model of OM saturation which represents the distribution of organic matter in a target reservoir.

Hydrodynamic reservoir simulation of unconventional field development with thermal EOR techniques requires improved capabilities of the reservoir simulation software. Today, commercial simulation software does not allow description of reservoir OM saturation in thermo-HDS via a complete detailed group-model. The main obstacle is the separation of mobile oil and BHC cannot be represented in thermo-HDS calculations.

Despite the fact that the complete specification of the initial OM distribution in the target reservoir was not realized in numerical experiments, the authors performed HDS with a partial specification of the OM saturation. The noticeable influence of the specification of the distribution of OM groups in the reservoir on the results of calculations and efficiency of thermal EOR (HWI) was determined.

This study demonstrates the development of a complex methodological approach for the enhancement of *in-situ* upgrading process simulation. The focus was on consistent experimental studies of kinetic mechanisms of organic matter transformations and their accurate reproduction in the numerical simulator.

An autoclave experiment, where subcritical water was injected at reservoir pressure, showed significant alteration of geochemical parameters. The numerical simulation subsequently recreated the autoclave experiment. Two cases were tested with different approaches and different types of pseudo-components. The history matched and validated kinetic model can be used later in field-scale modeling to evaluate the influence of the number of components and chemical reactions on the results of forecast calculations of thermal EOR.

The novel methodological approach developed in this paper can result in the advancement of the simulation procedure. This is the first attempt to take into account the fluidity of the solid bitumen and the changes in its mobility at elevated temperatures. The method in the presented form requires refinement to avoid uncertainties during phase changes: permeability modifications in the water-oil system during supercritical water injection, capillary forces, wettability, and upscaling procedure. In perspective, the

parameters obtained in the refined model such as the kinetic model, viscosity correlations, relative permeability curves, and operational parameters can be used in further field-scale modeling.

Chapter 6. High-pressure Air Injection method

6.1 High-pressure air injection on a laboratory scale

The field studied belongs to the North Kinel'sky oil and gas region of the South Tatar oil and gas area of the Volga-Ural oil and gas province. All identified oil deposits are confined to the roofing of the Tournaisian stage. The average depth of the formation according to borehole data is 1339 m. At depths below 1,000 m, the fracture gradient tends to be 15.83 kPa/m that limits downhole injection pressure to 21.4 MPa. The total thickness of the reservoir varies from 2.4 to 16.5 m. The thickness of the oil-saturated part is 1.2-13.8 m. Average porosity is in the range of 11-12% and permeability is in the range of 55 to 95 mD. The crude oil has a gravity of 33.2° API and dead oil viscosity, on average, of 13 mPa.s. Preliminary calculations of the combustion temperature predict low values due to low porosity, relatively oil viscosity, and low reservoir temperature.

This chapter is dedicated to the construction and validation of laboratory-scale numerical models of oxidation experiments to provide a proper HPAI kinetic model for oxidation and combustion reactions and estimate HPAI method feasibility for the Kirsanovsk oil field based on the results of oxidation studies. Before the field tests, physicochemical and thermodynamic characteristics of the process were studied to avoid any risks and uncertainties. The given research was published in ([Khakimova et al., 2020](#)).

6.1.1 Experimental setup

According to the methodology, the development of a thermodynamic model starts from High-Pressure Differential Scanning Calorimetry (HPDSC) and High-Pressure Ramped Temperature Oxidation (HPRTO) laboratory tests. They were carried out to obtain the temperature dependence of the thermal effect and to estimate the oxidation characteristics as a function of temperature. Then a laboratory experiment was conducted to simulate the process of HPAI itself on an MPCT. It allows validation of the kinetic model and technological parameters. This research focuses on the results of the MPCT

oxidation experiment, its further subsequent simulation to provide stoichiometry of the reactions, and field design parameters.

6.1.1.1 High-pressure ramped temperature oxidation

A schematic diagram of the HPRTO setup of the experiment on the oxidation of oil with a linear increase in temperature is given in [Figure 40](#).

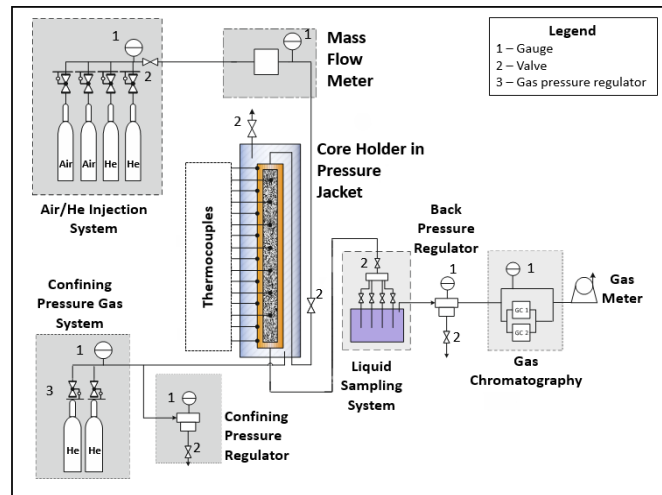


Figure 40. Scheme of the HPRTO setup ([Khakimova et al., 2020](#)).

The HPRTO Reactor is a thin-walled reactor with an outer diameter of 25.4 mm, a wall thickness of 1.65 mm, and a reactor length of 483 mm made of steel grade Inconel. A detailed description of the HPRTO system was presented in the ([Khakimova et al., 2020](#)).

The reactor was vertically installed in a pressure jacket, and the air was injected from top to bottom. The working pressure in the reactor was 12 MPa created by air from a high-pressure cylinder, while helium was injected into the annular space between the pressure jacket and the reactor to create a confining pressure. The start of the pressurization, air injection, temperature rise, other process events, and features of the HPRTO experiment are given in ([Khakimova et al., 2020](#)).

6.1.1.2 Medium pressure combustion tube

The experiment was carried out on the MPCT laboratory setup. The schematic representation of the MPCT installation is presented in Figure 41. The MPCT specification is given in Table 15.

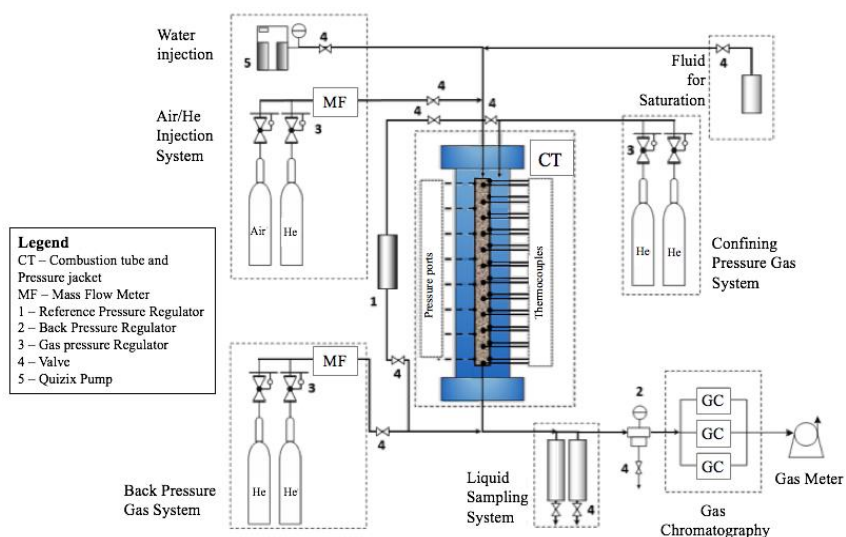


Figure 41. Scheme of the MPCT installation (Khakimova et al., 2020).

Table 15. MPCT specifications

Internal diameter x Length, mm	99.6 x 1837
Reactor volume, l	14.3
Reactor material	Inconel steel
Maximum pressure, MPa	21
Maximum operating temperature, °C	1200
A number of wall thermocouples, pcs.	12
A number of internal thermocouples, pcs.	12
The number of pressure ports in the reactor, pcs.	8

Prior to air injection, helium was injected to pressurize the system, and the first zone was heated up. The air injection started with a rate of 15.34 st./h and the start of temperature rise at a rate of 40°C/h. The end of air injection occurred after 20.44 hours and was followed by a helium injection at a rate of 15.34 st./h and then the pressure was dropped after 31.23 hours. The maximum temperature achieved in zone 1 was 526°C. Temperature profiles demonstrate that the combustion front did not reach the 11th and 12th zones due to the stopping of the air injection. The combustion front velocity with a

temperature of 350°C through zones 3-10 was 18.1 cm/h. The working pressure in the reactor was 12 MPa, the initial temperature was 27°C.

6.1.2 Experimental results

6.1.2.1 High-pressure ramped temperature oxidation

The temperature profiles recorded by axial thermocouples located on the corresponding 7 zones are shown in Figure 42. The negative temperature gradient is visible in the range from 290°C to 350°C. There is a distinct low-temperature oxidation interval, in which low-temperature oxidation reactions dominate for heavy oils, and a high-temperature oxidation interval, in which high-temperature oxidation reactions dominate (sharp temperature profiles). The molar concentrations of oxygen, nitrogen, helium, carbon monoxide, and carbon dioxide are presented in Figure 42. The start of hydrocarbon gas generation begins at about 300°C due to oil cracking, followed by a high-temperature oxidation interval with sharp temperature profiles, which may indicate the burning of the hydrocarbon gases which are formed.

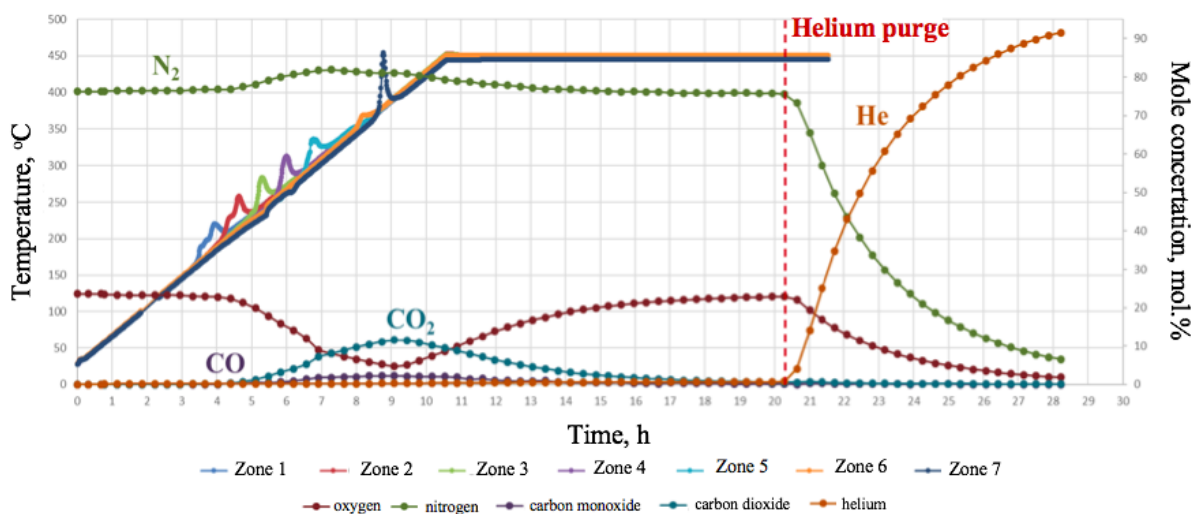


Figure 42. Centreline temperatures by zone gas mole concentrations

An increase in the nitrogen concentration at the production end (start of exothermic reactions) indicates the occurrence of low-temperature oxidation reactions where the air is consumed, and the generation of combustion gases does not compensate

for this consumption. According to the nitrogen concentration curve, the low-temperature and high-temperature oxidation reactions proceed simultaneously along the length of the reactor from the beginning to the end of the oxidation. The decrease in the nitrogen concentration at the outlet corresponds to the start of the high-temperature oxidation interval, which indicates a reduction in the proportion of low-temperature oxidation reactions or, in other words, oxygen addition reactions. The combustion initiation temperature value was determined from the results of the HPRTO experiment over the area of the highest temperature gradient of the first peak and is 160°C.

6.1.2.2 Medium pressure combustion tube

The temperature values for centerline thermocouples for 12 zones are shown in [Figure 43 \(left\)](#). The maximum temperature of zone 1 was 526°C. The first 2-4 zones are usually transition zones. By the time the air supply stopped, the combustion front did not reach the 11th and 12th zones. In zones 11 and 12, the temperatures were 435°C and 278°C respectively, which indicates that residual combustion occurred in these zones. When helium injection began, the heaters were not turned off. This allowed the combustion process to continue due to the air which remained in the model. With the pressure that was created in the experiment, the amount of oxygen (air) remaining in the system at the time of the transition to helium injection was sufficient for residual combustion to occur in the later zones. This process is visible in [Figure 43](#) in the period between 8 and 15 hours from the start of air injection.

After the temperature in the center of the zone reached its maximum, the heater of this zone was set to adiabatic control mode, maintaining the temperature on the core holder wall 20° C lower than the readings of the axial thermocouple. This is the reason for the change in the slope of the temperature profile during the cooling zone.

The velocities for the combustion front were calculated based on the rate of achievement in the zones of the bulk model with a temperature of 350°C. The progress through the combustion tube of the high-temperature combustion front (at a temperature of 350°C) was calculated. The combustion front velocity with a temperature of 350°C through zones 3-10 was 18.1 cm/h. The first two zones were not taken into account since

the front velocity had not yet stabilized and there was a delay in the propagation of the front from zone 1 to zone 2 due to the so-called “Plugs” of mobilized oil.

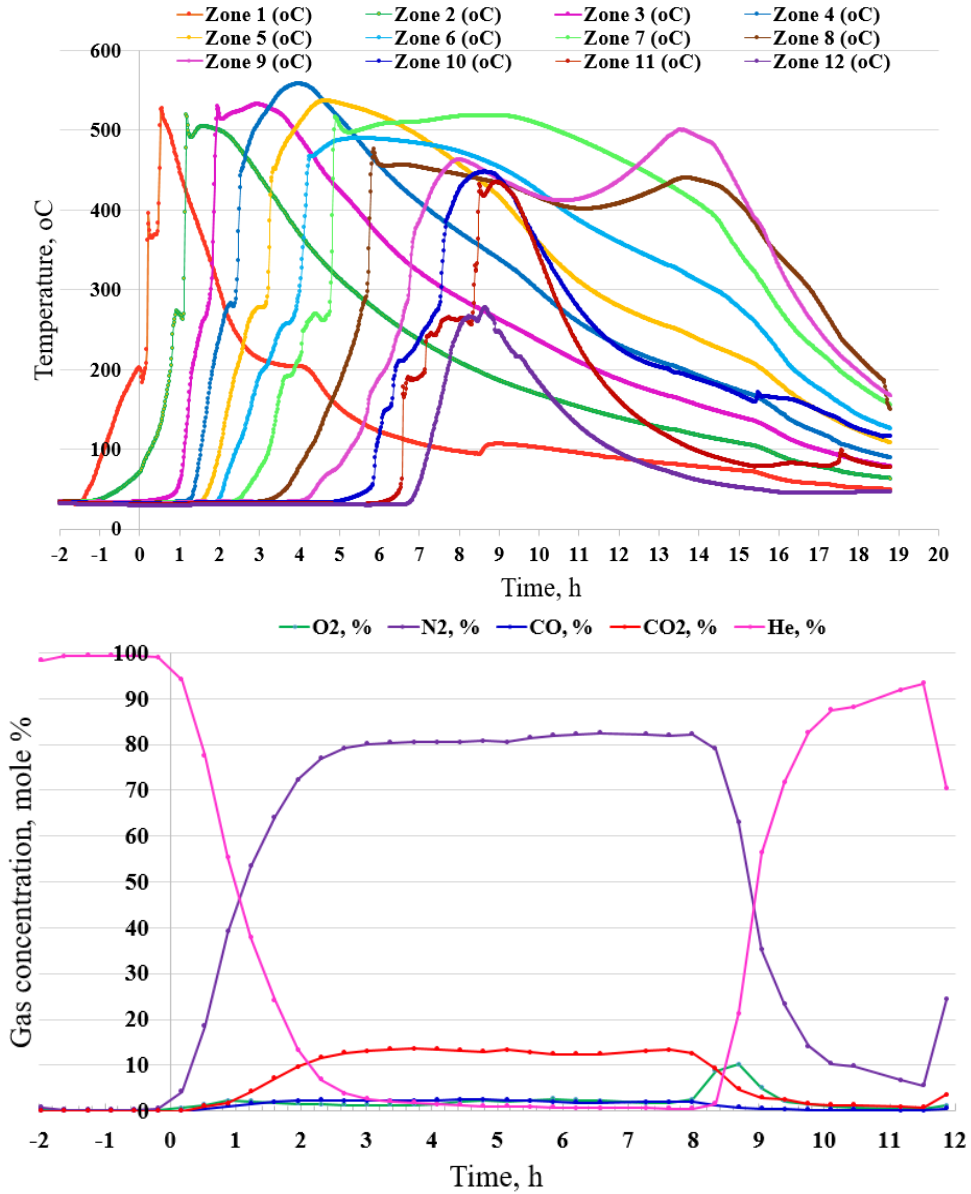


Figure 43. Temperature profiles on the centreline (top); Combustion gas mole concentrations (bottom)

Figure 43 (bottom) shows the molar concentration of oxygen, nitrogen, helium, carbon monoxide, and carbon dioxide. An increase in the yield of propane, n-butane, and other hydrocarbon gases occurred at the time of initiation of combustion which

corresponds to the zone of low-temperature oxidation. Another explanation of this effect is that at the initial stage of the combustion front, it does not capture the entire zone, but only some part of it. Accordingly, hydrocarbon gases were removed from these uncovered parts of the zone by the high-temperature oxidation process. The increase in nitrogen concentration at the reactor output occurred after the start of the combustion process. According to the composition change in [Figure 43 \(bottom\)](#) in the interval from 2.5 to 8 hours, stabilization of the component composition of gases leaving the MPCT was observed, which corresponds to the steady-state combustion mode.

6.1.3 Numerical modeling of the HPAI experiments

6.1.3.1 High-pressure ramped temperature oxidation numerical model

The digital model of the HPRTO experiment setup was constructed in the CMG STARS commercial simulator. The characteristics of the layers are specified considering the design of the experimental setup, which consists of a reactor, a steel wall, microfiber insulation, a copper part, and ceramic heaters. The thermophysical parameters were calibrated so that the actual temperature on the wall of the HPRTO coincided with the temperature of the corresponding layer in the numerical model. More details can be found in the paper ([Khakimova et al., 2020](#)).

6.1.3.2 Medium pressure combustion tube numerical model

A numerical model of the MPCT experimental setup was built to adapt the model of chemical reactions and kinetics of oxidative processes. It consists of 11 grid blocks in the radial direction, one block in the azimuthal direction, and 45 blocks in the vertical direction ([Figure 44](#)). Each of the 12 temperature zones is divided into three cells, the size of which is sufficient to represent the combustion process in the tube. However, in the first zone, an additional cell of much smaller size was added, into which air is injected. This is necessary so that the injected air enters the beginning of the combustion tube, and not into the center of the first cell.

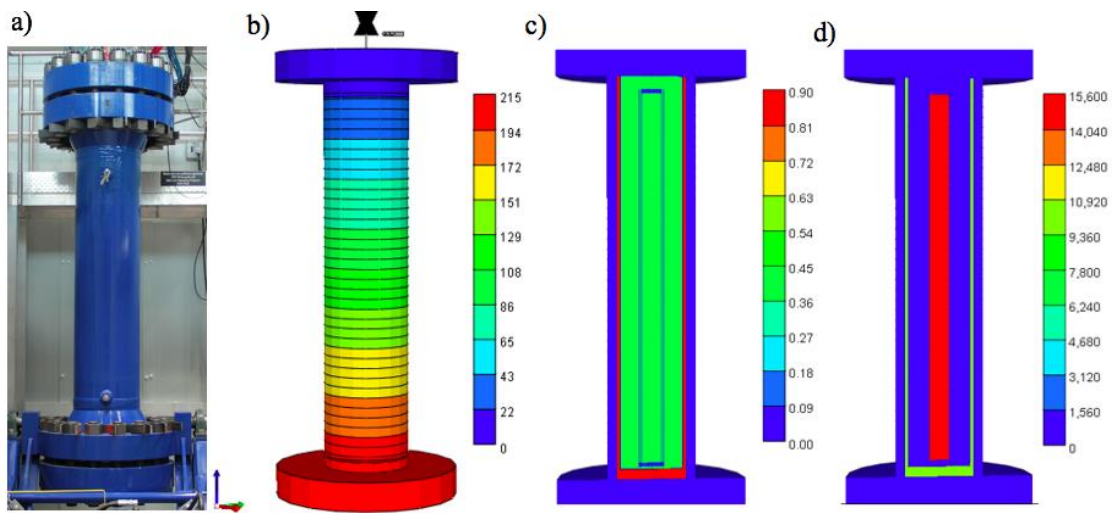


Figure 44. (a) MPCT equipment and its digital model in CMG STARS: (b) model grid, (c) initial porosity distribution, (d) initial permeability distribution

All layers of the combustion tube installation, including heaters installed from the outside, are reproduced in the numerical model of the experiment. The central cells represent a rock sample (1-3), the steel pipe wall (4), insulation (5), which consists of mineral wool, heating elements (6), insulation consisting of pyrite and helium (7), steel wall (8), an annulus filled with helium (9), and a pressure casing made of steel (10-11). The filtration-capacitive characteristics of the layers and the geometry are specified, taking into account the design of the experimental setup.

It was discovered that a full representation of the geometry of the pipe can lead to a reproduction of chemical transformations, as well as physical phenomena such as heat transfer and heat loss. Due to this, cells were added between the large steel flange and the flange covering the core holder and corresponding cells at the end of the core holder. The space around the core holder is filled with helium and pyrite, and the space between the steel cover and the pressure jacket is filled with helium.

The average values of heat capacity and thermal conductivity from the Kirsanovsk oil field were obtained during experiments carried out in the Skoltech laboratory and

further used in simulations. Thermal properties for other layers and types of materials were taken from Belgrave’s model.

There are some crucial factors affecting the performance of the numerical simulation of combustion tube tests: sensitivity of the model on the system parameters; a recreation of the properties of the combustion tube multilayer design; work of the heaters; reproduction of the processes preceding the air injection. A detailed description of the geometry replication process is presented in the article (Khakimova et al., 2020). The porosity and permeability characteristics of the layers and their sizes were established taking into account the design of the experimental setup and given in Table 16. Figure 45 (left) shows the scheme of the MPCT setup and Figure 45 (right) shows the schematic representation of the tube cross-section. More details on the model properties can be found in the article (Khakimova et al., 2020).

Table 16. The porosity, permeability, and diameters of the tube layers

Layer	Diameter, mm	Material	Porosity, %	Permeability, mD
1.	100	Rock	40	15600
2.	102	Steel	0	0
3.	120	Mineral wool	45	100
4.	164	Steel	0	0
5.	254	Porous thermal insulation + He	45	1000
6.	260	He	99	10000
7.	406	Steel	0	0
8.	620	Steel flanges	100	0

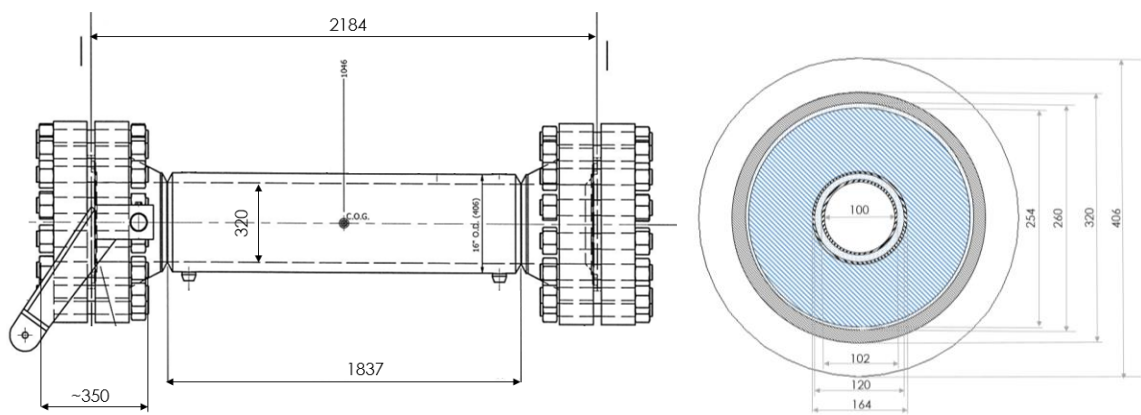


Figure 45. MPCT setup diagram and its cross-section

The numerical model created employs a comprehensive mathematical formulation that is capable of representing the major phenomenological effects observed in near-adiabatic combustion tubes such as mass-heat transfer, taking into account the properties of the medium, convection, delay, heat losses, and the secondary reactions (support of the reaction). The imperfect shape can be explained by the uniformity of the packing or/and due to combustion front "slip" and delay of the burning process.

The operation of the guard heaters causes significant convective circulatory movement to occur in the pressurized annulus of the combustion tube, which influences the temperatures measured in the sand pack. They depend on: operating pressure; Raleigh (or Grashof) number of the gas in the annulus; on-time of the heaters in response to the combustion front. There is a need to consider the radial and external heat transfers if high-pressure combustion tube tests are to be correctly interpreted and/or modeled. Combustion tubes of different designs, operated under identical conditions can produce different experimental results.

The next important aspect of adaptation of the model is the initialization of the model and reproduction of the injection conditions: 1) establishment of the initial temperatures in the cells; 2) accounting for the heat loss; 3) gradual increase of the pressure in the system by the preliminary pumping of helium into the system; 4) initiation of combustion; 5) maintaining the necessary temperatures with the heaters during the experiment; 6) switching to helium and the gradual release of pressure in the system.

The 1.83 m long combustion tube consists of 12 heating zones each 15.24 cm long, and the heaters are physically located on the heater support column at $j=4$. Each heating zone consists of a thermocouple inserted into the tube center, a thermocouple mounted on the exterior tube wall, a 1 kW wire-type heating element (HR_{nn}) wrapped around the heating zone. There is a 1.8 cm layer of mineral wool insulation wrapped around the tube and held in place by thin metal cladding. The center and wall thermocouples are located at the axial midpoint of each heating zone which is reflected in the numerical model.

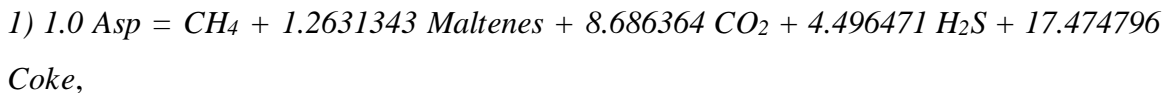
Heat loss coefficients to the surroundings are introduced, the ambient temperature of each cell including the initial heater temperature set as 26°C. The heaters distribute 1000 W of heat over three grid blocks per heater and they were set to adiabatic control, maintaining the temperature on the core holder wall 20°C lower than the indicators of the central thermocouple. That allows the reproduction of the angle of inclination of the temperature profile during the cooling of the zone.

6.1.4 HPAI numerical simulation results

6.1.4.1 Fluid and kinetic model for Kirsanovsk oil field

There have been several reaction combustion schemes published in the literature (Belgrave *et al.*, 1990; Sarathi *et al.*, 1999; Barzin *et al.*, 2010; Yang *et al.*, 2016). All of these schemes are similar in terms of reaction types in that they have low-temperature oxidation, thermal cracking, and high-temperature oxidation contributions. However, the schemes differ due to their definitions of pseudo-components. In this research, the following reaction scheme by (Belgrave *et al.*, 1990) was chosen.

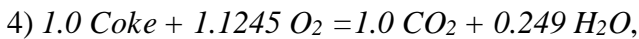
Thermal Cracking:



Low temperature oxidation:



High-temperature oxidation:



Based on this reaction scheme, the target oil was characterized by using three pseudocomponents: maltenes, asphaltenes, and coke. Description of the fluid model includes PVT properties of components in a mixture, k-value correlations, summarized in the article (Khakimova *et al.*, 2020). Oil saturation of the model was 73.9%, water saturation 11.1% and gas saturation 15%. Asphaltenes mole fraction was 0.005.

The history-matched Arrhenius kinetic parameters are summarized in Table 17.

Table 17. Kinetic parameters obtained from the history match

Reaction	A, 10 ⁹	E _a , kJ/mol	H _r , kJ/mol
1	2,760 hr ⁻¹	181.041	0
2	0.4 hr ⁻¹ kPa ^{-0.4246}	86.73	5.874*10 ²
3	9.01 hr ⁻¹ kPa ^{-4.7627}	185.6	3.14*10 ³
4	7.00 hr ⁻¹ kPa ⁻¹	34.763	4.71*10 ²

6.1.4.2 MPCT: history matching

The numerical modeling of the MPCT experiment and optimization process was carried out in the thermal hydrodynamic simulator CMG STARS. The model of chemical reactions and kinetics were history matched by varying the kinetic parameter (in particular, the pre-exponential factor in the first reaction), and the operation regimes of the heaters. Heat losses and thermal properties of certain layers were adjusted during this process to achieve the best match. Relative permeability curves have a significant impact on the results of the combustion tube simulation and are the essence of the adaptation of the model according to the results of the experiment. Figure 46 shows a comparison of temperature fronts of several zones.

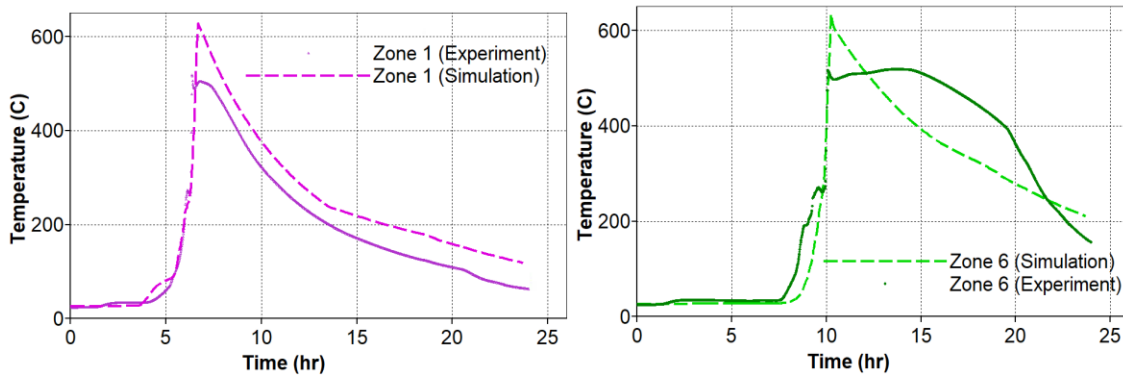


Figure 46. Temperature profiles: Zone 1 (left); Zone 6 (right)

Figure 47 presents the yield of molar concentrations of CO₂ in the experiment and numerical simulation and the yield of O₂ molar concentrations, as was observed in HPRTO.

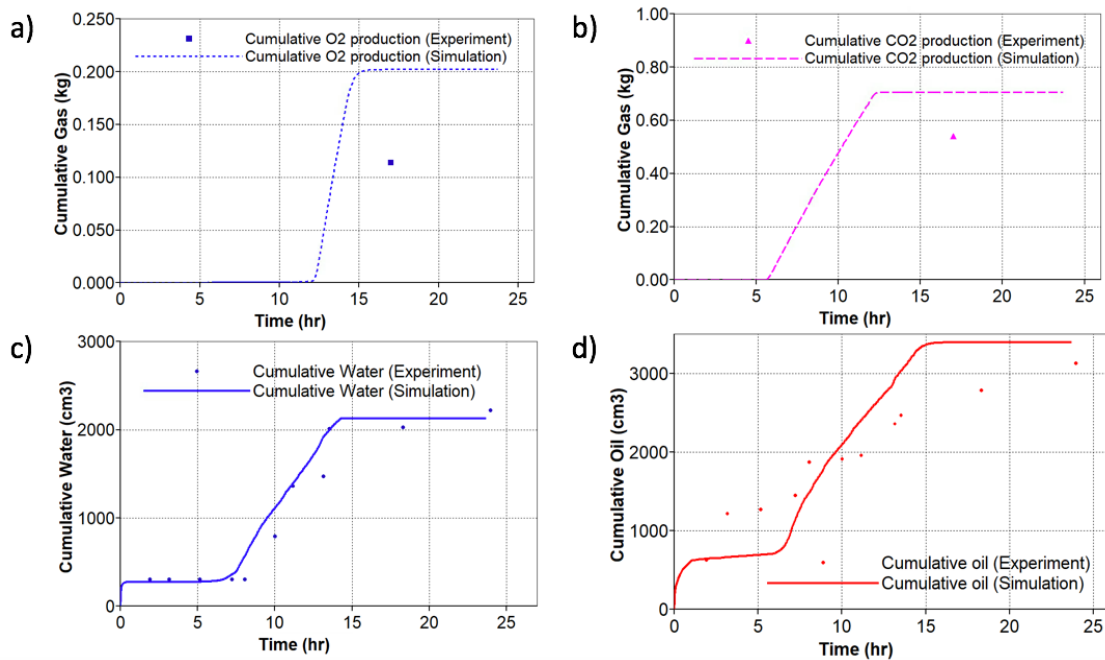


Figure 47. (a) Cumulative O₂, (b) CO₂, (c) water, and (d) oil production for experiment and simulation

Also, Figure 47 shows the dynamics of oil yield and the comparison of cumulative oil production for the experiment and numerical simulation. Figure 47 (right) shows the dynamics of water production and a comparison of the accumulated water production for the experiment and numerical simulation.

The first 5 zones show good agreement between the experimental curves and temperature profiles obtained in the simulation. The shape of zones 6–9 for modeling differs from the experimental curves, but the beginning of the combustion front coincides. This may be due to the combustion front "slip" and delay of the burning process. In Zones 7 and 8, a similar process is observed, in which a sharp drop in temperature turns into a smoother curve. In zones 10 and 11, it was possible to repeat the shape of the curves, and the peak temperature in zone 11. In Zone 12, the curve obtained by numerical simulation lags behind the experimental values, indicating a higher heat loss in the model. Table 18 shows the material balance of oil and water for the experiment and numerical simulation.

Table 18. Mass of the products for the experiment and simulation

	Experiment	Simulation
Mass of oil obtained, g	2564.26	2485.64
Oil burned, g	220	224.62
Mass of CO ₂ , g	544.59	820
Mass of O ₂ , g	114.4	0.45
Mass of water obtained, g	2220.9	2250.9
Air injected, g	799.81	794.5
Air consumed, g	688.8	681.5

Generally, there is a lack of commonly accepted standards in terms of simulation modeling. There are no universal hard rules available in the literature due to the complexity of the problem. In addition, the requirements vary depending on the objectives, desired accuracy, and time/budget of the particular reservoir. History match tolerance depends upon drive mechanisms and related key parameters, reservoir characteristics, study objectives, and data quality. Simple measures should be determined to assess the suitability of the developed model. For example, withdrawals for oil, water/gas rates, and cumulative volumes should be matched (Baker et al., 2006).

The resulting model gives a good agreement of the temperature profiles in all zones, an excellent agreement with the experimental values of the accumulated water and oil, and in the total oxygen consumption is obtained. The match for mass of obtained oil, water, burned oil, air injected and air consumed is within 3 percent. There is a discrepancy in the mole concentrations of O₂ and CO₂, and in the total oxygen consumption, which emphasizes the necessity of further investigation of phase transition behavior of target oil and basic chemical reaction model. However, this model repeats general features of the MPCT experiment (temperature peaks, front velocity, cumulative oil, and water), which are the most important characteristics of the oil recovery process by high-pressure air injection and could be tested in the full-field model.

6.2 Numerical simulation on a field-scale

It is crucial to avoid risks and take into account all the uncertainties that might arise during the pilot project. Thus, the physicochemical and thermodynamic characteristics of the process were also studied in this chapter. The methodology with consequent physical and numerical simulation of HPRTO and MPCT laboratory tests was applied to obtain the temperature dependence of the thermal effect and to estimate the

oxidation characteristics as a function of temperature. The details on the evaluation of the feasibility can be found in (Askarova et al., 2020a).

Results from numerical modeling of laboratory-scale oxidation experiments were further used during field-scale simulation to estimate the performance of the HPAI method. The field is a single-layer with seven oil deposits discovered in the formation of the Tournaisian stage of the Lower Carboniferous. The field is classified as simple by the degree of complexity of the geological structure. The gravity of the crude oil is 33.2° API. An average oil saturation is 75%. Other main characteristics of the individual subsections are presented in Table 19.

Table 19. Characteristics of the model

Characteristics	Subsection 1	Subsection 2	Subsection 3	Subsection 4
Number of active grids	20,486	40,434	14,447	13,327
Porosity, %	11.2	12	12.1	12.1
Permeability, mD	59	84	94	82
Pore volume, m ³	8,342,974	16,288,440	6,446,607	5,581,886
Initial geological oil reserves, m ³	781,532	2,405,516	1,365,192	1,087,928

The hydrodynamic model for HPAI simulation was created in CMG commercial software. The distribution of oil saturation is shown in Figure 48 where 4 subsections of interest were distinguished.

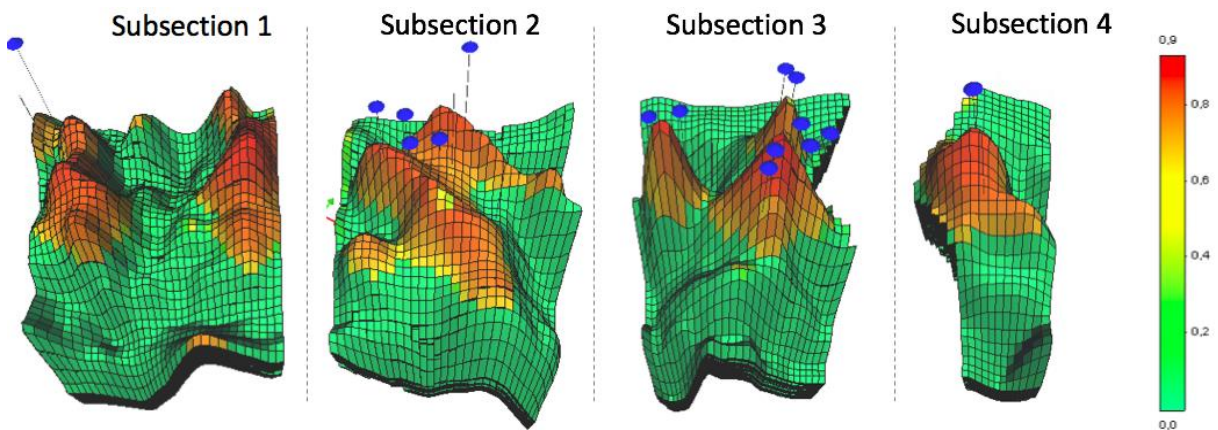


Figure 48. Oil saturation distribution of different subsections

Commonly, objective functions are selected to estimate the degree of discrepancy between the calculations by different sizes of the grid blocks. Stability analysis of the

large-block model serves as a base and then the thermophysical, chemical, and filtration parameters can be selected. According to the history matching of the MPCT experiment performed earlier, the pre-exponential Arrhenius parameters and relative permeability curves were obtained. These kinetic reactions and pseudo-compositional model (see [Sec. 5.4](#)) were transferred to the sector model. Four scenarios of field development were examined to evaluate the efficiency of air injection on individual subsections. The scenarios include 1) Primary recovery method (without injecting water or air); 2) Air injection; 3) Water injection; 4) Simultaneous injection of air and water. In all scenarios, production wells were launched with fluid production control - 50 m³/day and with a bottom hole pressure limitation - 2 atm.

Recent advances in air-injection based projects have allowed this method to be considered more seriously as a promising method for recovering heavy oil. It is believed that when the process is carried out correctly, the *in-situ* combustion method reduces the density and viscosity of the oil, while not producing complex emulsions. At the same time, operating costs per cubic meter of oil produced is lower due to higher well production rates and lower cost of working fuel.

Methods for assessing the financial and economic efficiency of an investment project, taking into account the time factor, involve bringing costs and incomes, spaced over time, to a base point in time, for example, to the date of the start of the project. The most important parameters are the capital cost of the wells, the additional cost of compressed air, and the discount rate. It is very important to consider the possibility of reducing capital investment and provide a scheme with sufficient spacing between the wells.

The main difference between air injection into the reservoir is the absence of costs for the transportation and storage of air, and the absence of costs for the purchase of air. However, it is important to consider the capital and operating costs of air compression and injection. The oil debit, the total well stock, the size of land plots for a given number of wells, and the volume of oil were determined by numerical modeling. The volume of oil is determined by taking into account the amount of oil produced, the rate of

technological losses, and its consumption for the process, and the coefficient of change in oil production. Further, development indicators were calculated for each scenario, including active wells, cumulative oil, water, and liquid production, oil recovery factor, water cut, injected volumes of water, and air. That allows further economical assessment and a decision was made based on these results.

The performance of each subsection is presented in Figure 49. Subsection 1 demonstrates promising predictions for Scenario 2 and Scenario 4, with 9% and 10% additional cumulative oil production respectively, in comparison with Scenario 3. Meanwhile, the high-temperatures in air-injection well cross-sections indicate combustion existence in Subsections 2 and 3 (see Figure 49, c, d).

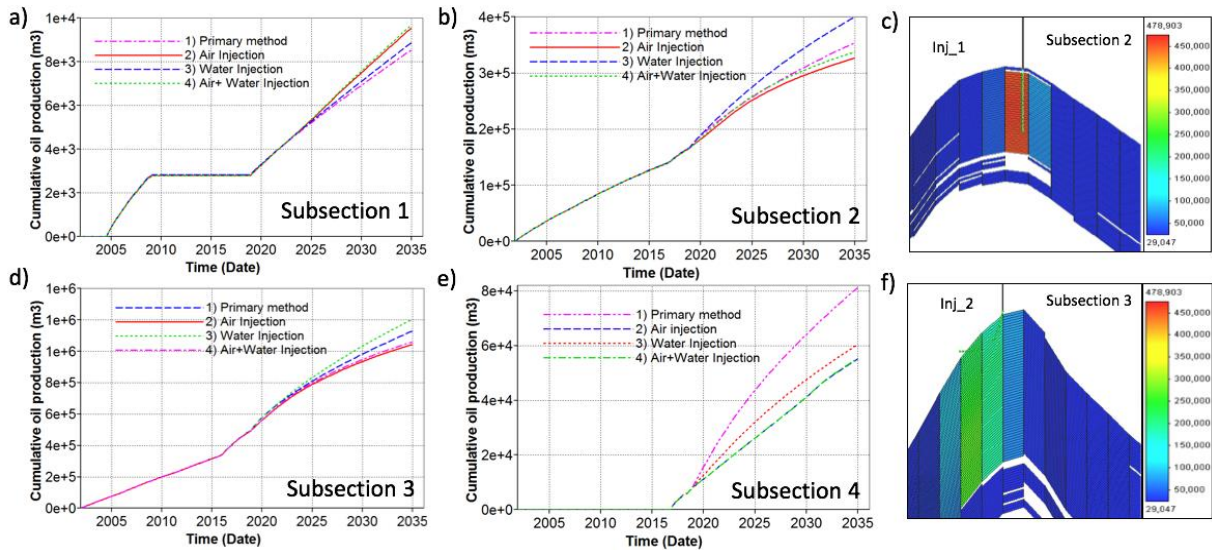


Figure 49. Cumulative oil production for 4 subsections (a,b,d,e) and temperature profiles for scenario 2 in subsections 2 (c); subsection 3 (f)

However, the amount of oxygen is insufficient to maintain the required pressure at a distance of more than 50 m from the well in Subsections 2, 3, and 4 due to insufficient injectivity of the injection wells. Combustion stops and air breaks into the producing wells. In the calculations for Scenario 2 and 4, restrictions were placed on the producing wells with respect to oxygen (shutting down the wells when the concentration of O_2 reached 2%). In the long run, the water injection and primary production demonstrate a better efficiency and more profitable with the given development system of Subsections

2, 3, and 4. It should be noted, the efficiency of water injection is overestimated, since in practice it does not show such effectiveness. Lack of water availability is another drawback of Scenario 3.

Further Subsections 2 and 3 were dealt with in detail to find the optimal injection scenario and to achieve the ultimate oil production. However, only the rearrangement of Subsection 3 (see Figure 50) demonstrated the effectiveness of air injection-based methods as to water injection.

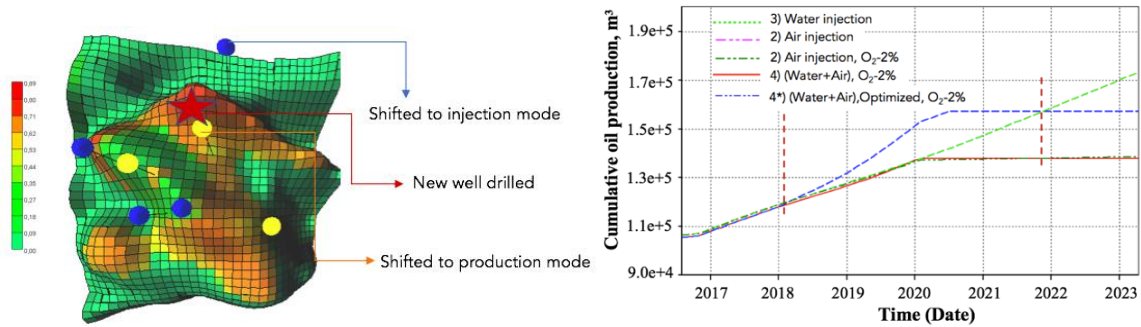


Figure 50. Optimization scenario (left) and cumulative oil production (right) for Subsection 3 before air breakthrough

The development system of this uplift was changed as follows: 1 well (yellow) was shifted from injection mode to production, another well (blue) from production to injection mode, and an additional well was drilled. See Figure 50 (left). In this case, an option with water + air injection is more effective than the option with water injection until 11.2021 m^3 is reached. See Figure 50 (right). The results showed that by optimizing the development system, it is possible to increase the efficiency of field development. The economical factor should play a key role in the identification of the best solution. The effectiveness of Scenarios 1 and 3 in these models is due to the high ratio of gas and oil mobility provided by relative permeability tables in the oil-gas system.

This chapter focuses on an assessment of the HPAI recovery technique feasibility for the target field. It was done through subsequent laboratory-scale HPRTO and MPCT experiments and their further 3D numerical modeling. A kinetic model of reactions occurring during combustion was validated against experimental results. Adapted fluid

model, relative permeability, kinetic model, and operational parameters obtained during the numerical simulation were used for the field upscaling.

Four different Scenarios were proposed and calculated for four individual subsections of the field. In Subsection 1 Scenario 2 adds 4% and Scenario 4, in its turn, adds 10% to cumulative oil production in comparison with Scenario 3. Injection of air into the reservoir does not lead to an increase in oil recovery in the long run for subsections 2, 3, and 4, due to rapid breakthroughs of air into producing wells within 3-4 years (oxygen concentration limit is 2%). For Subsection 3, the optimization with transferring injection well for into production, and production well into injection mode, as well as drilling an additional well, can lead to higher oil production (+16 %) until 2021 (after which production wells are shut off due to air breakthrough).

At present, the relative permeability curves in the oil-gas system, possible air breakthroughs into production wells, injectants (water and air) availability, and their costs are considered to be the main uncertainties greatly affecting the results.

6.3 Conclusions

In this chapter, an assessment of the feasibility of the HPAI recovery technique for the target field was carried out. Subsequent laboratory-scale HPRTO and MPCT experiments, and their further 3D numerical modeling were performed. The 3D numerical model of MPCT experiments has a multilayer design and proper heating regimes, which allowed us to avoid constructional uncertainties. As a result, the methodology that can combine laboratory and numerical modeling of the HPAI process as a possible EOR technique for Kirsanovsk oil at reservoir conditions was developed and applied. This approach helps provide a proper kinetic model for one of the existing reaction schemes of oil combustion, which could be used as a start model in full-field simulations. Indeed, numerical simulations gave a satisfactory correlation with experimental results: oil recovery factor – 0.89, oxidation front velocity - 18.1 cm/h, and optimal airflow rate – 220 st.m³/m³ in the MPCT experiment. However, the modeling of the HPRTO experiment did not give such a good correlation with experimental results. This was because during the HPRTO experiment displacement of oil and filtration effects

are negligible in comparison to the oil phase transition and oxidative behavior. A kinetic model of reactions occurring during combustion was validated against experimental results. Adapted fluid model, relative permeability, kinetic model, and operational parameters obtained during the numerical simulation were used for the field upscaling.

Four different field-wide development scenarios were considered to maximize oil production. The methods were tested on existing wells over 30 years and compared to assess the performance of air injection: primary recovery, air injection, water injection, and simultaneous injection of water and air. High temperatures in air-injection well cross-sections indicate the existence of combustion.

Injection of air into the reservoir does not lead to an increase in oil recovery in the long run for Subsections 2, 3, and 4 due to rapid breakthroughs of air into producing wells within 3–4 years (oxygen concentration limit is 2 %).

The number of problems and uncertainties raised during up-scaling were: relative permeability curves in the system gas-oil, a lack of sufficient air injectivity in part of the reservoir, relatively low porosity, pay zone thickness, and current well pattern.

The following recommendations were provided to Zarubezhneft: 1) Any pilot testing of air injection should monitor injection pressures and rates for changes in air injectivity due to concern about liquid blockage; 2) Nitrogen injectivity tests should be performed in several wells to support current geological characterization and gas-oil relative permeability to gas.

A numerical model of the combustion tube in this thesis employs a comprehensive formulation that is capable of representing the major phenomenological effects observed in near adiabatic combustion tubes such as mass-heat transfer taking into account the properties of the medium, convection, combustion delay, heat losses, and the support of secondary reactions. The model also takes into account the operation of guard heaters that causes significant convective circulatory movement to occur in the pressurized annulus influencing the temperatures measured in the sand pack. The numerical model validated against experimental results was further upscaled taking into account the areal heterogeneity, displacement effectivity due to low air injectivity,

convergence difficulties caused by high residual oil saturation, and high critical water saturation in the same grid block.

Chapter 7. Forward and reverse *in-situ* combustion

ISC is a very promising EOR method for improving the oil recovery factor for heavy oil fields and it is believed to be one of the most effective (Barzin et al., 2013; B. Chen, 2012; Gutiérrez, D. et al., 2012). Broadly, underground combustion might embody many different related techniques; however, forward combustion attracted the most attention (Gates C.F. and Ramey H.J., 1980; Moore, R. G. et al., 1996; Speight, 2013) In this method, energy and material transport are provided through porous media. The heat and combustion gases reduce the viscosity of the driven oil, which consequently increases its mobility. There are two types of combustion distinguished, depending on the movement of the hot front: forward and reverse combustion. (Perry et al., 1960; Speight, 2013)

The work presented in this chapter is devoted to a unique set of forward and reverse combustion tube (CT) experiments to gain insights into the kinetics and the physics of the process and to predict the performance of the ISC method for the light oil carbonate reservoir (Askarova et al., 2020b). The importance of the research is related to the application of reverse combustion that is generally believed to be unprofitable. However, reverse combustion might have advantages over forward combustion under certain conditions or might serve as a reservoir preheating technique. Field application of the process hinges on the existence of adequate air permeability and the rate of the reaction under reservoir conditions. These experiments give the opportunity to build and validate the numerical models of forward and reverse combustion conducted at reservoir conditions and test their field application using different scenarios.

7.1 Experimental study of forward and reverse combustion

Experimental forward and reverse combustion tube tests were conducted on HPCT using restored state core samples from the light carbonate oil field. The core materials were prepared by cleaning the core in the modified Soxhlet-type extractor, dried, and fired overnight in an oven at 350°C to remove the residual hydrocarbons. The clean cores were crushed to sand-like particle size and sieved to remove fine material. An

oil sample with 30° API for the test was also selected from the reservoir and centrifuged to remove water.

The objective of the dry forward and reverse combustion tube experiments using a 100 mm HPCT system was to investigate and compare the *in-situ* combustion behavior in the two different process configurations. The tests were performed at a pressure of 27.2 MPa (4,000 psia) using synthetic air (21.28-mole percent oxygen, the balance being nitrogen) at an air injection flux of 40.4 m³(ST)/m²h at ignition temperature 175°C. The first three zones of both forward and reverse tests were heated to ignition temperature to initiate the process. Figure 51 below shows a schematic diagram of the HPCT experimental setup where forward and reverse combustion tests were conducted.

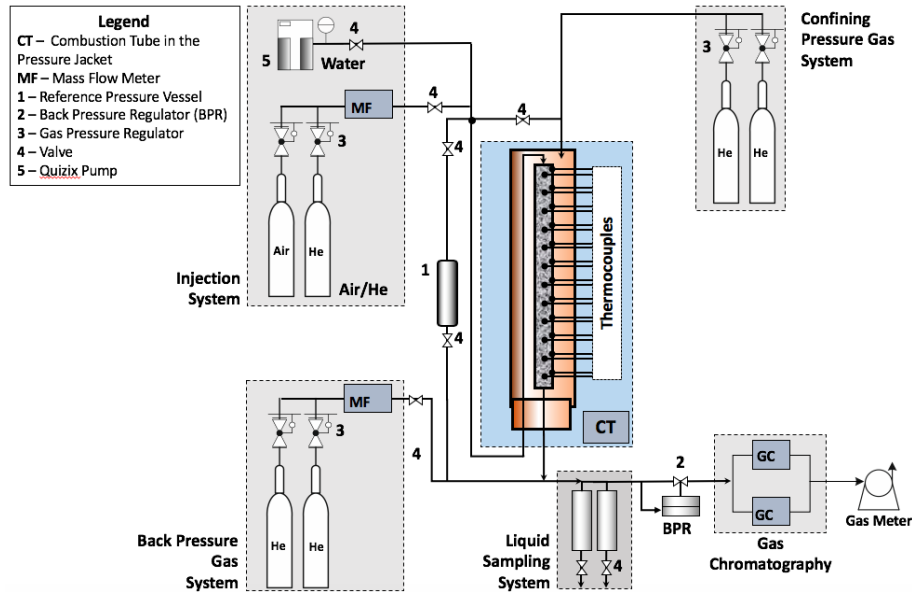


Figure 51. High-pressure combustion tube experimental setup

The combustion consists of a sand pack in a thin-walled tube, thermal insulation, heater support column, electrical heaters, and thermocouples in the center of the sand pack, as well as wall-thermocouples (Sibbald, L. et al., 1998; Smith and Perkins, 1973). The system of heaters and thermocouples were implemented to avoid radial heat loss and to ensure that the process is not driven by heater regimes. After the packing, the tube was sealed, insulated, and placed into the high-pressure jacket. The tests were carried out on

the same experimental setup, and under the same conditions except the fact that during the reverse combustion test the air was injected from the bottom. In this case, the end zone was heated and the combustion zone moved in the opposite direction to the airflow. It should be noted, that the test configurations were selected to minimize the number of equipment parameters that were changed. According to our assumptions and published literature (Lasaki et al., 1985; Onishi et al., 2006) the dominant mechanisms during the ISC process are not the flue gas flooding or gravity segregation, but a thermal effect. The input parameters of both experiments are summarized in Table 20.

The work was conducted using the oil samples from the reservoir under study and restored state core at the reservoir pressure and conditions that would be encountered in the field. After packing, the tube was sealed, insulated, and inserted into the pressure jacket. Air was passed through the packed core, then a vacuum was applied. Then the pack was saturated with brine and the porosity was determined (approximately similar for both experiments). Brine was further pumped to measure the pack’s permeability. It is difficult to establish the same values during the experiments, but permeability variation is believed to be not very significant for the combustion process. Also, during numerical experiments, the exact conditions on the validated numerical model can be recreated. The actual value of permeability has very little effect on the mechanics of the combustion process. The only requirement for permeability is that it must be adequate to permit air injection at a pressure compatible with overburden at an acceptable compression cost. (Sarathy, P.S., 2016) As mentioned in (Perry et al., 1960), permeability variation should not be high, but it is not critical as in water flooding.

Table 20. Input parameters of forward and reverse combustion tube tests

	Forward combustion	Reverse combustion
Number of zones	33	
Tube diameter	100 mm	
Pressure	27.2 MPa	
Air Injection Flux	40.4 m ³ (ST)/m ² h	
Ignition Temperature	175°C	
API	30	
Porosity	45.4%	43.2%
Permeability	33.6 Darcy	19.5 Darcy
Reservoir Temperature	100 °C	

The average molecular weight of original oil	217 g/mol			
	Before Pressure Up	At the start of Air Injection	Before Pressure Up	At the start of Air Injection
So	70.3	66.5	71.3	69.0
Sw	29.7	33.5	28.7	31.0
Asphaltenes mass fraction	11.93%			
Sulfur content	0.47			
H/C ratio	1.81			
Air injection	Top-down		Bottom-up	
Oil viscosity	89/55/27 mPa·s at 15°C/25°C/40°C			
Original oil density	0.8795/0.8725/0.8615 g/cm ³ at 15°C/25°C/40°C			
Time of helium purge: hours after the start of air injection	8.8		5.5	

These experiments were conducted to obtain the information regarding the stoichiometry and implement field design parameters, analyze the combustion front, product gas composition, and temperature profiles.

7.1.1. Experimental part

7.1.1.1 Forward combustion

The core holder of the HPCT equipment was oriented vertically, the air was injected top-down, and fluids produced during the experiment were collected at the bottom of the tube. Water was initially injected at 1.0 ml/min to pressurize the system and was terminated shortly after the start of air injection. The core was preheated to the reservoir temperature of 100°C. As was already mentioned, the first three zones (first 15 cm) of the combustion tube were preheated to the ignition temperature of 175°C one hour before the start of air injection. When the ignition temperature was achieved, synthetic air was injected into the top inlet of the core. The start of the temperature rise can be observed in Zones 2 and 3 indicating the start of the ignition after 40 minutes of air injection. The combustion tube was on adiabatic control where wall temperatures were set to track the core temperatures within 5°C to minimize heat losses.

7.1.1.2 Reverse combustion

The configuration of the reverse combustion is similar to forward combustion and the core holder was also oriented vertically. However, the air was injected from the bottom up. Both ignition and production were carried out from the top. In this such case,

the injected air flows towards the preheated end of the tube. Water is injected with the same flux as during forward mode and the core is gradually preheated to reservoir temperature. The pressure fluctuations were observed during the first hour that resulted in an alteration of the air injection rate. Further, it stabilized at the above-noted designed injection rate, the air reached the top end of the core where ignition zones were located.

The system was maintained in near-adiabatic mode to track the core temperatures within 5°C as in the forward combustion experiment using the heat supplied externally. Thus, the radial temperature gradient in any plane normal to the axis of the tube approaches zero. Initially, the tube was at reservoir pressure and temperature, except at one end where it was heated to a predetermined “ignition” temperature. When the prescribed ignition temperature was achieved, the air was injected from the “cold” end of the tube (in the case of the reverse combustion test). As the oxygen in the air stream contacted the hot oil, a localized exothermic reaction occurred. The generated heat was conducted and convected away from the reaction zone so that definite temperature and concentration profiles were rapidly established and moved uniformly in the direction opposite of that of airflow.

The reverse combustion front advanced downward through the core in the opposite direction to that of the injected airflow. At 5.6 hours after the start of air injection the leading edge of the high-temperature front reached Zone 30, air injection was terminated and helium was injected at the same rate as the air. Wall heaters were not turned off when the helium purge was initiated, enabling the continuation of the burning process by consuming part of the air that was stored ahead of the combustion front. The helium injection continued for 7.38 hours and then the system was bled down. Liquid production was intermittently collected for later analyses; also online gas composition analysis was carried out.

7.1.2. Experimental results

7.1.2.1 Forward combustion

The centerline temperature profiles for each zone of the combustion tube are presented in [Figure 52](#) including the processes preceding the air injection (marked as “Air

on”). The heating of the three ignition zones started 1 hour before the start of the air injection.

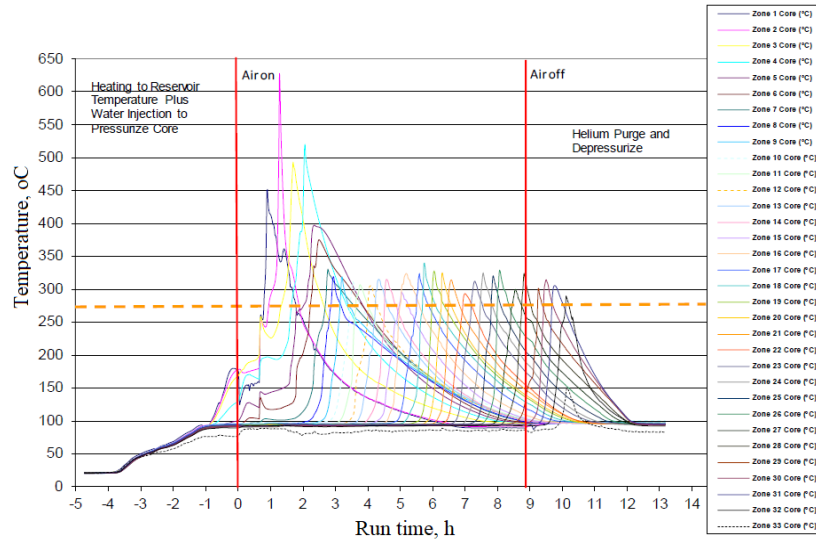


Figure 52. Forward combustion test temperature profiles

The first six zones demonstrated the maximum peak temperatures in comparison with other zones and ranged from 375°C to 626°C. The air injection was terminated after Zone 28 reached 324°C. However, the following four zones (29, 30, 31, 32) displayed temperature levels similar to upstream zones due to continued combustion with oxygen remaining in the tube. Their achieved peak temperatures were in the range of 290°C to 314°C. It should be noted, that the operating pressure of 27.2 MPa is higher than the critical pressure of water.

The front velocity (see Figure 53) was calculated at the selected temperature of 275°C. The temperature that defines the combustion velocity is selected on the basis of the temperature range where the oxidation reactions occur. These oxidation reactions are responsible for the mobilization of the oil in-situ. In the case of heavy oils, the combustion temperature defining the front velocity exceeds 350°C. In the case of light oils, mobilization of the oil is primarily associated with the combustion/oxidation reactions that occur in the low-temperature range.

The slope of this plot gives the 275°C front velocity at the air injection flux used in the test. According to the given slope of the front-location, the advancement rate of the

leading edge was 0.176 m/h at an air flux of 40.4 m³(ST)/m²h. Following Figure 53 the front velocity would not change significantly for the 290-330°C front temperatures at the above-mentioned air flux.

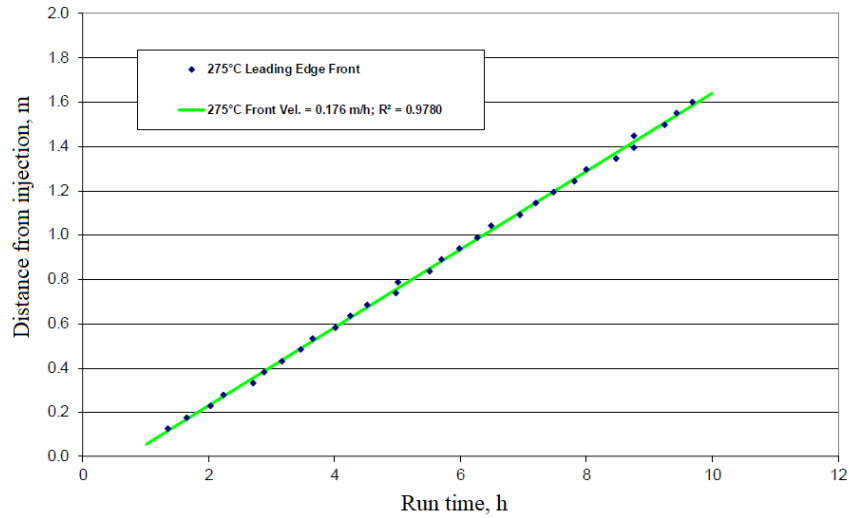


Figure 53. Forward combustion front locations

The production of main combustion gases such as oxygen, nitrogen, carbon dioxide, and carbon monoxide as a function of the runtime is given in Figure 54.

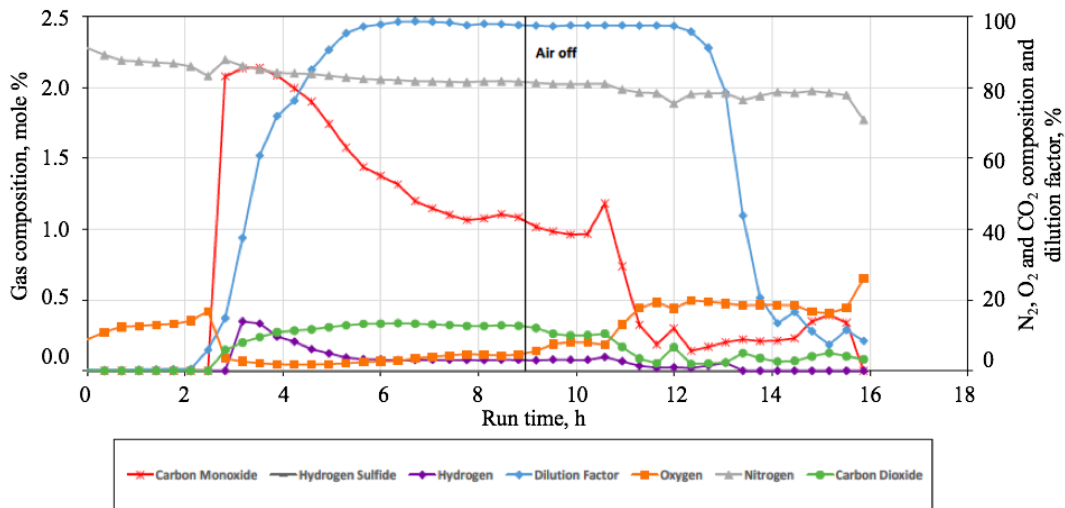


Figure 54. Produced combustion gas compositions for forward combustion test

During the first 2.5 hours after the start of air injection, all the gases produced were collected inside a trap. The gas was accidentally vented out without going through the gas chromatographs. Consequently, only a small fraction of gas residue was analyzed.

A steady production of carbon dioxide at about 13% can be observed in Figure 54. It indicates favorable bond-scission type reactions that are confirmed by good burning characteristics. The observed temperatures were not very high, and therefore the level of carbon dioxide was not attributed to the decomposition of the carbonate core (Engler et al., 1989). The combustion gas composition results from the laboratory experiments correlate well with field-scale observations. The overall oxygen utilization was 61.5%, and unconsumed oxygen was partially due to unburned oxygen produced throughout the air injection period, but primarily due to stored oxygen in the burned section of the combustion tube test. It was later displaced during helium purge which resulted in an oxygen peak in Figure 54. Figure 55 below shows the cumulative production of oil and water over time.

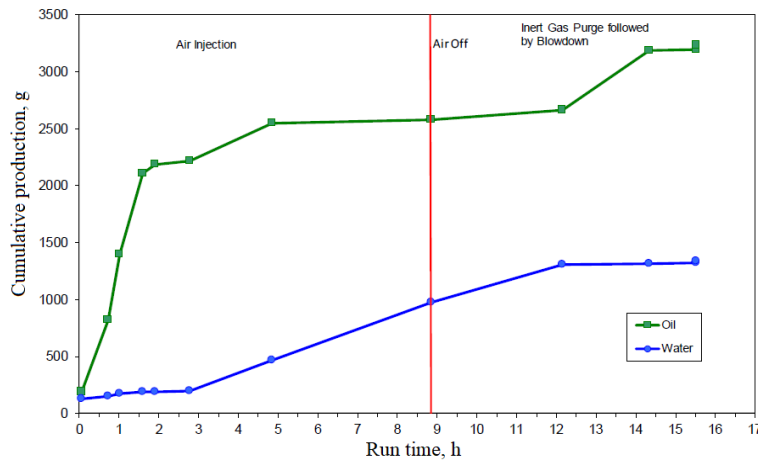


Figure 55. Forward combustion oil and water production cumulative masses

According to the experiment, 3236.5 grams of oil were produced, which corresponds to a recovery coefficient of 91.4%, taking into account the very small amount of initial oil in the lines.

7.1.2.2 Reverse combustion

The reverse combustion tube test was conducted in order to investigate the ISC behavior of the restored state core in a reverse mode. The centerline temperatures are presented in Figure 56.

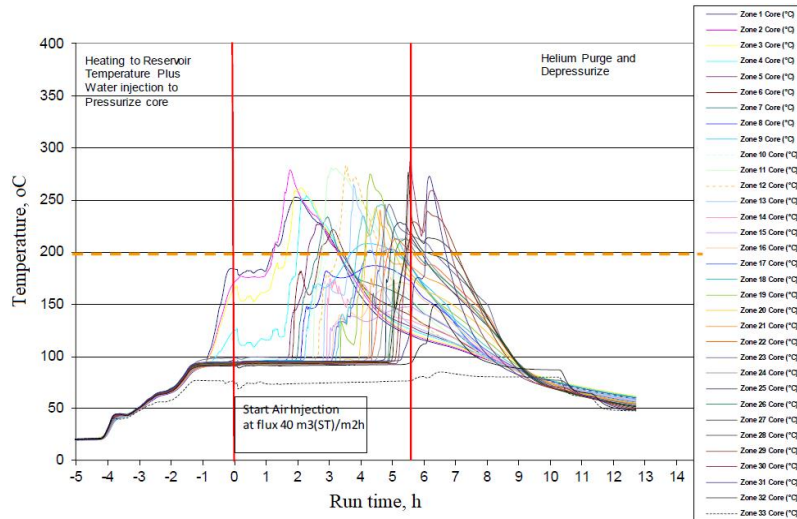


Figure 56. Reverse combustion test temperature profiles

As with the forward mode, the heating of the three ignition zones started one hour prior to the start of air injection. The maximum peak temperatures for the first four zones are above 250°C, while the subsequent Zones 5-10 peak at temperatures less than 250°C. The following zones under numbers 11, 12, and 13 again exceed 250°C peaks, while the next three zones remain below 200°C. Mid zones demonstrated relatively low-temperature peaks, and from Zone 17 they started to increase and achieved the highest level at 288°C at Zone 30. Lower peak temperatures can be explained by the kinetics of the reactions occurring during reverse combustion. The air injection was terminated after 5.6 hours after the start of air injection and helium was injected when the leading edge of the high-temperature front reached Zone 30.

The front velocity for the reverse combustion was calculated at the selected 200°C, which is represented by the horizontal dashed line in Figure 56. The time when each zone attained this temperature was plotted against the corresponding thermocouple location for zones 3 to 30. Two distinct stabilized combustion zones were observed

during the reverse combustion test (see Figure 57). The first stable section corresponds to the first seven zones with relatively high peak temperatures.

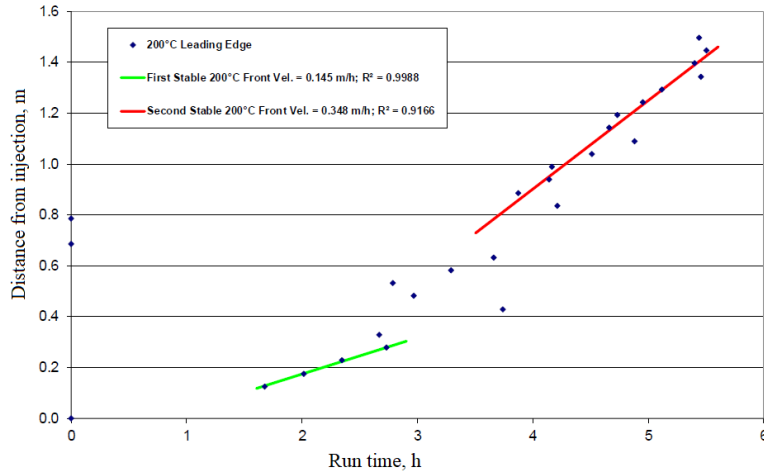


Figure 57. Reverse combustion front locations

The advancement rate of the 200°C leading edge at an air flux of 40.4 m³(ST)/m²h was 0.145 m/h for the period 1.67 to 2.73 hours, and 0.348 m/h for the period 3.87 to 5.50 hours. Between 2.8 and 4.0 hours, the advance of the front was unstable, with low temperature (< 200°C) peaks. The product gas concentrations as a function of runtime are presented in Figure 58.

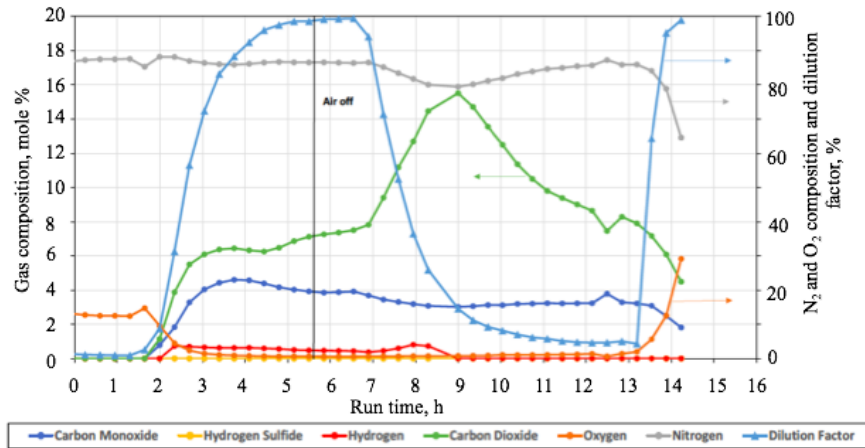


Figure 58. Reverse combustion produced combustion gas compositions

For the typical sandstone combustion test in the high-temperature (bond-scission) mode, CO₂ concentration is 12-15%, and CO is 1.0 to 3.0%. For these carbonate combustion tests, similar levels were observed, although the levels of CO during the reverse combustion test were higher, possibly due to less stable combustion characteristics.

The production of the main combustion gases shows oxygen, nitrogen, carbon dioxide, and carbon monoxide. No measurable hydrocarbon was produced during the first 1.5 hours after the start of air injection, only trace quantities of oxygen and nitrogen, slightly diluted by helium. Ignition was observed at 1.13 hours, the first traces of carbon dioxide and light hydrocarbon were detected by the gas chromatograph at around 1.6 hours.

The level of carbon dioxide production remained between 6 to 8% for the first 7 hours, which indicates the gas production during the air injection period. However, typical favorable conditions for bond-scission type reactions consistent with favorable burning characteristics normally result in carbon dioxide production at levels of 12-15%. In combustion tube tests on carbonate cores that exceed 500°C (typical of heavy oil combustion) or where water co-injection is used (e.g. wet combustion), CO₂ level exceeding 16%, and sometimes reaching 30% have been observed due to the decomposition of the carbonate core material. In the reverse combustion test temperatures did not exceed much more than 300°C resulting in a lower level of CO₂.

Nevertheless, oxygen consumption was nearly complete, indicating reactions with oxygen consumption but the without production of carbon oxides. It can be explained by water formation or liquid phase hydrocarbon oxidation. The unconsumed oxygen and the stored oxygen in the burned section were displaced during the helium purge and appeared as an oxygen peak during the depressurization. The overall apparent atomic hydrogen to carbon (H/C) ratio was 3.9 which is considerably higher than usual the 1.2 in the forward combustion test. It indicates oxygen addition reactions between the injected air and the significant quantity of warm, residual oil in the core pack. This feature is one of the less

attractive features of reverse combustion. Figure 59 presents the cumulative liquid production over time.

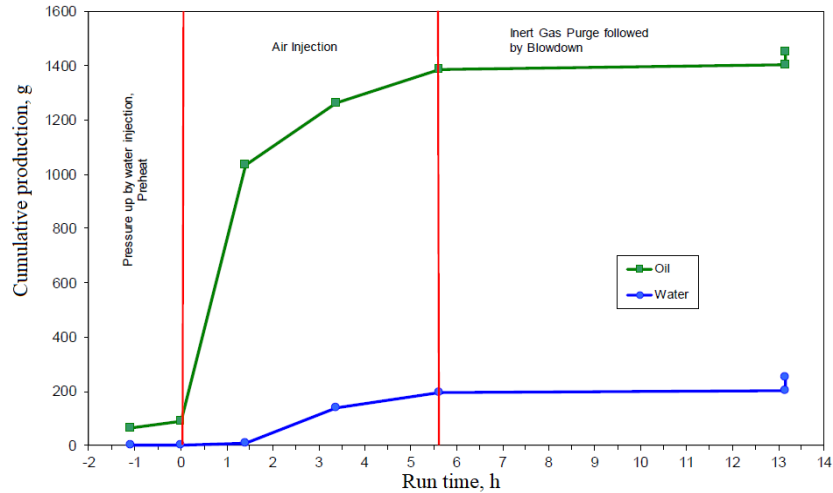


Figure 59. Reverse combustion oil and water production cumulative masses

Oil production amounted to 1,451 grams including lines, which gives 42.5% recovery of the OOIP. There was 4% consumed as fuel, another 1% was consumed as fuel gas, and 50% remained as residual on the core in the one-dimensional reverse combustion tube experiment. Initial water in the system was 1596 grams, 250.8 grams were produced as a liquid, 25.2 grams were produced as gas, and 1,361.4 grams remained as residual water.

Combustion tube tests were performed to assess the suitability and potential of the selected oil reservoir for the implementation of an air injection-based EOR. Also, they can provide useful information regarding the combustion characteristics of the studied rock/oil system. These parameters are influenced by a wide range of factors, such as properties of the fluid, experimental pressure and temperatures, permeability, porosity, and composition of the rock matrix.

The maximum peak temperature for the forward combustion test was 626°C, while in reverse combustion the maximum recorded temperature was only 288°C. The average peak temperatures are generally a function of the air flux and dependent on heat

loss thus should be a subject of further studies during the numerical simulation. Table 21 provides a summary of stabilized combustion parameters for both tests.

Table 21. Summary of stabilized combustion parameters

	Forward combustion	Reverse combustion	
Combustion front, °C Leading edge	275	200	
Time interval by velocity, h	1.35 to 10.11	1.67 to 2.73	3.87 to 5.5
Gas chromatograph interval, h	4.23 to 9.17	3.1 to 4.5	5.3 to 7.1
Air fuel ratio, m ³ (ST)/kg	10.84	13.52	13.38
Combustion front velocity, m/h	0.176	0.145	0.348
Air required, m ³ (ST)/kg	229.5	279.49	116.08
Fuel required, kg/m ³	17.82	19.97	8.45
Apparent atomic H/C ratio	1.45	5.10	4.69
The percent oxygen Utilization, %	84.2	96.62	97.37
The percent conversion of reacted O ₂ to carbon oxides	72.4	38.37	41.33
(CO ₂ +CO)/CO ratio	11.13	2.43	2.87
(CO ₂ +CO)N ₂ ratio	0.17	0.12	0.13
Mole percent O ₂ , %	21.28	21.04	
N ₂ /O ₂ ratio	3.69	3.75	

Reverse combustion manifested two distinct velocity periods with the front velocity of 0.145 m/h at the first stage and 0.348 m/h at the second based on the produced carbon dioxide. These two sections were considered as stabilized combustion zones. As with the peak temperatures, the front velocity is affected by air flux and heat loss reduces it. The combustion front development and front velocities are crucial for the prediction of field-scale performance.

Oil recovery for the forward combustion was as high as 91.4% of the initial oil in place with 2.4% remaining residual, while only 43% was produced as liquids during the reverse combustion process with 50% remained as residual on the core. This result can be explained by the API values of the oil samples. Forward combustion has a wide range of oils from 10 to 40° API, while for reverse combustion 5 to 20° API is considered to be favorable. This parameter is also a subject of history matching.

The reverse combustion required a higher amount of air at the first stable section than during forward combustion. However, when the temperatures started to increase again and the front velocity slope became steeper the air requirement decreased sharply. The overall air requirement was 253.5 m³(ST)/m³ and 146.9 m³(ST)/m³ for forward and reverse experiments, respectively. The air requirements determine the compression capacity, affecting the overall project economics.

In contrast with sandstone reservoirs, in carbonate reservoirs resulting in 12-15% CO₂ concentration and 1.0 to 3.0% CO, there are reactions other than HTO, LTO, but also carbonate decomposition with the products of reaction being CO₂, CO, O₂, N₂, and water (Sarathy, P.S., 2016). Generally, during heavy oil combustion tests on carbonate core exceeding 500°C or wet combustion, CO₂ might be in the range of 16-30% due to the decomposition of the carbonate core material. According to some literature, the decomposition reaction of carbonates (Olszak-Humienik and Jablonski, 2015) is assumed to take place at temperatures above 700°C (Engler et al., 1989). Thus, at the given maximum temperature (300°C) the contribution of dolomite and calcite can be insignificant, similarly to (Khakimova et al., 2020).

Dependence on initial temperatures was not evaluated within these experiments. However, it might affect the peak temperatures and the combustion-zone velocities. Both experimental and numerical tests should focus on the determination of the kinetic parameters and chemical reactions adequately describing the processes.

7.2 Numerical simulation of forward combustion

Different tools can be used to study and assess the possible performance of the target oil field. As was described previously in Chapter 5, experimental and numerical calculations are conducted under reservoir conditions. Further, the obtained numerical model is validated against experimental results and transferred to field scale to predict the oil recovery indicators. Within this research J. Belgrave (Belgrave et al., 1993) kinetic model, its activation energy terms, and other kinetic parameters were used as main assumptions. The following variables should be history matched to ensure the reliability of the created numerical model (Belgrave et al., 1993):

- temperature profiles;
- the produced gas composition is matched by adjustment of the kinetics and the oxidation stoichiometry;
- fluid production rates depend on the relative permeability curves.

The modeling and optimization process was carried out in the thermal hydrodynamic simulator CMG STARS widely used for thermal recovery processes.

7.2.1 A common approach to numerical modeling of combustion tube test

The digital model of the HPCT experimental setup (see [Figure 60](#)) was created in a similar fashion as described in [Section 5.3](#). However, it was adjusted to incorporate the distinctive features of the HPCT equipment geometry and its heater regimes. According to experimental studies, radial heat transfers can significantly distort temperatures recorded inside the sand pack. Thermal convection in the annulus can also affect the results, as well as the nature of the pressurizing gas in the annulus. Thus, radial and external heat transfers of HPCT tests should be correctly interpreted and modeled.

[Figure 60](#) presents a longitudinal section of a block-centered cylindrical grid displaying the distribution of initial oil saturation, permeability, and porosity. The size of the grid mesh was determined during previous simulations in [Section 5.3](#) as well as important heat transfer elements of the assembly.

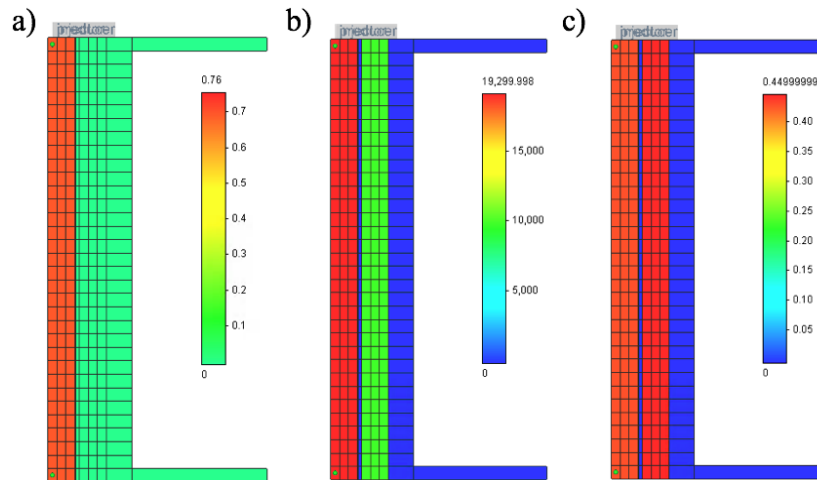


Figure 60. A numerical model of the HPCT installation in CMG: (a) initial oil saturation; (b) permeability; (c) porosity

All-important features of the equipment were incorporated. Outside the sand pack, there is a combustion tube followed by fibrous insulation, heater support column, electrical heaters, annular space, and a pressure jacket. The pressure shell flanges have also been included and serve as a thermal sink. Each temperature zone is divided into three, and temperature levels in each of these central blocks (of three) and on the corresponding wall cell determine the quality of the heaters implemented through the heater support column to simulate the experimental adiabatic heating. Between the combustion tube and the heater, there is a layer representing thermal insulation that prevents overheating of certain areas of the tube. The thickness of this layer and its thermal properties are crucial factors affecting the response of the heaters. “Near-adiabatic” mode was implemented, thus some offset temperature should be specified between the tube-wall and sand pack. In addition, “set-point” control is implemented to establish a constant tube-wall temperature along the core length. In this case, the constant sand pack temperature is maintained ahead of the combustion front that replicates the reservoir conditions.

7.2.2 Numerical modeling of forward ISC

This numerical model takes account of the fluid and heat dynamics and representative chemical reactions that take place within the core during the ISC process. The selection of chemical reactions and their kinetic parameters was carried out through the validation of a numerical model of the combustion tube (CT) experiment based on the experimental results. The comprehensive approach of (Belgrave et al., 1993) that can reproduce the major oxidation-related phenomena and predicting the combustion performance over a broad range of operating conditions was used as an initial assumption. The modeling and optimization process was carried out in the thermal hydrodynamic simulator CMG STARS. The creation of a fluid model was carried out, taking into account the pseudo-component composition of the model fluid. The oil was characterized by two liquid pseudo-components such as Maltenes and Asphaltenes (Similarly to Section 5.3). The viscosity and volatility models of the crude oil also should be specified accurately to capture the oil displacement physics. Andrade’s equation is

often used due to its simplicity. However, there are instabilities at steam and combustion temperatures, and a result unrealistic, low viscosities in this range. Thus, Walther's equation is a better approach for curve-fitting and extrapolation. Figure 61 demonstrates the difference discussed above for extrapolations using Andrade and Walther equations.

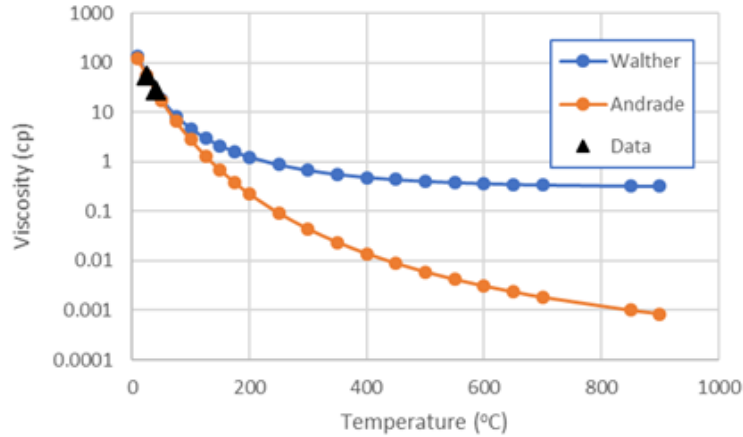
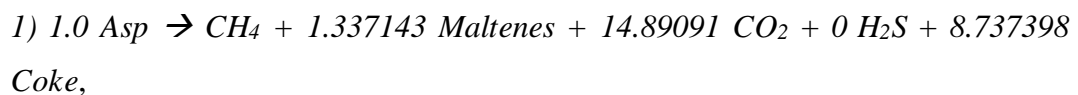


Figure 61. The difference in viscosity extrapolations for heavy oil using the Andrade and Walther equations

Volatility represented by K-values of the oleic pseudo-components should be considered since it considerably affects the fuel available for the combustion process. For instance, with very light oils, combustion tends to be more stable at higher pressures as there is a greater tendency for the oil to remain in the liquid state. While the “Asphaltenes” pseudo-component is non-volatile, the K-values can be obtained by correlations against specific gravity or molecular weight in WinProp. In cases when Maltenes are too volatile, too little oil is available to fuel the combustion.

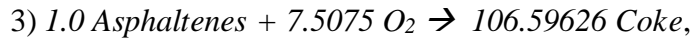
The reaction scheme consists of four reactions that are capable of representing the ISC process (Belgrave, J.D.M. et al., 1997; Belgrave et al., 1993; Moore, R. G. et al., 1996). The stoichiometry of the reaction was calculated according to the experimental results.

Thermal Cracking:



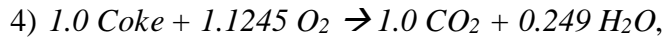
Thermal cracking is accompanied by an insignificant absorption of energy and leads to oil upgrading, aquathermolysis (formation of H₂S, H₂, CO₂). This reaction is important in terms of compositional changes and gas evolution.

Low-temperature oxidation:



These exothermic reactions are responsible for polymerization (an increase of oil viscosity), most of the fuel for heavy oil combustion, and spontaneous ignition.

High-temperature oxidation:



This exothermic reaction is critical for heavy oil displacement and produces most of the carbon oxides.

The temperature profiles for particular zones of the combustion tube obtained during simulation are presented in [Figure 62](#).

The model effectively maintains the desired core/tube wall temperature difference. The shape of the computed heater response compares favorably with the experimental heater profiles. Downward progression of the combustion front and annular convection were demonstrated. Temperature profiles obtained during numerical simulations demonstrated a very good match with experimental data. Particularly the start of the temperature rise was reproduced very well. A comparison of the history-matched cumulative oil, water, and gas cumulative production and experimental data are presented in [Figure 63](#). It shows satisfactory agreement between experimental data and simulation results.

Below is the material balance of oil and water for the experiment and numerical simulation in [Table 22](#). The difference between experimental and simulation results of cumulative oil and water production was 3.6 and 1.1%, respectively.

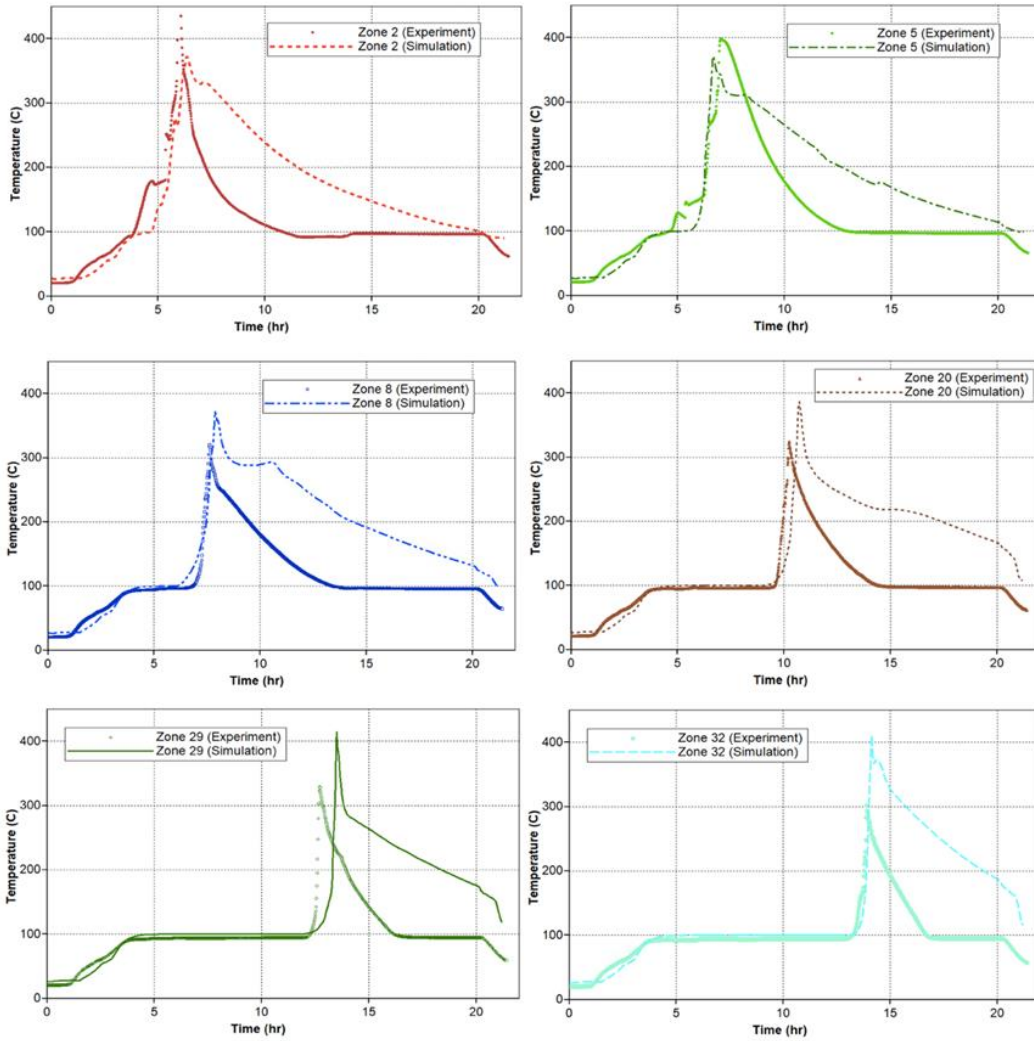


Figure 62. Simulation results: forward combustion temperature profiles

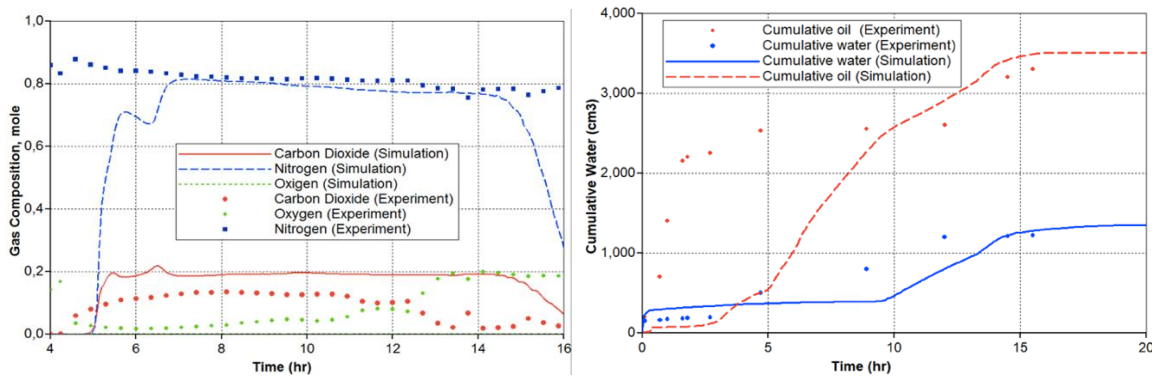


Figure 63. Simulation results: forward combustion produced combustion gas compositions (left); forward combustion oil and water cumulative production (right)

Table 22. Comparison of the cumulative production for the experiment and simulation

Cumulative production	Experiment	Simulation
Oil, cm ³	3300	3421
Water, cm ³	1220	1234

A good agreement of temperature peaks in all zones can be observed, as well as cumulative water and oil productions that have a good match with experimental values. There is a good match between carbon dioxide and nitrogen. However, a significant discrepancy in the mole concentrations of O₂ is observed and should be further investigated in detail. The created model recreates the general features and could be tested in the full-field model.

7.3 Conclusions

The work was conducted to study the combustion behavior of the oil sample from the target field and evaluate its burning characteristics, incremental production of oil, and water, air, and fuel requirements. Forward and unique reverse ISC combustion methods were examined to predict feasibility for their application in the target oil field.

- Unique HPCT laboratory tests on a 100 mm diameter high-pressure combustion tube using actual reservoir samples were performed, at a pressure of 27 MPa and an air injection flux of 40 m³(ST)/m²h at an ignition temperature of 175°C.
- Favorable test results were confirmed by the propagation of a steady combustion front through the core pack and a stable product gas composition for both tests.
- The oil recovery was 91.4% for the forward combustion and 43% for the reverse combustion tests. For the forward combustion of the 3533 grams of oil initially in the system, the above mentioned 91.4% was produced as liquids, 4.4% was consumed as fuel, 0.4% was produced as fuel gas and 2.4% remained as residual. Similarly, for reverse combustion 43% was produced as liquids, 4% was consumed as fuel, 1% was produced as fuel gas and 50% remained as residual on the core in the one-dimensional reverse combustion tube experiment.

Reverse combustion can be used as a preheating method before steam flooding or other EOR technique. The initial oil saturation of the given reservoir was comparatively high and the viscosity of initial oil also was lowered during reverse combustion, thus forward combustion could be performed further to achieve a higher oil recovery. Reverse combustion pre-treatment can lead to the development of highly permeable paths between wells. The reverse combustion tests on oil samples with API in the range of 5 to 20° API in comparison with the oil sample presented in this research also could reveal more insights about the reverse combustion process.

Under given conditions forward combustion process demonstrated better performance and was more efficient at mobilizing oil from the core pack in comparison with the reverse combustion test. Generally, this method is more technically developed and showed higher recovery factors. However, it has viscosity limitations. Reverse combustion, in its turn, can be applicable for very heavy crude oil, low permeability reservoirs, and can serve as a preheating method. Meanwhile, there is a probability of spontaneous ignition, combustion instabilities, and the possibility of shifting to forward mode. Since there is no available experimental data in the domain of increased-pressure operation, this research provides an important set of experimental data obtained under the reservoir conditions that would be encountered in the field. Both methods have high-cost air compression and risks associated with oxygen breakthrough. Thus, it is crucial to conduct the numerical modeling of the experiments, further validate the numerical models against experimental results, and perform the field-scale modeling to predict the performance of both methods. Also, this process will allow the determination of favorable conditions where reverse combustion can be successfully applied. Reverse combustion must be further studied using different oil and core samples. Further numerical simulation of the reverse combustion experiment can reproduce the possible combustion channels in response to different operational variables and heterogeneities in the permeability.

A methodological approach that combines laboratory and numerical studies validated during HPAI simulation in [Chapter 5](#) was applied for numerical simulation of

the ISC process. History matching was performed to compare the numerical results against the experimental results and to validate the kinetic model. The kinetic model for light carbonate oil combustion was tested and tuned for further employment during the field-scale simulation. Numerical simulation of forward combustion demonstrated excellent results. It can be further applied as a basis for the simulation of reverse combustion as well as tests on oil samples with API in the range of 5 to 20° API to obtain more information about the reverse combustion process.

Chapter 8. Summary, conclusions, and recommendations

8.1 Summary

This research consists of case studies with subsequent laboratory investigations, numerical simulation, and validation against experimental data, and further field-scale simulation. Simulation of the experimental tests is important for the design and optimization of the process, as well as for calculation of the decision variables like cumulative oil, recovery factor, and net present value. Numerical modeling serves as a tool to distinguish the process features, to interpret the reverse combustion laboratory test, and to estimate the performance of the method. The model of kinetic reactions obtained and validated during history-matching of the processes studied in this research can be used in order to make reasonable and comprehensive decisions on the stage of early planning of reservoir development.

The main goal of this study was to conduct a comprehensive experimental and numerical modeling of thermal EOR to select a development methodology on the example of specific objects. The methodology was based on experimental studies of HWI, supercritical water injection, HPAI, and ISC and their subsequent numerical modeling using experimental data with the aim of predicting the feasibility of the method.

8.2 Conclusions

The following conclusions were derived that correspond to the objectives of the research:

1. A numerical model of the laboratory equipment that is capable of representing the major phenomenological effects observed in near adiabatic combustion tubes such as mass-heat transfer taking into account the properties of the medium, convection, combustion delay, heat losses, and the support of secondary reactions.

2. The efficiency of oil displacement by HWI for the studied deep heavy carbonate oil field is confirmed by numerical simulation. The numerical model and implementation of aquathermolysis reactions demonstrate a good match of temperature profiles and experimental and simulation values of cumulative fluid output. The data

obtained during this research can be applied in the up-scaled model for further feasibility studies.

3. The importance of an accurate specification of a group-model of OM saturation representing the distribution of organic matter in a target reservoir was described. Some limitations such as the inability of the separation of mobile oil and “bonded” hydrocarbons separation were described. The complex methodological approach for the enhancement of *in-situ* upgrading process simulation was developed.

4. The numerical simulations of HPRTO and MPCT tests gave a satisfactory correlation with experimental results. Also, the estimation of the HPAI recovery technique feasibility was carried at the field-scale. Four different scenarios were proposed and calculated for four individual Subsections of the field. Injection of air into the reservoir did not lead to an increase in oil recovery in the long run for subsections 2, 3, and 4 due to rapid breakthroughs of air into producing wells within 3–4 years (oxygen concentration limit is 2 %). Optimization of one subsection was performed to achieve the best performance.

5. The oil recovery for the forward combustion and the reverse combustion tests were 91.4% and 43%, respectively. It was determined, that reverse combustion can be used as a preheating method before steam flooding or other EOR technique. The reverse combustion tests on oil samples with API in the range of 5 to 20 °API in comparison with the oil sample presented in this research also could reveal more insights about the reverse combustion process. Both methods have high-cost air compression and risks associated with oxygen breakthrough. Numerical simulation of forward combustion displayed a satisfactory correlation with experimental results.

8.2 Contribution to the knowledge

1. An aquathermolysis kinetic model was adapted from the steam injection process and introduced into the numerical model simulating the HWI process for the first time. The vigorous workflow that consists of a subsequent experimental and numerical study of HWI was also presented in this research. The data, such as cementation technology, fluid model, relative permeability curves, kinetic model, and operational

parameters obtained during this research can be directly transferred to the upscaled model for further feasibility studies.

2. The importance of an accurate specification of a group-model of OM saturation representing the distribution of organic matter in a target reservoir was proved. Some limitations of the commercial software were defined such as the inability to separate mobile oil and bonded hydrocarbon. A few suggestions were made in the framework of thermal EOR calculations. Also, this research includes the development of a complex methodological approach for the enhancement of in situ upgrading process simulation. The main focus was on consistent experimental studies of kinetic mechanisms of organic matter transformations and their accurate reproduction in the numerical simulator.

3. A methodology that includes the laboratory and numerical modeling of the HPAI process was introduced. A numerical model of a combustion tube in this thesis employs a comprehensive formulation that is capable of representing the major phenomenological effects observed in near adiabatic combustion tubes such as mass-heat transfer taking into account the properties of the medium, convection, combustion delay, heat losses, the support of secondary reactions. The model also takes into account the operation of guard heaters that cause significant convective circulatory movement to occur in the pressurized annulus influencing the temperatures measured in the sand pack. The numerical model validated against experimental results was further upscaled taking into account the areal heterogeneity, displacement effectivity due to low air injectivity, convergence difficulties caused by high residual oil saturation, and high critical water saturation in the same grid block.

4. A unique experimental study of forward and reverse combustion was conducted. Valuable data for further numerical simulation of forward and reverse combustion was provided. The data that were not available before for reverse combustion at reservoir conditions were obtained and closely studied to understand the mechanism of this process. Conditions, where the application of reverse combustion becomes possible were determined: as a preheating method before steam flooding or other EOR technique,

in the reservoir with low effective permeability and on oil samples with API in the range of 5 to 20° API.

8.4 Recommendations

The following questions are subjects for further investigations.

8.4.1 HWI

- The experimental and numerical results obtained during HWI tests should be further used for field-scale modeling based on which the optimal rate, optimal injection temperature, and volume of the injectant in the reservoir should be validated and adjusted.

- The implemented kinetic model should be verified on other cases of HWI on the carbonate oil fields.

- The numerical model could be enhanced with the implementation of a heterogeneous model through dual porosity-dual permeability modeling and reaction of calcite decomposition.

8.4.2 Supercritical water injection

- A natural progression of this work is the refinement of the methodology to avoid uncertainties during phase changes: permeability modifications in the water-oil system during supercritical water injection, capillary forces, wettability, and upscaling procedure.

- Further, the parameters obtained in the refined model such as kinetic model, viscosity correlations, relative permeability curves, and operational parameters should be used in field-scale modeling and compared to the base-case scenario results.

8.4.3 HPAI

- The discrepancy in the mole concentrations of O₂ and CO₂, and the total oxygen consumption must be further investigated with a focus on phase transition behavior of target oil and basic chemical reaction model.

- Sufficient relative permeability curves in the system gas-oil should be provided by the company. The current well pattern and development system should be optimized,

and a sector with higher porosity and bigger pay zone thickness should be considered in the future.

- Any pilot testing of air injection should monitor injection pressures and rates for changes in air injectivity due to liquid blockage concern. A lack of sufficient air injectivity in part of the reservoir should be addressed.

- Nitrogen injectivity tests should be performed in several wells to support current geological characterization and gas-oil relative permeability to gas.

8.4.4 ISC

- In this work, a reverse test was conducted on a test configuration that was selected to minimize the number of equipment parameters. A future combustion tube test of reverse combustion, with oil production in a downward direction, would provide valuable insights. The orientation of the combustion tube test during reverse combustion, permeability values, the effect of carbon decomposition, and other factors affecting the performance of reverse combustion should be examined further during additional laboratory tests and numerical investigations with the implementation of the chemical model.

- The number of reverse combustion tests on oil samples with API in the range of 5 to 20°API should be carried out to provide more insights about the reverse combustion process.

- Considerably more work will need to be done to determine the kinetic model of reverse combustion, taking into account the possible vapor combustion.

References

- Abdallah, W., Buckley, J.S., Carnegie, A., Edwards, J., Herold, B., Fordham, E., Graue, A., Habashy, T., N., S., Signer, C., Hussain, H., Montaron, B., Ziauddin, M., 2007. Fundamentals of Wettability, Oilfield Review.
- Adams, R.H., Khan, A.M., 1969. Cyclic Steam Injection Project Performance Analysis and Some Results of a Continuous Steam Displacement Pilot. *J. Pet. Technol.* 21, 95–100. <https://doi.org/10.2118/1916-pa>
- Al-Hadhrami, H. S., Blunt, M.J., 2001. Thermally induced wettability alteration to improve oil recovery in fractured reservoirs, in: *SPE Reservoir Evaluation and Engineering*. pp. 179–186. <https://doi.org/10.2523/59289-ms>
- Alajmi, A. F., Algharaib, M., Gharbi, R., 2009. Experimental evaluation of heavy oil recovery by hot water injection in a middle eastern reservoir. *SPE Middle East Oil Gas Show Conf. MEOS, Proc.* 2, 1–14.
- Alpak, F.O., Vink, J.C., 2018. Rapid and accurate simulation of the In-situ Conversion Process using upscaled dynamic models. *J. Pet. Sci. Eng.* 161, 636–656. <https://doi.org/10.1016/j.petrol.2017.11.011>
- Alvarado, V., Manrique, E., 2010. Enhanced oil recovery: An update review. *Energies* 3, 1529–1575. <https://doi.org/10.3390/en3091529>
- Askarova, A., Cheremisin, Alexander, Belgrave, J., Solovyev, A., Mehta, R., Cheremisin, Alexey, 2020a. Evaluation of the subject geological area suitability for oil recovery by High-Pressure Air Injection method 7–14.
- Askarova, A., Popov, E., Ursenbach, M., Moore, G., 2020b. Experimental Investigations of Forward and Reverse Combustion for Increasing Oil Recovery of a Real Oil Field. *Energies* 13, 1–16. <https://doi.org/10.3390/en13174581>
- Askarova, A., Turakhanov, A., Markovic, S., Popov, E., Maksakov, K., Usachev, G., Karpov, V., Cheremisin, A., 2020c. Thermal enhanced oil recovery in deep heavy oil carbonates: Experimental and numerical study on a hot water injection performance. *J. Pet. Sci. Eng.* 194, 107456.

<https://doi.org/https://doi.org/10.1016/j.petrol.2020.107456>

- Askarova, A., Turakhanov, A., Mukhina, E., Cheremisin, Alexander, Cheremisin, Alexey, 2020d. Unconventional Reservoirs: Methodological Approaches for Thermal EOR Simulation, in: Unconventional Resources Technology Conference. pp. 4–5. <https://doi.org/10.15530/urtec-2020-2112>
- B. Hyne, J., D. Clark, P., A. Clarke, R., Koo, J., W. Greidanus, J., Tyrer, J.D., Verona, D., 1982. Aquathermolysis of heavy oils. *Rev. Tec. INTEVEP* 2, 87–94.
- Baker, R.O., Chugh, S., McBurney, C., McKishnie, R., 2006. History matching standards; quality control and risk analysis for simulation. *Can. Int. Pet. Conf. 2006, CIPC 2006*. <https://doi.org/10.2118/2006-129>
- Barzin, Y., Moore, R.G., Mehta, S.A., Mallory, D.G., Ursenbach, M.G., Tabasinejad, F., 2010. Role of vapor phase in oxidation/combustion kinetics of high-pressure air injection (HPAI). *Proc. - SPE Annu. Tech. Conf. Exhib. 7*, 5581–5598. <https://doi.org/10.2118/135641-ms>
- Barzin, Y., Moore, R.G., Mehta, S.A., Ursenbach, M.G., Tabasinejad, F., 2013. A Comprehensive Kinetics Model for Light Oil Oxidation/Combustion Reactions under High Pressure Air Injection Process (HPAI). <https://doi.org/10.2118/166483-ms>
- Bauman, J.H., Deo, M.D., 2011. Parameter Space Reduction and Sensitivity Analysis in Complex Thermal Subsurface Production Processes. *Energy & Fuels* 25, 251–259. <https://doi.org/10.1021/ef101225g>
- Behar, F., Lewan, M.D., Lorant, F., Vandenbroucke, M., 2003. Comparison of artificial maturation of lignite in hydrous and nonhydrous conditions. *Org. Geochem.* 34, 575–600. [https://doi.org/10.1016/S0146-6380\(02\)00241-3](https://doi.org/10.1016/S0146-6380(02)00241-3)
- Behar, F., Lewan, M.D., Lorant, F., Vandenbroucke, M., 2003. Comparison of artificial maturation of lignite in hydrous and nonhydrous conditions. *Org. Geochem.* 34, 575–600. [https://doi.org/https://doi.org/10.1016/S0146-6380\(02\)00241-3](https://doi.org/https://doi.org/10.1016/S0146-6380(02)00241-3)
- Belgrave, J.D.M., Moore R.G., Ursenbach M.G., 1997. Comprehensive Kinetic Models for the Aquathermolysis of Heavy Oils. *J. Can. Pet. Technol.* 36, 38–44.
- Belgrave, J., 2019. Belgrave's Oil and Gas Corporation [WWW Document]. *Cycl. Air Inject. Stimul. Sand*

Control. Upgrad. Oil.

Belgrave, J.D.M., Moore, R. G., Ursenbach, M. G., Bennion, D.W., 1993. A Comprehensive Approach to In-Situ Combustion Modeling. SPE Adv. Technol. Ser. 1, 98–107.

Bentley, R. W., 2002. Oil forecasts, past and present. Energy Explor. Exploit. 20–21, 481–492.

<https://doi.org/10.1260/014459802321615108>

Bentley, R W, 2002. Global oil & gas depletion: an overview. Energy Policy 30, 189–205.

[https://doi.org/https://doi.org/10.1016/S0301-4215\(01\)00144-6](https://doi.org/https://doi.org/10.1016/S0301-4215(01)00144-6)

Berry, V.J., Parrish, D.R., n.d. A Theoretical Analysis of Heat Flow in Reverse Combustion ABSTRACT.

Bhat, S.K., Kovsky, A.R., 1998. Permeability modification of diatomite during hot fluid injection, in: SPE Annual Western Regional Meeting in Bakersfield, California. pp. 1–8. <https://doi.org/10.2523/46210-ms>

Bhattacharya, S., Mallory, D.G., Moore, R.G., Ursenbach, M.G., Mehta, S.A., 2016. SPE-180451-MS

Vapor Phase Combustion in Accelerating Rate Calorimetry for Air-Injection EOR Processes. SPE West. Reg. Meet. held Anchorage 23–26.

Bousaid, I.S., Ramey, H.J., 1968. Oxidation of Crude Oil in Porous Media. Soc. Pet. Eng. J. 8, 137–148.

<https://doi.org/10.2118/1937-pa>

Bousaid, I.S., 1991. Hot-water and steamflood studies using Kern River oil, in: International Thermal

Operations Symposium, Bakersfield, California. pp. 187–200. <https://doi.org/10.2118/21543-ms>

Bowman, C.H., Gilbert S., 1969. A Successful Cyclic Steam Injection Project in the Santa Barbara Field, Eastern Venezuela. J Pet. Technol. 21, 1531–1539.

Braun, R.L., Burnham, A.K., 1992. PMOD: a flexible model of oil and gas generation, cracking, and

expulsion. Org. Geochem. 19, 161–172. [https://doi.org/https://doi.org/10.1016/0146-6380\(92\)90034-](https://doi.org/https://doi.org/10.1016/0146-6380(92)90034-)

U

Braun, R.L., Burnham, A.K., 1990. Mathematical model of oil generation, degradation, and expulsion.

Energy & Fuels 4, 132–146. <https://doi.org/10.1021/ef00020a002>

Briggs, P.J., Baron, P.R., Fulleylove, R.J., Wright, M.S., 2007. Development of Heavy-Oil Reservoirs. J.

Pet. Technol. <https://doi.org/10.2118/15748-pa>

- Burger, J.G., 1978. Chapter 8 In-Situ Recovery of Oil from Oil Sands, in: Chilingarian, G. V, Yen, T.F.B.T.-D. in P.S. (Eds.), *Developments in Petroleum Science*. Elsevier, pp. 191–212.
[https://doi.org/https://doi.org/10.1016/S0376-7361\(08\)70067-0](https://doi.org/https://doi.org/10.1016/S0376-7361(08)70067-0)
- Burnham, A.K., Day, R.L., Hardy, M.P., Wallman, P.H., 2010. AMSO's Novel Approach to In-Situ Oil Shale Recovery. pp. 149–160. <https://doi.org/10.1021/bk-2010-1032.ch008>
- Butler, R.M., 2004. The behavior of non-condensable gas in SAGD-A rationalization. *J. Can. Pet. Technol.* 43, 28–34.
- Cassinat, J.C., Payette, M.C., Taylor, D.B., Cimolai, M.P., 2002. Optimizing Waterflood Performance by Utilizing Hot Water Injection in a High Paraffin Content Reservoir, in: *SPE Symposium on Improved Oil Recovery*. pp. 199–211. <https://doi.org/10.2523/75141-ms>
- Castrup, S., 2019. Data analytics for steam injection projects. *SPE West. Reg. Meet. Proc.* 2019, 23–26.
<https://doi.org/10.2118/195328-ms>
- Chen, Bo, 2012. Investigation of in-situ combustion kinetics using the isoconventional principle. Stanford University.
- Chen, B., 2012. INVESTIGATION OF IN-SITU COMBUSTION KINETICS USING THE ISOCONVERSIONAL PRINCIPLE. Stanford University.
- Chong, L., Sanguinito, S., Goodman, A.L., Myshakin, E.M., 2021. Molecular characterization of carbon dioxide, methane, and water adsorption in micropore space of kerogen matrix. *Fuel* 283, 119254.
<https://doi.org/https://doi.org/10.1016/j.fuel.2020.119254>
- Clark, P. D., Dowling, N. I., Lesage, K. L., Hyne, J.B., 1987. Chemistry of organosulphur compound types occurring in heavy oil sands:5. Reaction of thiophene and tetrahydrothiophene with aqueous Group VIII B metal species at high temperature. *Fuel* 66, 1699–1702. [https://doi.org/10.1016/0016-2361\(87\)90366-8](https://doi.org/10.1016/0016-2361(87)90366-8)
- Clark, P.D., Dowling, N.I., Lesage, K.L., Hyne, J.B., 1987. Chemistry of organosulphur compound types occurring in heavy oil sands:5. Reaction of thiophene and tetrahydrothiophene with aqueous Group VIII B metal species at high temperature. *Fuel* 66, 1699–1702. [https://doi.org/10.1016/0016-2361\(87\)90366-8](https://doi.org/10.1016/0016-2361(87)90366-8)

- CMG, 2016. STARS User Guide, Calgary, Alberta, Computer Modeling Group (CMG).
- Crawford, P.M., Killen, J.C., 2010. New challenges and directions in oil shale development technologies, in: ACS Symposium Series. American Chemical Society, pp. 21–60. <https://doi.org/10.1021/bk-2010-1032.ch002>
- Dickson, J. L., Leahy-Dios, A., Wylie, P. L., 2011. Development of improved-hydrocarbon-recovery-screening methods. *JPT, J. Pet. Technol.* 63, 43–44. <https://doi.org/10.2118/0111-0043-jpt>
- Dietz, D.N., Weijdema, J., 1968. Reverse combustion seldom feasible. *Prod. Mon.; (United States)* 32:5.
- Dong, F., Feng, Z., Yang, D., Zhao, Y., Elsworth, D., 2018. Permeability Evolution of Pyrolytically-Fractured Oil Shale under In Situ Conditions. *Energies* 11. <https://doi.org/10.3390/en11113033>
- Dornan, R.G., 1990. Hot waterflood in a post-steamflood reservoir: a case history in the Kern River Field, California, in: 60th California Regional Meeting in Ventura, California. pp. 329–337. <https://doi.org/10.2523/20050-ms>
- Ehlimir, E.O., Orisa, E.F., 2018. The Influence of Wettability on Relative Permeability and Oil Recovery Scheme. *Int. J. Eng. Mod. Technol.* 4, 54. <https://doi.org/DOI:10.13140/RG.2.2.32581.09440>
- Elkins, L.F., Skov, A.M., Martin, P.J., Lutton, D.R., 1974. Experimental Fireflood - Carlyle Field, Kansas. Fall Meet. Soc. Pet. Eng. AIME. <https://doi.org/10.2118/5014-MS>
- Engler, P., Santana, M.W., Mittleman, M.L., Balazs, D., 1989. Non-isothermal, in situ XRD analysis of dolomite decomposition. *Thermochim. Acta* 140, 67–76. [https://doi.org/https://doi.org/10.1016/0040-6031\(89\)87285-5](https://doi.org/https://doi.org/10.1016/0040-6031(89)87285-5)
- Erickson, A., Legerski, J.R., Steece F.V., 1993. An appraisal of high pressure air injection (HPAI) on the in situ combustion results from deep, high temperature, high gravity oil reservoirs, in: Jubilee Anniversary Field Conference. pp. 259–270.
- Erofeev, A.A., Mitrushkin, D.A., Meretin, A.S., Pachezhertsev, A.A., Karpov, I.A., Demo, V.O., 2016. Simulation of thermal recovery methods for development of the bazhenov formation. *Soc. Pet. Eng. - SPE Russ. Pet. Technol. Conf. Exhib.* 2016 2432–2449. <https://doi.org/10.2118/182131-ms>
- Fadaei, H., Debenest, G., Kamp, A.M., Quintard, M., Renard, G., 2010. How the In-Situ Combustion Process Works in a Fractured System: 2D Core- and Block-Scale Simulation 118–130.

- Fadaei, H., Castanier, L.M., Kamp, A.M., Debenest, G., Quintard, M., Renard, G., 2011. Experimental and Numerical Analysis of In-Situ Combustion in a Fractured Core. SPE J. 16, 358–373.
<https://doi.org/10.2118/141117-PA>
- Fan, H., 2003. The effects of reservoir minerals on the composition changes of heavy oil during steam stimulation. J. Can. Pet. Technol. 42, 11–14. <https://doi.org/10.2118/03-03-N1>
- Fan, Y., Durlofsky, L.J., Tchelepi, H.A., 2010. Numerical simulation of the in-situ upgrading of oil shale. SPE J. 15, 368–381. <https://doi.org/10.2118/118958-PA>
- Fassihi, M.R., Brigham, W.E., Ramey, H.J., 1984. Reaction Kinetics of In-Situ Combustion : Part 2- Modeling. Soc. Pet. Eng. J. 408–416.
- Fassihi, M.R., Yannimaras, D. V., Westfall, E.E., Gillham, T.H., 1996. Economics of light oil air injection projects, in: SPE/DOE Tenth Symposium on Improved Oil Recovery, Tulsa, Oklahoma. pp. 501–509.
<https://doi.org/10.2118/35393-ms>
- Gao, Y., Chen, M., 2020. Numerical modeling on thermoelastoplastic responses of Karamay oil sand reservoir upon steam circulation considering phase change of bitumen. J. Pet. Sci. Eng. 187, 106745.
<https://doi.org/https://doi.org/10.1016/j.petrol.2019.106745>
- Gates C.F., Ramey H.J., 1980. A Method for Engineering In-Situ Combustion Oil Recovery Projects. Soc. Pet. Eng. J. 32. <https://doi.org/10.2118/7149-PA>
- Gjini, D., Buzi, X., Mastmann, M., Tare, S., 1999. Experience with cyclic in situ combustion in Albania, in: 1999 CSPG and Petroleum Society Joint Convention, Calgary, Alberta, Canada. pp. 1–7.
<https://doi.org/10.2118/99-51>
- Glandt, C.A., Pieteron, R., Dombrowski, A., Balzarini, M.A., E, S.W., 1999. Coral Creek Field Study SPE-52198-MS, in: SPE Mid-Continent Operations Symposium, Oklahoma, USA. pp. 1–11.
- Goodyear, S.G., Reynolds, C.B., Townsley, P.H., Woods, C.L., 1996. Hot water flooding for high permeability viscous oil fields, in: Proceedings - SPE Symposium on Improved Oil Recovery. pp. 289–299. <https://doi.org/10.2118/35373-ms>
- Guangshou, S., Tiyaoyao, Z., Linsong, C., Yunxian, W., 2009. Aquathermolysis of conventional heavy oil with superheated steam 289–293. <https://doi.org/10.1007/s12182-009-0046-4>

- Guangshou, Song, Tiyaoyao, Z., Linsong, C., Yunxian, W., 2009. Aquathermolysis of conventional heavy oil with superheated steam 289–293. <https://doi.org/10.1007/s12182-009-0046-4>
- Gunn, R.D., Krantz, W.B., 1987. Underground Coal Gasification: Development of Theory, Laboratory Experimentation, Interpretation & Correlation With the Hanna Field Tests, National Technical Information Service.
- Gunn, R.D., Krantz, W.B., 1980. Reverse Combustion Instabilities in Tar Sands and Coal. Soc. Pet. Eng. J. 20, 267–277. <https://doi.org/10.2118/6735-PA>
- Gutiérrez, D., Moore, R. G., Ursenbach, M. G., Mehta, S. A., 2012. The ABCs of in-situ-combustion simulations: From laboratory experiments to field scale, in: Journal of Canadian Petroleum Technology. <https://doi.org/10.2118/148754-PA>
- Gutiérrez, D., Moore, R.G., Ursenbach, M.G., Mehta, S.A., 2012. The ABCs of In-Situ-Combustion Simulations: From Laboratory Experiments to Field Scale. J. Can. Pet. Technol. 51, 256–267. <https://doi.org/10.2118/148754-PA>
- Gutierrez, D., Taylor, A.R., Kumar, V., Ursenbach, M.G., Moore, R.G., Mehta, S.A., 2007. Recovery Factors in High-Pressure Air Injection Projects Revisited, in: SPE Annual Technical Conference and Exhibition. Society of Petroleum Engineers. <https://doi.org/10.2118/108429-MS>
- Gutiérrez, D., Taylor, A.R., Kumar, V.K., Ursenbach, M.G., Moore, R.G., Mehta, S.A., 2008. Recovery factors in high-pressure air injection project revisited. SPE Reserv. Eval. Eng. 11, 1097–1106. <https://doi.org/10.2118/108429-PA>
- Hao, Y., Lu, M., Dong, C., Jia, J., Su, Y., Sheng, G., 2016. Experimental Investigation on Oil Enhancement Mechanism of Hot Water Injection in tight reservoirs. Open Phys. 14, 703–713. <https://doi.org/10.1515/phys-2016-0079>
- Hascakir, B., Kovscek, A.R., 2014. Analysis of in-situ combustion performance in heterogeneous media. Soc. Pet. Eng. - SPE Heavy Oil Conf. Canada 2014 1, 80–97. <https://doi.org/10.2118/170008-ms>
- Hayashitani, M., Bennion, D.W., Donnelly, J.K., Moore, R.G., 1978. Thermal Cracking Models For Athabasca Oil Sands Oil, in: SPE Annual Fall Technical Conference and Exhibition. <https://doi.org/10.2118/7549-MS>

- Hazra, K.G., Lee, K.J., Economides, C.E., Moridis, G., 2013. Comparison of Heating Methods for In-situ Oil Shale Extraction. <https://doi.org/https://doi.org/10.3997/2214-4609.20142631>
- Hong, K.C., 1987. Guidelines for Converting Steamflood To Waterflood. SPE Reserv. Eng. (Society Pet. Eng. 2, 67–76. <https://doi.org/10.2118/13605-PA>
- Huygen, H.H.A., Huitt, J. L., 1996. Wellbore heat losses and casing temperatures during steam injection, in: Spring Meeting of the Eastern District, API Division of Production. pp. 25–32.
- Hyne, J.B., Clark, P.D., Clarke, R.A., Koo, J., Greidanus, J.W., Tyrer, J.D., Verona, D., 1982. Aquathermolysis of heavy oils. Rev. Tec. INTEVEP 2, 87–94.
- IEA, 2020. Oil 2020 [WWW Document]. IEA.
- Ismail, N.B., Klock, K.A., Hascakir, B., 2016. In-Situ Combustion Experience in Heavy Oil Carbonate. <https://doi.org/10.2118/180724-ms>
- Jardine, D., Wilshart, J.W., 1982. Carbonate Reservoir Description. Soc. Pet. Eng. - Int. Pet. Exhib. Tech. Symp. IPETS 1982 1–35. <https://doi.org/10.2523/10010-ms>
- Jha, B., Verkoczy K. N., 1985. OIL RECOVERY BY THERMAL METHODS. Present. 36 th Annu. Tech. Meet. Pet.
- Johnson L A, J., Fahy, L.J., Romanowski L J, J., 1978. Echoing in situ combustion oil recovery project in a Utah tar sand, in: Annual Technical Conference and Exhibition of Society of Petroleum Engineers. United States.
- Jupp, T.E., Woods, A.W., 2003. Thermally driven reaction fronts in porous media. J. Fluid Mech. 484, 329–346. <https://doi.org/10.1017/S0022112003004348>
- Kamari, A., Mohammadi, A.H., 2014. Screening of Enhanced Oil Recovery Methods., in: Handbook on Oil Production Research. Nova Science Publishers, NY, pp. 10–25.
- Kang, Z., Zhao, Y., Yang, D., 2020a. Review of oil shale in-situ conversion technology. Appl. Energy 269, 115121. <https://doi.org/https://doi.org/10.1016/j.apenergy.2020.115121>
- Kang, Z., Zhao, Y., Yang, D., Tian, L., Li, X., 2020b. A pilot investigation of pyrolysis from oil and gas extraction from oil shale by in-situ superheated steam injection. J. Pet. Sci. Eng. 186, 106785. <https://doi.org/https://doi.org/10.1016/j.petrol.2019.106785>

- Kapadia, P.R., Kallos, M. S., Gates, I.D., 2010. A Comprehensive Kinetic Theory to Model Thermolysis, Aquathermolysis, Gasification, Combustion, and Oxidation of Athabasca Bitumen Hydrogen Generation from Pyrolysis and Aquathermolysis : Experimental Data, in: Improved Oil Recovery Symposium. pp. 1–31.
- Kapadia, P.R., Kallos, M.S., Leskiw, C., Gates, I. D., 2009. Potential for hydrogen generation during in situ combustion of bitumen, in: Society of Petroleum Engineers - EUROPEC/EAGE Conference and Exhibition 2009. pp. 8–11.
- Kapadia, P.R., Wang, J., Kallos, M.S., Gates, I.D., 2012. New thermal-reactive reservoir engineering model predicts hydrogen sulfide generation in Steam Assisted Gravity Drainage. *J. Pet. Sci. Eng.* 94–95, 100–111. <https://doi.org/10.1016/j.petrol.2012.06.030>
- Kapadia, P.R., Wang, J., Kallos, M.S., Gates, I.D., 2012. Journal of Petroleum Science and Engineering New thermal-reactive reservoir engineering model predicts hydrogen sulfide generation in Steam Assisted Gravity Drainage. *J. Pet. Sci. Eng.* 94–95, 100–111. <https://doi.org/10.1016/j.petrol.2012.06.030>
- Kazak, E.S., Kazak, A. V, 2019. A novel laboratory method for reliable water content determination of shale reservoir rocks. *J. Pet. Sci. Eng.* 183, 106301. <https://doi.org/https://doi.org/10.1016/j.petrol.2019.106301>
- Khakimova, L., Askarova, A., Popov, E., Moore, R.G., Solovyev, A., Simakov, Y., Afanasiev, I., Belgrave, J., Cheremisin, A., 2020. High-pressure air injection laboratory-scale numerical models of oxidation experiments for Kirsanovskoye oil field. *J. Pet. Sci. Eng.* 188, 106796. <https://doi.org/10.1016/J.PETROL.2019.106796>
- Kim, T.W., Kovsky, A., 2017. High-Temperature Imbibition for Enhanced Recovery from Diatomite 1–21.
- Kim, T.W., Kovsky, A., 2017. SPE-185632-MS High-Temperature Imbibition for Enhanced Recovery from Diatomite 1–21.
- Kisler, J. P., Shallcross, D. C., 1997. An improved model for the oxidation processes of light crude oil. *Chem. Eng. Res. Des.* <https://doi.org/10.1205/026387697523859>

- Kokorev, V.I., Darishchev, V.I., Akhmadeishin, I.A., Shchekoldin, K.A., Boksernam, A.A., 2014. The Results of the Field Tests and Prospects of Termogas Development of Bazhenov Formation in OJSC RITEK, in: SPE Russian Oil and Gas Exploration & Production Technical Conference and Exhibition. Society of Petroleum Engineers. <https://doi.org/10.2118/171172-MS>
- Kovscek, A.R., Diabira, I., Castanier, L.M., 2000. An experimental investigation of permeability and porosity alteration in diatomite during hot fluid injection, in: SPE/AAPG Western Regional Meetings. pp. 315–326. <https://doi.org/10.2523/62558-ms>
- Kristensen, M.R., Gerritsen, M.G., Thomsen, P.G., Michelsen, M.L., Stenby, E.H., 2006. Efficient Reaction Integration for In-Situ Combustion Simulation. *Transp. Porous Media Porous Med* 1–32.
- Kudryavtsev, P., 2014. SPE-169542-MS Towards Dynamic Control of In-situ Combustion : Effect of Initial Oil and Water Saturations 1–12.
- Lamoureux-Var, V., Lorant, F., 2005. H₂S artificial formation as a result of steam injection for EOR: A compositional kinetic approach, in: SPE/PS-CIM/CHOA International Thermal Operations and Heavy Oil Symposium Proceedings. pp. 1–4. <https://doi.org/10.2523/97810-ms>
- Lasaki, G., Martel, R., DOE John Fahy, us L., 1985. Numerical Simulation of Combined Reverse Combustion and Steamflooding for Oil Recovery in a Utah Tar Sand. *Soc. Pet. Eng. J.* 227–234.
- Lee, K., Moridis, G.J., Ehlig-Economides, C.A., 2016. A comprehensive simulation model of kerogen pyrolysis for the in-situ upgrading of oil shales. *SPE J.* 21, 1612–1630. <https://doi.org/10.2118/173299-PA>
- Lee, K., Moridis, G.J., Ehlig-Economides, C.A., 2014. Oil shale in-situ upgrading by steam flowing in vertical hydraulic fractures. *Soc. Pet. Eng. - SPE USA Unconv. Resour. Conf.* 2014 1980, 673–685.
- Lee, K.J., Finsterle, S., Moridis, G.J., 2018a. Estimating the reaction parameters of oil shale pyrolysis and oil shale grade using temperature transient analysis and inverse modeling. *J. Pet. Sci. Eng.* 165, 765–776. <https://doi.org/10.1016/j.petrol.2018.03.020>
- Lee, K.J., Finsterle, S., Moridis, G.J., 2018b. Analyzing the impact of reaction models on the production of hydrocarbons from thermally upgraded oil shales. *J. Pet. Sci. Eng.* 168, 448–464. <https://doi.org/https://doi.org/10.1016/j.petrol.2018.05.021>

- Lee, K.J., Moridis, G.J., Ehlig-Economides, C.A., 2017. Numerical simulation of diverse thermal in situ upgrading processes for the hydrocarbon production from kerogen in oil shale reservoirs. *Energy Explor. Exploit.* 35, 315–337. <https://doi.org/10.1177/0144598716689354>
- Lewan, M.D., 1997. Experiments on the role of water in petroleum formation. *Geochim. Cosmochim. Acta* 61, 3691–3723. [https://doi.org/10.1016/S0016-7037\(97\)00176-2](https://doi.org/10.1016/S0016-7037(97)00176-2)
- Lewan, M.D., Roy, S., 2011. Role of water in hydrocarbon generation from Type-I kerogen in Mahogany oil shale of the Green River Formation. *Org. Geochem.* 42, 31–41. <https://doi.org/https://doi.org/10.1016/j.orggeochem.2010.10.004>
- Lewan, M.D., Winters, J.C., McDonald, J.H., 1979. Generation of oil-like pyrolyzates from organic-rich shales. *Science* 203, 897–9. <https://doi.org/10.1126/science.203.4383.897>
- Li, Y., KANG, Z., XUE, Z., ZHENG, S., 2018. Theories and practices of carbonate reservoirs development in China. *Pet. Explor. Dev.* 45, 712–722. [https://doi.org/10.1016/S1876-3804\(18\)30074-0](https://doi.org/10.1016/S1876-3804(18)30074-0)
- Liang, T., Zou, Y.-R., Zhan, Z.-W., Lin, X.-H., Shi, J., Peng, P., 2020. An evaluation of kerogen molecular structures during artificial maturation. *Fuel* 265, 116979. <https://doi.org/https://doi.org/10.1016/j.fuel.2019.116979>
- Lin, C.Y., Co Chen, W.H., Co Lee, S.T., Culham, W.E., 1984. Numerical Simulation of Combustion Tube Experiments and the Associated Kinetics of In-Situ Combustion Processes. *Soc. Pet. Eng. AIME* 657–666. <https://doi.org/doi:10.2118/11074-PA>
- Luong, D., Sephton, M.A., Watson, J.S., 2015. Subcritical water extraction of organic matter from sedimentary rocks. *Anal. Chim. Acta* 879, 48–57. <https://doi.org/10.1016/j.aca.2015.04.027>
- Maes, J., Muggeridge, A.H., Jackson, M.D., Quintard, M., Lapene, A., 2016. Modelling in-situ upgrading of heavy oil using operator splitting method. *Comput. Geosci.* 20, 581–594. <https://doi.org/10.1007/s10596-015-9495-6>
- Mallory, D.G., Moore, R.G., Mehta, S.A., 2018. Ramped Temperature Oxidation Testing and In Situ Combustion Projects. *Energy & Fuels* 32, 8040–8056. <https://doi.org/10.1021/acs.energyfuels.8b00760>
- Martinez, A.R., McMichael, C.L., 1998. Classification of Petroleum reserves, in: 15 Th World Petroleum

Congress. pp. 209–2010.

McGee, R., Frain, M., Hagen, S., 2011. Combined Miscible Drive Enhanced Pleito Creek Oil production. Oil Gas J.

McGlade, C., Sondak, G., Han, M., 2018. Whatever happened to Enhanced Oil Recovery [WWW Document]. iea. URL <https://www.iea.org/commentaries/whatever-happened-to-enhanced-oil-recovery> (accessed 8.20.20).

Meijssen, T.E.M., Emmen, J., Fowler, T.D., 2014. In-situ Oil Shale Development in Jordan through ICP Technology, in: Abu Dhabi International Petroleum Exhibition and Conference. Society of Petroleum Engineers. <https://doi.org/10.2118/172135-MS>

Messner, G.L., Stalling, D.R., 1990. Dual injection with steam and hot water in the Kern River field - A case history, in: International Technical Meeting. pp. 851–8515.

Montes, A.R., Moore, R.G., Mehta, S.A., Ursenbach, M.G., Gutierrez, D., 2018. Is high-pressure air injection (HPAI) simply a flue-gas flood? Can. Int. Pet. Conf. 2008.

Moore, R. G., Lareshen, C.J., Ursenbach, M. G., Mehta, S. A., Belgrave, J .D. M., 1996. Combustion/Oxidation Behavior of Athabasca Oil Sands Bitumen, in: Improved Oil Recovery Symposium. Society of Petroleum Engineers, pp. 1–8. <https://doi.org/10.2118/35392-MS>

Moore, R.G., Mehta, S.A., Ursenbach, M.G., 2007a. A Guide to High Pressure Air Injection (HPAI) Based Oil Recovery. <https://doi.org/10.2118/75207-ms>

Moore, R.G., Mehta, S.A., Ursenbach, M.G., 2007b. A Guide to High Pressure Air Injection (HPAI) Based Oil Recovery, in: SPE/DOE Improved Oil Recovery Symposium. pp. 1–7. <https://doi.org/10.2523/75207-ms>

Mukhina, E., Askarova, A., Kalacheva, D., Leushina, E., Kozlova, E., Cheremisin, Alexander, Morozov, N., Dvoretzkaya, E., Demo, V., Cheremisin, Alexey, 2020. Hydrocarbon saturation for an unconventional reservoir in details, in: Society of Petroleum Engineers - SPE Russian Petroleum Technology Conference 2019, RPTC 2019. pp. 1–17. <https://doi.org/10.2118/196743-ms>

Murer, A.S., McClennen, K.L., Ellison, T. K., Larson, D. C., Timmer, R. S., Thomsen, M. A., Wolcott, K. D., 2000. Steam injection project in heavy-oil diatomite. SPE Reserv. Eval. Eng. 3, 2–12.

<https://doi.org/10.2118/60853-PA>

Needham, R.B., Doe, P.H., 1987. Polymer Flooding Review. JPT, J. Pet. Technol. 1503–1507.

<https://doi.org/10.2118/17140-PA>

Olszak-Humienik, M., Jablonski, M., 2015. Thermal behavior of natural dolomite. J. Therm. Anal.

Calorim. 119, 2239–2248. <https://doi.org/10.1007/s10973-014-4301-6>

Onishi, T., Okatsu, K., Teramoto, T., 2006. History matching with combustion-tube tests for light-oil air injection project, in: SPE International Oil&Gas Conference and Exhibition. pp. 1–6.

Oskouei, S.J.P., Maini, B., Moore, R.G., Mehta, S.A., 2010. Experimental evaluation of SAGD-ISC hybrid recovery method, in: Canadian Unconventional Resources & International Petroleum Conference. pp.

1–10. <https://doi.org/10.2118/137836-ms>

Pang, H., Jin, Y., Gao, Y., 2019. Evaluation of elastic property changes in Karamay oil sand reservoir during thermal stimulation. Energy Sci. Eng. <https://doi.org/10.1002/ese3.342>

Pederson, J., Sitorus, J., 2001. Geothermal Hot-Water Flood -Balam South Telisa Sand, Sumatra,

Indonesia, in: SPE Asia Pasific Oil and Gas Conference and Exhibition in Jakarta, Indonesia. pp. 1–7.

<https://doi.org/10.2523/68724-ms>

Perry, R.H., Green, D.O.N.W., Campbell, J.M., 1960. Reverse Combustion-A New Oil Recovery Technique. Soc. Pet. Technol. <https://doi.org/10.2118/1500-G>

Popov, E., Kalmykov, A., Cheremisin, A., Bychkov, A., Bondarenko, T., Morozov, N., Karpov, I., 2017.

Laboratory investigations of hydrous pyrolysis as ternary enhanced oil recovery method for

Bazhenov formation. J. Pet. Sci. Eng. 156, 852–857. <https://doi.org/10.1016/j.petrol.2017.06.017>

Pu, W., Zhao, S., Hu, L., Varfolomeev, M.A., Yuan, C., Wang L., Rodionov, N.O., 2019. Thermal effect caused by low temperature oxidation of heavy crude oil and its in-situ combustion behavior. J. Pet.

Sci. Eng. 184, 1–8. <https://doi.org/10.1016/j.petrol.2019.106521>

Pu, W., Zhao, S., Hu, L., Varfolomeev, M.A., 2019. Journal of Petroleum Science and Engineering

Thermal effect caused by low temperature oxidation of heavy crude oil and its in-situ combustion

behavior 184, 106521. <https://doi.org/10.1016/j.petrol.2019.106521>

Pwaga, S., Iluore C., Hundseth O., Perales F.J., Idrees M.U., 2010. Comparative Study of Different EOR

Methods, Department of Petroleum Engineering. Trondheim, Norway.

- Reed, R.L., Tracht, J.H., 1960. Experimental Aspects of Reverse Combustion in Tar , Sands. Pet. Trans. AIME 219, 99–108.
- Rego, F. B., Botechia, V. E., Schiozer, D. J., 2017. Heavy oil recovery by polymer flooding and hot water injection using numerical simulation. J. Pet. Sci. Eng. 153, 187–196.
<https://doi.org/10.1016/j.petrol.2017.03.033>
- Rodriguez, E., Ordonez, A., Comas, J.C., Trujillo Portillo, M.L., Belgrave, J.D.M., 2012. A Framework for Consolidating Air Injection Experimental Data. SPE Lat. Am. Caribb. Pet. Eng. Conf.
<https://doi.org/10.2118/152048-MS>
- Romanowski L J, J., Thomas, K.P., 1985. Reverse combustion in asphalt ridge tar sand. United States.
- Ryan, R.C., Fowler, T.D., Beer, G.L., Nair, V., 2010. Shell’s In Situ Conversion Process—From Laboratory to Field Pilots. pp. 161–183. <https://doi.org/10.1021/bk-2010-1032.ch009>
- Sarathy, P.S., 2016. In-situ combustion handbook - principles and practices.
- Satter, A., 1965. Heat Losses During Flow of Steam Down a Wellbore, in: SPE Production Research Symposium 1966. pp. 845–851. <https://doi.org/10.2118/1071-pa>
- Shen, C.W., 1989. Laboratory hot waterfloods prior to and following steamfloods., in: SPE California Regional Meeting in Bakersfield, California. pp. 97–101. <https://doi.org/10.2118/18754-ms>
- Shilov, E., Cheremisin, A., Maksakov, K., Kharlanov, S., 2019. Huff-n-puff experimental studies of CO₂ with heavy oil. Energies 12, 1–15. <https://doi.org/10.3390/en12224308>
- Shojaiepour, M., Kharrat, R., Hashemi, A., 2014. Experimental and Simulation Study of In-situ Combustion Process in Carbonate Fractured Porous Media. J. Japan Pet. Inst. 57, 208–215.
- Sibbald, L., Moore, R. G., Bennion, D.W., Chmilar, B. J., Ursenbach, M. G., 1998. In situ combustion experimental studies using a combustion tube system with stressed core capability, in: Annual Technical Meeting. pp. 1–18.
- Sibbald, L., Moore, R. G., Bennion, D. W., Chmilar, B. J., Ursenbach, M. G., 1988. In-situ combustion experimental studies using a combustion tube system with a stressed core capability, in: The 39th Annual Technical Meeting of the Petroleum Society of CIM. pp. 1–18.

- Siskin, M., Katritzky, A.R., 2001. Reactivity of Organic Compounds in Superheated Water: General Background. *Chem. Rev.* 101, 825–836. <https://doi.org/10.1021/cr000088z>
- Smith, T.K., Perkins, F.W., 1973. Experimental and Numerical Studies of the Wet Combustion Recovery Process. *J. Can. Pet. Technol.* 13, 44–54.
- Sola, B.S., Rashidi, F., 2008. Experimental study of hot water injection into low-permeability carbonate rocks. *Energy and Fuels* 22, 2353–2361. <https://doi.org/10.1021/ef800009r>
- Speight G.J., 2016. Oil recovery, in: Speight, J.G. (Ed.), *Introduction to Enhanced Recovery Methods for Heavy Oil and Tar Sands (Second Edition)*. Gulf Professional Publishing, Boston, p. 493. <https://doi.org/https://doi.org/10.1016/B978-0-12-849906-1.00019-9>
- Speight, J.G., 2019. Chapter 3 - Thermal Methods of Recovery, in: Speight, J.G.B.T.-H.O.R. and U. (Ed.), . Gulf Professional Publishing, pp. 113–168. <https://doi.org/https://doi.org/10.1016/B978-0-12-813025-4.00003-9>
- Speight, J.G., 2013. Chapter 5 - Thermal Methods of Recovery, in: Speight, J.G.B.T.-O.S.P.P. (Ed.), . Gulf Professional Publishing, Boston, pp. 111–137. <https://doi.org/https://doi.org/10.1016/B978-0-12-404572-9.00005-X>
- Stone, T. W., Li, G., Pallister, I., 2013. A Comparison of Analytic and Segmented Heat and Quality Loss in Thermal Steam Injection Wells, in: *SPE Reservoir Simulation Symposium Held in The Woodlands*. pp. 1–11.
- Stosur, J.J., 1977. CHAPTER 34 - IN SITU COMBUSTION METHOD FOR OIL RECOVERY STATE OF THE ART AND POTENTIAL, in: Meyer, R.F., Bamea, J., Grenon, M.B.T.-T.F.S. of N.-M.P. and G. (Eds.), . Pergamon, pp. 611–623. <https://doi.org/https://doi.org/10.1016/B978-0-08-021735-2.50044-6>
- Sun, Y., Kang, S., Wang, S., He, L., Guo, W., Li, Q., Deng, S., 2019. Subcritical Water Extraction of Huadian Oil Shale at 300 °c. *Energy and Fuels* 33, 2106–2114. <https://doi.org/10.1021/acs.energyfuels.8b04431>
- Surguchev, L.M., Reich, E. M., Berenblyum, R. A., Schipanov, A. A., 2010. Improved oil recovery methods: Applicability screening and potential evaluation, in: *Society of Petroleum Engineers - SPE*

- Russian Oil and Gas Technical Conference and Exhibition 2010. pp. 2–7.
<https://doi.org/10.2118/134742-ms>
- Sutherland, R. B., Hammawa, H., Moore, R. G., Mehta, S. A., Ursenbach, M. G., 2007. Mitigating explosion risks in high pressure air injection compressors. *J. Can. Pet. Technol.* 46, 55–60.
<https://doi.org/10.2118/07-08-06>
- Symington, W.A., Kaminsky, R.D., Meurer, W.P., Otten, G.A., Thomas, M.M., Yeakel, J.D., 2010. ExxonMobil's Electrofrac™ Process for *In Situ* Oil Shale Conversion. pp. 185–216.
<https://doi.org/10.1021/bk-2010-1032.ch010>
- Taber, J. J., Martin, F. D., 1983. Technical screening guides for the enhanced recovery of oil. Proc. - SPE Annu. Tech. Conf. Exhib. 1983-October. <https://doi.org/10.2523/12069-ms>
- Tadema, H.J., Wiejdem, J., 1970. Spontaneous ignition of oil sands. *Oil Gas J* 68:50.
- Tamanyan, B.P., 2015. Aquathermolysis of crude oils and natural bitumen : chemistry , catalysts and prospects for industrial implementation. *Russ. Chem. Rev.* 84, 1145–1175.
<https://doi.org/10.1070/RCR4500>
- Tamanyan, 2015. Aquathermolysis of crude oils and natural bitumen : chemistry , catalysts and prospects for industrial implementation. *Russ. Chem. Rev.* 84, 1145–1175. <https://doi.org/10.1070/RCR4500>
- Tang, G.Q., Kovscek, A.R., 2008. An experimental investigation of the effect of temperature on recovery of heavy oil from diatomite. *SPE Repr. Ser.* 163–179.
- Terry, R.E., 2001. Enhanced oil recovery. *Encycl. Phys. Sci. Technol.*
- Thomas, S., 2008. Enhanced oil recovery - an overview. *Oil Gas Sci. Technol.* 63, 9–19.
<https://doi.org/10.2516/ogst>
- Tiwari, P., Deo, M., Lin, C.L., Miller, J.D., 2013. Characterization of oil shale pore structure before and after pyrolysis by using X-ray micro CT. *Fuel* 107, 547–554.
<https://doi.org/10.1016/J.FUEL.2013.01.006>
- U.S. Energy Information Administration, 2020. Assumptions to the Annual Energy Outlook 2015 - Oil and Gas Supply Module, U.S. Energy Information Administration.
- Ungerer, P., Behar, F., Villalba, M., Heum, O.R., Audibert, A., 1988. Kinetic modelling of oil cracking.

Org. Geochem. [https://doi.org/10.1016/0146-6380\(88\)90238-0](https://doi.org/10.1016/0146-6380(88)90238-0)

Wang, H.Y., 2017. A Numerical Study of Thermal-Hydraulic-Mechanical Simulation With Application of Thermal Recovery in Fractured Shale-Gas Reservoirs. *SPE Reserv. Eval. Eng.* 20, 513–531.

<https://doi.org/10.2118/183637-pa>

Wang, X., Zhao, Y.-P., 2020. The time-temperature-maturity relationship: A chemical kinetic model of kerogen evolution based on a developed molecule-maturity index. *Fuel* 278, 118264.

<https://doi.org/https://doi.org/10.1016/j.fuel.2020.118264>

Warren, J.E., Reed R.I., Price H.S., 1960. Theoretical Consideration of Reverse Combustion in Tar Sands.

Watts, B.C., Hall, T.F., 1997. The Horse Creek Air Injection Project: Overview, in: *SPE Rocky Mountain Regional Meeting*, Casper, Wyoming. pp. 143–154.

Wellington, S.L., Berchenko, I.E., Rouffignac, E.P., 2005. In situ thermal processing of an oil shale formation to produce a desired product. US Pat. US6880633 B2.

White, M., Chick, L., Mcvay, G., 2010. Impact of Geothermic Well Temperatures and Residence Time on the In-situ Production of Hydrocarbon Gases from Green River Formation Oil Shale Subsurface Simulation PNNL [WWW Document]. 30th Oil Shale Symp. URL http://www.costar-mines.org/oss/30/presentation/Presentation_07-1-White_Mark.pdf (accessed 5.21.20).

Wu, Z., Liu, H., 2019. Investigation of hot-water flooding after steam injection to improve oil recovery in thin heavy-oil reservoir. *J. Pet. Explor. Prod. Technol.* 9, 1547–1554. <https://doi.org/10.1007/s13202-018-0568-7>

Xu, H. H., Okazawa, N. E., Moore, R. G., Mehta, S. A., Laureshen, C. J., Ursenbach, M. G., Mallory, D. G., 2001. In Situ upgrading of heavy oil. *J. Can. Pet. Technol.* 40, 45–53.

Yang, M., Harding, T.G., Chen, Z., 2017. An Improved Kinetics Model for in Situ Combustion of Pre-Steamed Oil Sands. *Energy and Fuels* 31, 3546–3556.

<https://doi.org/10.1021/acs.energyfuels.6b02582>

Yang, X., Gates, I. D., 2009. Combustion kinetics of Athabasca bitumen from 1D combustion tube experiments. *Nat. Resour. Res.* 18, 193–211. <https://doi.org/10.1007/s11053-009-9095-z>

Yang, M., Chen, Z., 2016. An Improved Reaction Kinetics Model Of In-Situ Combustion For Pre-Steamed

Oil Sands, in: SPE Canada Heavy Oil Technical Conference. pp. 1–16.

Yang, X., Gates, I.D., 2009. Combustion kinetics of Athabasca bitumen from 1D combustion tube experiments. *Nat. Resour. Res.* <https://doi.org/10.1007/s11053-009-9095-z>

Yasar, M., Trauth, D.M., Klein, M.T., 2001. Articles Reaction Environment on Pathways and Selectivities 504–509.

Yoshioka, Y., Sasaki, K., Takatsu K., Sugai, Y., 2017. Screening of Major Chemical Reactions in In-Situ Combustion Process for Bitumen Production from Oil Sands Reservoirs. *Int. J. Pet. Petrochemical Eng.* 3, 82–92. <https://doi.org/10.20431/2454-7980.0304008>

Youtsos, M.S.K., Mastorakos, E., Cant, R.S., 2013. Numerical simulation of thermal and reaction fronts for oil shale upgrading. *Chem. Eng. Sci.* 94, 200–213.
<https://doi.org/https://doi.org/10.1016/j.ces.2013.02.040>